9th German-Greek-Polish Symposium

Recent Advances in Mechanics

September 4 – 9, 2016, Kolympari, Crete, Greece

Book of Abstracts

Edited by:

John. T. Katsikadelis, National Technical University of Athens and
Georgios E. Stavroulakis, Technical University of Crete

Organized by

Hellenic Society of Theoretical and Applied Mechanics

Technical University of Crete, Greece

9th German-Greek-Polish Symposium

Recent Advances in Mechanics

September 4 – 9, 2016
Kolympari, Crete, Greece

Book of Abstracts

Organized by

Hellenic Society of Theoretical and Applied Mechanics and

Technical University of Crete

Chairman:
J.T. Katsikadelis, National Technical University of Athens

Co-chairmen:
R Kienzler, University of Bremen, Germany
W. Kurnik, Technical University of Warsaw, Poland

Editors: J.T. Katsikadelis &
G.E. Stavroulakis

Editors: J.T. Katsikadelis & G.E. Stavroulakis

Technical Assistance: M. Bakatsaki

Published by the Technical University of Crete, 2016

ISBN 978-960-8475-25-0

Organized by the

- Hellenic Society of Theoretical and Applied Mechanics
- Technical University of Crete

Sponsored by the

- National Technical University of Athens
- Technical University of Crete

International Organizing Committee

Chairman:

- Prof. **J.T. Katsikadelis**, National Technical University of Athens

Co-chairmen:

- Prof. **R Kienzler**, University of Bremen, Germany
- Prof. **W. Kurnik**, Technical University of Warsaw, Poland

Local Organizing Committee

Chairman:

- Prof. **G.E. Stavroulakis,** Technical University of Crete

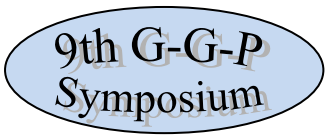

TABLE OF CONTENTS

Abstracts of Oral Presentation

PREFACE

The German-Greek-Polish Symposia are organized regularly every three years in one of the participating countries. These special meetings were initiated by Profs. R. Bogacz, A. Kounadis and O. Mahrenholtz in 1991 and continued after 2000 by Profs J.T. Katsikadelis, R. Kienzler and W. Kurnik. They have a more than 25 years old "history".

- 1st, September 1991 in Pułtusk, Poland
- 2nd, September 1996 in Bad Honnef, Germany
- 3rd, September 1998 in Xanthi, Greece
- 4th, September 2001 in Pułtusk, Poland
- 5th, September 2004 in Bad Honnef, Germany
- 6th, September 2007 in Alexandroupolis, Greece.
- 7th, September 2010 in Poznań, Poland
- 8th, September 2013 in Goslar, Germany

The present German-Greek-Polish Symposium is the 9th of the series. It is locally organized by the Technical University of Crete and takes place in Kolympari, Chania, Greece, hosted by the Orthodox Academy of Crete www.oac.gr.

The fundamental purpose of these meetings has been to bring together about 15 expert participants from Germany, Greece and Poland each, especially young researchers, and discuss the latest advances in the wide field of Applied Mechanics. Throughout, the presentations attempt to achieve the highest scientific level and the Symposia have been very successful both in terms of advancing scientific progress and furthering friendship and personal interaction among the participants. Distinguished people of mechanics have participated in the Symposia. Most of the presented contributions at the Symposium are published in special issues of the AAM.

Prof. J.T. Katsikadelis, PhD, Dr. Eng, Dr. h.c.
Chairman of the Symposium

Prof. G.E. Stavroulakis, Dr. Ing. Hab. Prof. h.c.
Chairman of the Local Organizing Committee

Athens, August 2016

GENERAL INFORMATION

Conference Organization

Prof. **John T. Katsikadelis**,
Institute of Structural Analysis & Aseismic Research
School of Civil Engineering
National Technical University of Athens
GR-157 73 Zografou, Athens, Greece
Tel: +30 210 7721652
E-mail: jkats@central.ntua.gr

Prof. **Georgios E. Stavroulakis**
Technical University of Crete
School of Production Engineering and Management
University Campus, Kounoupidiana
R-73100 Chania, Greece
Tel: +30 2821037418
E-mail: gestavr@dpem.tuc.gr

Secretariat:

Mrs. **Maria Bakatsaki**
Institute of Computational Mechanics and Optimization
School of Production Engineering and Management
Technical University of Crete
University Campus, Kounoupidiana
GR-73100 Chania, Greece
Tel. +30-28210-37241 Fax: +30-28210-37486

email: 9ggp@isc.tuc.gr

PROGRAMME OVERVIEW

9th GGP — Crete, Sepbember 4-9, 2016

	Sunday	Monday	Tuesday	Wednesday	Thursday	Friday
7:30-8:30		Breakfast	Breakfast	Breakfast	Breakfast	Breakfast
9:00-9.30		Opening	Katsikadelis	excursion	Weber	Yiotis
9:30-10:00		Ceremony	Rauter	to	Tylikowski	Korzeb
10:00-10:30			Kurnik	Eleftherna	Stavroulakis	Tsopelas
10:30-11:00		Coffee break	Coffee break	Museum	Coffee break	Coffee break
11:00-11:30		Burczynski	Hartmann	and	Schwarz	
11:30-12:00		Kienzler	Maczak	Rethymnon	Provatidis	Closure
12:00-12:30		Manolis	Triantafyllou	city	Korczak	
12:45-14:30		Lunch	Lunch		Lunch	Lunch
14:30-15:00		Sumelka	Naumenko		Tsipsis	Departure
15:00-15:30		Natsiavas	Koumousis		Kuczma	
15:30-16:00		Bogacz	Charalambakis		Frischmuth	
16:00-16:30	Arrival	break	break		Zisis	
16:30-17:00	of	Silbermann	Kaessmair	back to	break	
17:00-17:30	Participants	Sumarac	Spiliopoulos	venue		
17:30-18:00		Liolios	Kowalewski			
20:00-21:00	Dinner	Dinner	Dinner	Dinner	Cretan Dinner	

GENERATION OF NEW GRAPHENE-LIKE MATERIALS

Prof. T. Burczyński[1], **Dr A. Mrozek**[2], **Dr hab. W.Kuś**[3]
[1]Institute of Fundamental Technological Research, Polish Academy of Sciences, Warsaw, Poland
[2]AGH University of Science and Technology, Cracow, Poland
[3]Institute of Computational Mechanics and Engineering, Silesian University of Technology, Gliwice, Poland

Abstract: *The paper describes an application of a hybrid algorithm to optimal searching for new, stable atomic arrangements of two-dimensional graphene-like carbon lattices. Interactions between atoms are modeled using the AIREBO potential, especially developed for carbon and hydrocarbon materials. Validation of the obtained results and examples of the models of the new grapheme-like materials are presented.*

1. Introduction

Carbon atoms form various types of bondings and spatial configurations. This ability is determined by the atoms' hybridization states, which depend on their particular electronic configuration. This phenomenon is responsible for the existence of many different allotropes of the carbon. Graphene-like materials can be classified as periodic, flat atomic networks, made of stable configurations of carbon atoms in certain hybridization states. Since the stable configurations of atoms correspond to the global minima on the Potential Energy Surface (PES), such a task can be considered as a special optimization problem. However, the number of local minima increases almost exponentially with the number of atoms in the structure, thus searching for the global minimum on a PES became a non-trivial, NP-hard problem.

2. Hybrid algorithm

The hybrid algorithm combines the parallel evolutionary algorithm prepared by the authors, and the classical conjugated-gradient minimization of the total potential energy of the optimized atomic system. Since the processed structure is considered as an atomic model, the behavior and the potential energy of carbon atoms are determined using the **A**daptive **I**ntermolecular **R**eactive **E**mpirical **B**ond **O**rder (AIREBO) potential developed for molecular dynamics simulations of hydrocarbons [2].

The fitness function is formulated as the total potential energy of the considered atomic system, i.e., the total sum of all potential energies of particular atomic interactions. The AIREBO potential in the following form is used in computation:

$$FF = \sum_{i} \sum_{j \neq i} \left(E_{ij}^{REBO} + E_{ij}^{LJ} + \sum_{k \neq i,j} \sum_{l \neq i,j,k} E_{kijl}^{TORSION} \right) \tag{1}$$

where: E^{REBO} corresponds to the short range interactions between covalently bonded pair of atoms, E^{LJ} is responsible for the long range interactions and is computed in a simplified way, using the Lennard-Jones-like function with additional distance-dependent switching functions and $E^{TORSIONAL}$ is torsional potential which depends on the neighboring atom's dihedral angles. Detailed description of the proposed algorithm is presented in [1].

3. New graphene-like materials

In order to validate the accuracy of the results, certain arrangements of carbon atoms already known from literature have been examined, e.g. the supergraphene (triclinic unit cell containing 8 carbon atoms) and the graphyne (triclinic unit cell containing 12 carbon atoms). Since all the tests yield promising results, the proposed optimization algorithm has been applied to search for new stable configurations of a given number of carbon atoms in a unit cell of given size and periodic boundaries [1]. For eight carbon atoms placed in the 4 Å ×7 Å rectangular unit cell obtained a stable flat network named X (Figure 1A) and for the same number of carbon atoms placed in the rectangular unit cell 4 Å ×6 Å obtained a stable flat network named Y (Figure 1B).

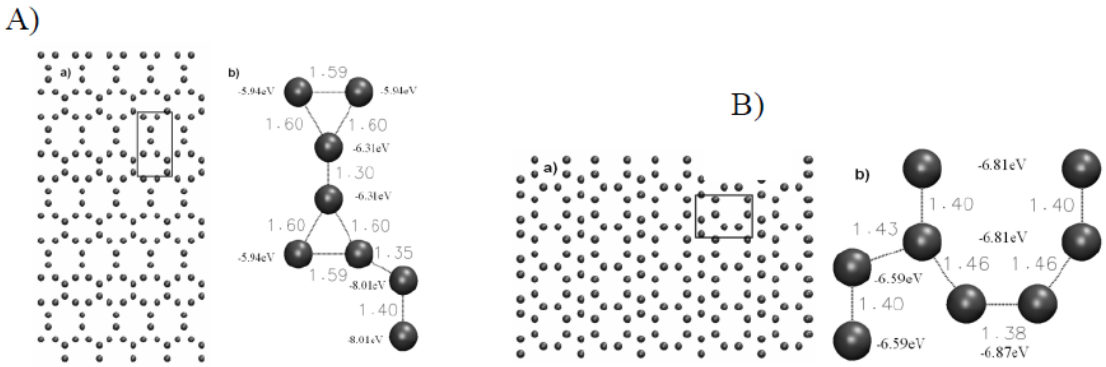

Figure 1: Layout of new stable carbon networks X (A) and Y (B) found by the hybrid algorithm

4. Conclusions

The main purpose of this paper was to present the hybrid parallel algorithm, applied to searching for new 2D graphene-like materials. The proposed method is able to find already-known structures like supergraphene and graphyne as well as new stable ones, named X and Y. Examples performed for new carbon networks clearly show that the final form and properties of optimized structures depend on the assumed size, type and atomic density of the unit cell. Thus, the considered topology optimization problem can be reformulated and applied to searching for a molecular structure with predefined material properties, not only in the case of carbon-based structures.

5. References

[1] Mrozek A., Kuś W., Burczyński T., "Nano level optimization of graphene allotropes by means of hybrid parallel evolutionary algorithm", *Computational Material Science, Vol 106, 2015, pp.* 161-169.

[2] Stuart S.J., Tutein J.A., Harsison A., " A reactive potential for hydracarbons with intermolecular interactions". *J. Chemical Physics, Vol. 112, 2000, pp.* 6472- 6486.

ON DISPLACEMENTS AND STRESSES IN A SECOND-ORDER CONSISTENT PLATE THEORY

Prof. Dr.-Ing. R. Kienzler[1], **Dr.-Ing. P. Schneider**[1]
[1]University of Bremen,
Bremen Institute for Mechanical Engineering, Germany

Abstract: *Using the uniform-approximation technique in combination with the pseudo-reduction method, a consistent second-order plate theory has been derived, which does not rely on any a priori assumptions nor on shear- or thickness-strain-correction factors. In the talk, it is shown how the displacement and stress distributions can be calculated once the governing PDEs have been solved*

1. Consistent second-order linear plate theory

Plates belong to the family of thin plane structures. The characteristic dimension in thickness direction h is much smaller than the characteristic in-plane dimension a. Thus the plate parameter $c^2 = h^2/12a^2$ appears as a small quantity, i.e., $c^2 \ll 1$. The derivation of a consistent linear, second-order plate theory has been reported in several papers, cf. e.g., Schneider et al [1]. In the following, we concentrate on plates with constant thickness made of an isotropic material (Young's E, Poisson's ratio ν). In extension of these earlier investigations, we introduce here energetic averages $\tilde{w}$ and $\tilde{\psi}_\alpha$ of the transverse displacement w and the slopes ψ_α, respectively, of the plate middle surface, as

$$\begin{aligned} c^2\tilde{w} &= c^2 w + \frac{3}{10}\frac{\nu}{1-\nu}c^4\Delta w + O(c^6), \\ c^2\tilde{\psi}_\alpha &= -c^2 w_{,\alpha} - \frac{3}{10}\frac{8+\nu}{1-\nu}c^4\Delta w_{,\alpha} - \frac{6}{5}\varepsilon_{3\alpha\beta}c^2\psi_{,\beta} + O(c^6) \end{aligned} \qquad (1)$$

(Δ is the two-dimensional Laplace operator, $\Delta() = ()_{,11} + ()_{,22}$, and $\varepsilon_{3\alpha\beta}$ is the completely screw-symmetric, third-order permutation tensor). The quantity ψ is defined as $\psi = \psi_{2,1} - \psi_{1,2} \triangleq rot\,\psi_\alpha$ and may be regarded as a measure of the transverse-shear deformation. This ψ is next to $\tilde{w}$ one of our two main variables which are governed (after pseudo reduction) by two main PDEs

$$\begin{aligned} \Delta\Delta\tilde{w} &= \frac{a^3}{K}\left(P - \frac{6}{5}\frac{2-\nu}{1-\nu}c^2\Delta P\right) + O(c^6), \\ c^2\left(\psi - \frac{6}{5}c^2\Delta\psi\right) &= 0 + O(c^6), \end{aligned} \qquad (2)$$

K is the classical plate stiffness $K = Eh^3/12(1-\nu^2)$ and P is the transverse load applied through the upper and lower plate faces $(x_3 = \pm h/2a)$.

The stress resultants are calculated as bending moments ($\delta_{\alpha\beta}$ Kronecker's tensor of unity) and transverse shear forces, respectively, via

$$\begin{aligned} \tilde{M}_{\alpha\beta} &= -\frac{K}{a}\left\{\left(1 + \frac{12}{5(1-\nu)}\right)\left((1-\nu)\tilde{w}_{,\alpha\beta} + \nu\tilde{w}_{,\gamma\gamma}\delta_{\alpha\beta}\right)\right. \\ &\quad \left. + \frac{3}{5}(1-\nu)c^2(\varepsilon_{3\alpha\gamma}\psi_{,\beta} + \varepsilon_{3\beta\gamma}\psi_{,\alpha})_{,\gamma}\right\} + \frac{6}{5}\frac{\nu}{1-\nu}c^2a^2P\delta_{\alpha\beta} + O(c^6), \qquad (3) \\ \tilde{Q}_\beta &= -\frac{K}{a^2}\left\{\Delta\tilde{w}_{,\beta} + \frac{1}{2}(1-\nu)\varepsilon_{3\beta\gamma}\psi_{,\gamma}\right\} - \frac{6}{5}\frac{2-\nu}{1-\nu}c^2aP_{,\beta} + O(c^6). \end{aligned}$$

Higher-order stress resultants are also involved and calculated but turn out to be expressible as linear combinations of the classical stress resultants.

Finally, the boundary conditions are given by

$$\begin{aligned} M^*_{\alpha\beta} n_\alpha &= \tilde{M}_{\alpha\beta} n_\alpha \big|_\Gamma \quad \text{or} \quad \psi^*_\beta = \tilde{\psi}_\beta \big|_\Gamma , \\ Q^*_\alpha n_\alpha &= \tilde{Q}_\alpha n_\alpha \big|_\Gamma \quad \text{or} \quad w^* = \tilde{w} \big|_\Gamma , \end{aligned} \qquad (4)$$

where $M^*_{\alpha\beta}$ and Q^*_α are the prescribed stress resultants and ψ^*_β and w^* are the prescribed displacement quantities along the boundary Γ of the mid-plane.

2. Displacement and stresses

With eqs. (1) - (4) the governing equations of the consistent second-order plate theory are given and can be solved by analytical or numerical methods. However, the stress distribution cannot be calculated, since by the pseudo-reduction method (cf. Schneider and Kienzler [2]) not all of the displacement coefficients are determined. They may be chosen a posteriori, i.e., without having any influence on the governing equations, to fulfill the boundary conditions along the plate faces and the local equilibrium conditions. This will be shown in the presentation.

3. Discussion

In the talk, the proposed second-order plate theory will be compared with other theories existing in the literature. We will assess and validate the theories of Reissner/Mindlin, Zhilin, Marguerre, Verkua, Ambartsumyan and Reddy.

4. References

[1] Schneider, P., Kienzler, R., and Böhm, M., "Modeling of consistent second-order plate theories for anisotropic materials", *Zeitschrift für Angewandte Mathematik und Mechanics*, Vol. 94, 2013, pp. 21-42.

[2] Schneider, P., and Kienzler, R., "An algorithm for automatisation of pseudo reductions of PDE systems arising from the uniform-approximation technique", In H. Altenbach & V.A. Eremeyev (eds.), *Shell-like Structures; Nonclassical theories and applications*, Springer, Heidelberg, 2011, pp. 377-390.

9th German-Greek-Polish Symposium
Recent Advances in Mechanics
September 04-09, 2016
Kolympari, Chania, GREECE

NANO-SIZED HETEROGENEITIES IN A MATRIX BY BEM AND FEM

Prof. G.D. Manolis[1], Assoc. Prof. S.L. Parvanova[2], Dipl. Ing. G.P. Vasilev[2], Prof. P.S. Dineva[3]
[1]Aristotle University, Thessaloniki, Greece
[2]University of Architecture, Civil Engineering and Geodesy, Sofia, Bulgaria
[3]Bulgarian Academy of Sciences, Sofia, Bulgaria

Abstract: *This work addresses the elastodynamic problem for a finite-sized, elastic solid matrix containing multiple nano-heterogeneities of arbitrary shape, number and geometric configuration. The problem is formulated under plane strain conditions under time-harmonic motions. We evaluate the non-uniform stress and strain fields that develop in the heterogeneous solid matrix for dynamic loads along the matrix boundaries.*

1. Introduction

The mechanical model used here is based on a combination of classical elastodynamic theory for the bulk solid under non-classical boundary conditions, supplemented with a localized constitutive law for the solid-inclusion interface in the framework of the Gurtin-Murdoch [1] theory of surface elasticity. We use (a) a 2D boundary element method (BEM) [2] with frequency-dependent fundamental solutions for the bulk solid and (b) the finite element method (FEM) software package ANSYS [3] augmented by a macro-finite element for representing surface effects on the contour of the nano-inclusions. The accuracy of the numerical solutions obtained for the dynamic stress concentration factor and for the diffracted displacement wave field is satisfactorily established. Then, comparison studies are conducted so to gauge the BEM and FEM performance. Finally, the authors acknowledge support by the Bulgarian NSF under Grant No. DFNI-I02/12.

2. BEM and FEM Formulations and Numerical Results

Consider wave motion in the plane for a Cartesian coordinate system, where a finite-sized, elastic and isotropic solid with boundary Γ is subjected to time-harmonic loads of frequency ω, see Fig. 1(a). The solid matrix contains multiple nano-inclusions with boundaries Γ_I^n or nano-cavities Γ_H^n, where *n=1, 2,…N*, of arbitrary shape, number, size and configuration. The material properties (Lamè constants and density) are denoted as λ_M, μ_M, ρ_M for the solid matrix and $\lambda_{I,n}, \mu_{I,n}, \rho_{I,n}$ for the *n-th* inclusion. Furthermore, the displacement vector $u_i\left(x_1, x_2, \omega\right)$, *i, j*=1, 2, the stresses σ_{ij} and the traction vector $t_i = \sigma_{ij} n_j$, (n_j: outward pointing unit normal vector) satisfy the equations of motion in the bulk solid:

$$\sigma_{ij,i} + \rho\omega^2 u_j = 0;\ \sigma_{ij} = C_{ijkl}^M u_{k,l}^M \ \ (matrix);\ C_{ijkl}^{I,n} u_{k,l}^{I,n} \ \ (inclus);\ C_{ijkl} = \lambda\delta_{ij}\delta_{kl} + \mu\left(\delta_{ik}\delta_{jl} + \delta_{il}\delta_{jk}\right) \ \ (1)$$

Following surface elasticity theory, the *n-th* interface between a nano-inclusion and the matrix is regarded as a thin material film with mechanical properties $\lambda^{S,n}, \mu^{S,n}$ and surface tension $\tau^{0,n}$. The constitutive law along interfaces between matrix and inclusion for the localized stress and strain is

$$\sigma^{sur} = \tau^0 + \left(2\mu^s + \lambda^s\right)\varepsilon^{sur} \qquad (2)$$

The boundary conditions along Γ_I^M are (a) continuity of the displacements as $u_i^I = u_i^M = u_i$ and (b) interface equilibrium conditions along the arc length $s \equiv \Gamma_I^M$ written in terms of the local normal and tangential (n,t) coordinates. These lead to the following relation between tractions along any interface from the side of the heterogeneity t_i^I and from the side of the surrounding matrix t_i^M :

$$\begin{Bmatrix} t_1^I + t_1^M \\ t_2^I + t_2^M \end{Bmatrix}_k = \boldsymbol{f}_k^{sur} + \boldsymbol{T}_k^{sur} \begin{Bmatrix} u_1 \\ u_2 \end{Bmatrix}_k \qquad (3)$$

This relation is defined for traction matrix $\mathbf{T}_k^{sur}$ and the surface force vector $\mathbf{f}_k^{sur}$. The BVP defined above can be reformulated as a BEM solution [2] using a set of integral equations along all boundaries based on the Betti's reciprocity theorem, plus a set of frequency-dependent fundamental solutions for in-plane wave motion. Surface effects given by Eq. (3) are then introduced at the boundaries. For the FEM formulation, the ANSYS [3] environment has user-programmable features capabilities, which allow for the incorporation of type of

element developed outside the program. Thus, surface effects are implemented by conversion of the $\boldsymbol{T}^{sur}$ matrix into a single macro-FE, which is attached along the contact inclusion-matrix interface.

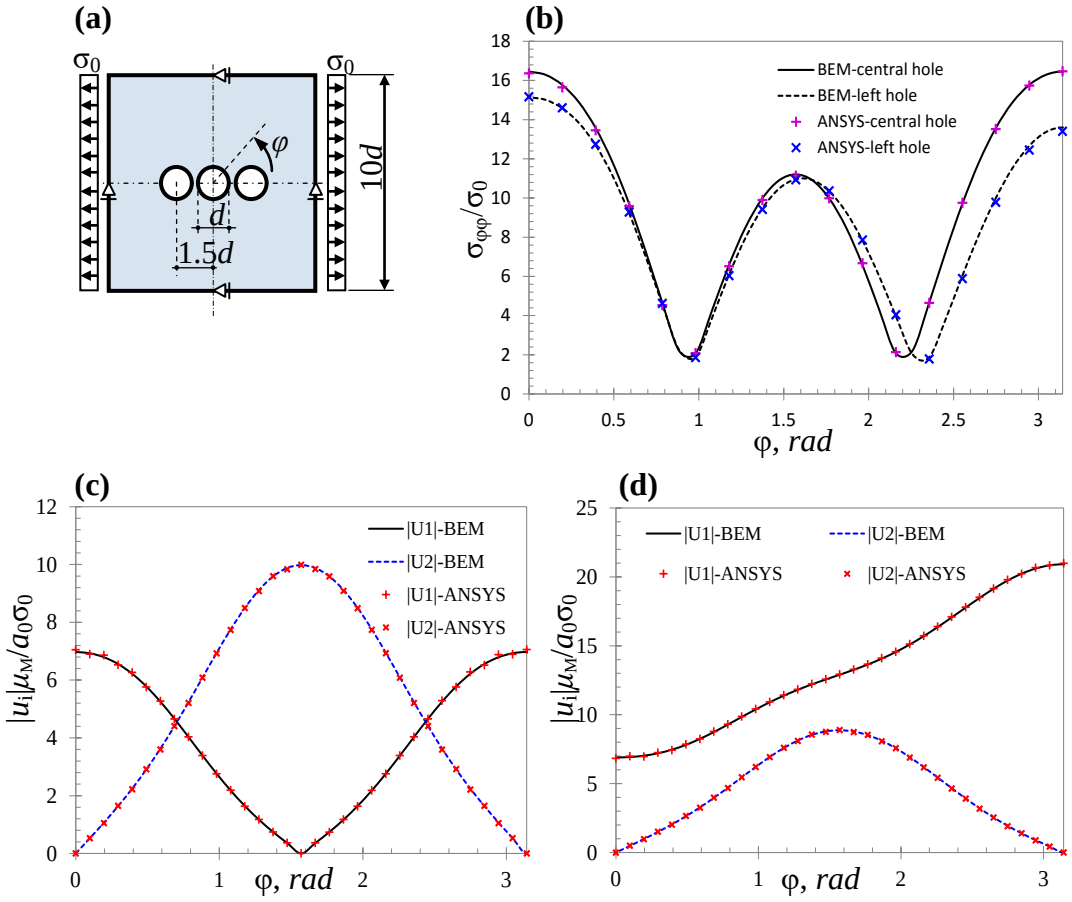

FIGURE 1: a) Three cavities in a square matrix; (b) normalized hoop stresses at the central and left cavities; normalized displacement amplitudes for (c) the central and (d) the left cavity

Consider three circular cavities embedded in a square solid matrix, see Fig. 1(a). The matrix is subjected tensile forces σ_0 applied horizontally. The cavity diameters are $d = 2a_0$ the size of the square plate is 10*d*, and interface effects are measured by parameter $s = K_S / (2\mu_M a_0) = 0.5$. Damping is 5% and Poisson's ratio is 0.26. Rigid body motion is avoided by constraining four edge nodes. The BEM mesh comprises 128 elements, 32 per each cavity contour and 32 for the matrix perimeter, while the FEM mesh comprises 2100 quadratic elements. The results obtained are plotted in Figs. 1 (b)-(d), for a normalized frequency of $\Omega = \omega d / C_P = 0.24$. Figure 2(b) depicts the normalized hoop stresses $|\sigma_{\varphi\varphi} / \sigma_0|$ versus polar angle φ, while Figs. 1(c), (d) plot the real and imaginary displacements normalized as $u_i \mu_M / a_0 \sigma_0$, $i = 1, 2$. The percentage difference in the normalized displacement components obtained by the BEM and FEM solutions ranges from *0.01–1.0%* for most cases, but can reach up to *2%* for low values at the edges $\varphi=0$ and $\varphi=\pi$.

3. References

[1] Gurtin, M.E., Murdoch, A.I., "A continuum theory of elastic material surfaces", *Arch. Rat. Mech. Anal.* Vol. 57, 1975, pp. 291–323.

[2] Parvanova, S., Manolis, G.D., Dineva, P., "Wave scattering by nanoheterogeneities embedded in an elastic matrix via BEM", *Eng. Anal. Bound. Elem.* Vol. 56, 2015, pp. 57–69.

[3] ANSYS, *Release 10.0, Structural Mechanics Package.* Canonsburg, Pennsylvania, 2009.

9th German-Greek-Polish Symposium
Recent Advances in Mechanics
September 04-09, 2016
Kolympari, Chania, GREECE

ON FRACTIONAL MECHANICS CONCEPTS

Dr. Habil. Eng. W. Sumelka, Prof. T. Łodygowski,
Poznan University of Technology, Institute of Structural Engineering, Poland

Abstract: *During the talk recent concepts of fractional mechanics will be summarized. Special attention will be focused on the original formulation by the Authors - especially the problem of the virtual boundary which appears as a result of non-local action in the model. Some remarks on numerical implementation, as well as illustrative examples will be provided.*

1. Introduction

Fractional Continuum Mechanics (FCM) it is a generalisation of the Classical Continuum Mechanics (CCM) utilising Fractional Calculus (FC) (the branch of mathematical analysis which deals with differential equations of arbitrary order [6]). The first concepts in this subject are these proposed by Klimek [4], Lazopoulos [5], equivalent concepts of Atanackovic et al. [1] and Carpinteri et al. [2], or finally the one by Drapaca et al. [3]. It is important, that except the concept presented in [3], previous one were defined for 1D problems and small strains. Of fundamental meaning is also the fact that these authors consider different physical units of fractional deformation e.g. in [4, 1, 2] we have $[m^{1-\alpha}]$, in [5] $[m^{-\alpha}]$, or in [3] $[m^{3-\alpha_{1k}-\alpha_{2k}-\alpha_{3k}}]$ k = 1; 2; 3 for strain tensor components, where *m* denotes meter, and the parameter α is in general different then 1.

In the paper [8] different concept of FCM was presented. In this version of FCM the fractional strain is without physical unit, as in the CCM, and the non-local action bases on the length scale parameter which is given explicitly and is simultaneously related to the terminals of fractional differential operator. Furthermore, this formulation is stated for 3D problems and finite deformations [7,9]. Recently, it was shown [10], that this concept, is able to mimic the behaviour of micro-beams made of the polymer SU-8.

During the talk some details about the problem of the virtual boundary, which appears as a result of non-local action in the model, will be discussed. Crucial remarks on numerical implementation will be stated, as well as illustrative examples will be provided (cf. Fig. 1).

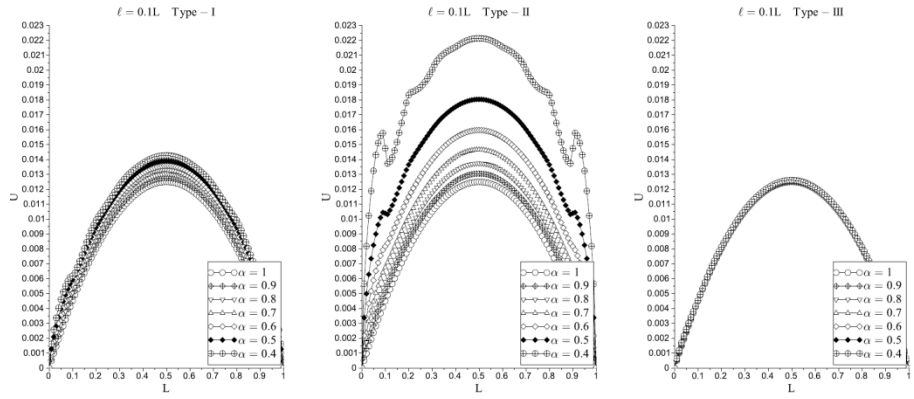

FIGURE 1: Displacement (*U*) in a 1D fractional body (*L*) (for length scale *l=10%L* and different orders α) for three different concepts of treating virtual points outside the body (Types I, II and III) - fixed ends (*U(x=0)= U(x=L)=0*), under body load (*b=0.1*).

2. References

[1] T.M. Atanackovic and B. Stankovic. Generalized wave equation in nonlocal elasticity. Acta Mechanica, 208(1-2):1–10, 2009.

[2] A. Carpinteri, P. Cornetti, and A. Sapora. A fractional calculus approach to nonlocal elasticity. European Physical Journal Special Topics, 193:193–204, 2011.

[3] C.S. Drapaca and S. Sivaloganathan. A fractional model of continuum mechanics. Journal of Elasticity, 107:107–123, 2012.

[4] M. Klimek. Fractional sequential mechanics—models with symmetric fractional derivative. Czechoslovak Journal of Physics, 51(12):1348–1354, 2001.

[5] K.A. Lazopoulos. Non-local continuum mechanics and fractional calculus. Mechanics Research Communications, 33:753–757, 2006.

[6] I. Podlubny. Geometric and physical interpretation of fractional integration and fractional differentiation. Fractional Calculus and Applied Analysis, 5(4):367–386, 2002.

[7] W. Sumelka. Application of fractional continuum mechanics to rate independent plasticity. Acta Mechanica, 255(11):3247–3264, 2014.

[8] W. Sumelka. Thermoelasticity in the framework of the fractional continuum mechanics. Journal of Thermal Stresses, 37(6):678–706, 2014.

[9] W. Sumelka, R. Zaera, and J. Fernández-Sáez. A theoretical analysis of the free axial vibration of non-local rods with fractional continuum mechanics. Meccanica, 50(9):2309–2323, 2015.

[10] W. Sumelka, T. Blaszczyk, C. Liebold, Fractional Euler-Bernoulli beams: theory, numerical study and experimental validation, European Journal of Mechanics - A/Solids, 54, pp. 243-251, 2015

9th German-Greek-Polish Symposium
Recent Advances in Mechanics
September 04-09, 2016
Kolympari, Chania, GREECE

ON A CONSISTENT APPLICATION OF NEWTON'S LAW TO MECHANICAL SYSTEMS WITH MOTION CONSTRAINTS

S. Natsiavas, E. Paraskevopoulos
Department of Mechanical Engineering, Aristotle University, 54 124 Thessaloniki, Greece

Abstract: *This study is focused on a class of discrete mechanical systems subject to equality motion constraints involving time and acatastatic terms. In addition, their original configuration manifold possesses time dependent geometric properties. The emphasis is placed on a proper application of Newton's law of motion. The final set of equations of motion appears as a system of second order ordinary differential equations.*

1. Introduction

Research on the dynamics of mechanical systems subject to motion constraints is a traditional and quite favorable topic among researchers with different backgrounds [1-3]. This is in part due to the fact that this area, as seen under the prism of analytical mechanics, is still challenging and several theoretical aspects related to it remain unexplored and are amenable to improvement, despite the long tradition on the subject. Another driving factor is that a better understanding of the fundamentals in this area provides a stronger foundation and offers substantial help in the efforts to solve difficult engineering problems by deriving and employing new, more advanced, accurate and robust numerical techniques [2].

Among the many beautiful theoretical subjects of Analytical Dynamics, a central place is occupied by those referring to the derivation and solution of the equations of motion of systems subject to time dependent equality constraints. Over the last decades, it has become apparent that many of the theoretical questions in this area, related to engineering problems, can be answered in an illustrative and complete way by employing fundamental concepts of differential geometry [4, 5]. Based on this observation, the main objective of this work is to use such concepts in order to provide a better theoretical foundation for treating a class of constrained mechanical systems. Specifically, the present study represents an extension of recent work of the authors on discrete scleronomic systems [6]. Again, the emphasis is put on interpreting and explaining several demanding theoretical aspects, which are of keen interest to the engineering community. In addition, the main philosophical approach adopted in this work is that the safest and deepest principle of Mechanics is Newton's law of motion.

2. Application of Newton's law – Equations of motion

In this work, it is assumed that the original configuration manifold possesses time dependent geometric properties. Moreover, the system is subject to a set of k time dependent acatastatic motion constraints with form

$$\dot{\psi}^R(q,\underline{v},t) \equiv a_i^R(q,t)v^i + a_0^R(q,t) = 0 \quad (R=1,\ldots,k). \tag{1}$$

When a constraint is holonomic, Eq. (1) can be integrated and cast in the form

$$\phi^R(q,t) = 0.$$

The derivation of the equations of motion is based on a consistent application of Newton's law of motion, similar to that performed in an earlier study [6]. One of the basic ideas in that study was to consider the configuration manifold M as the total space of a fiber bundle with base space M_A and fibers consisting of the Cartesian product manifold $M_C = M_1 \times \cdots \times M_k$, where the single dimensional manifolds M_R, $R=1,\ldots,k$, are related to the action of the R-th motion constraint. After incorporating the appropriate modifications and omitting the details, the equations of motion can be put in the form

$$(g_{ij}\overline{v}^j + \overline{g}_{i0})^{\cdot} - (\overline{\Lambda}^{\ell}_{ji}\overline{g}_{\ell k} + \overline{\Lambda}^{0}_{ji}\overline{g}_{0k})\overline{v}^j\overline{v}^k + (\overline{\Lambda}^{\ell}_{ji}\overline{g}_{\ell 0} + \overline{\Lambda}^{0}_{ji}\overline{g}_{00} + \overline{\Lambda}^{\ell}_{0i}\overline{g}_{\ell j} + \overline{\Lambda}^{0}_{0i}\overline{g}_{0j})\overline{v}^j$$
$$+ \overline{\Lambda}^{\ell}_{0i}\overline{g}_{\ell 0} + \overline{\Lambda}^{0}_{0i}\overline{g}_{00} - f_i = \sum\nolimits_{R=1}^{k} a_i^R[(\overline{m}_{RR}\dot{\overline{\lambda}}^R + \overline{m}_{R0})^{\cdot} + \overline{c}_{RR}\dot{\overline{\lambda}}^R + \overline{k}_{RR}\overline{\lambda}^R - \overline{f}_R], \tag{2}$$

where

$$(g_{ij}\overline{v}^j)^{\cdot} = (g_{ij}\overline{v}^j)_{,\ell}\overline{v}^{\ell} + (g_{ij}\overline{v}^j)_{,0} \quad \text{and} \quad (\overline{m}_{RR}\dot{\overline{\lambda}}^R)^{\cdot} = (\overline{m}_{RR}\dot{\overline{\lambda}}^R)_{,R}\dot{\overline{\lambda}}^R + (\overline{m}_{RR}\dot{\overline{\lambda}}^R)_{,0}.$$

Moreover, quantities g_{ij} and Λ^i_{jk} represent components of the metric tensor and affinities, while c^i_R and c^i_{R0} correspond to components of special vectors, for each constraint R, satisfying the conditions

$$a_i^R c_R^i = 1 \quad \text{and} \quad a_i^R c_{R0}^i = -a_0^R \quad (R=1,\ldots,k;\ i=1,\ldots,n) \tag{3}$$

The convention on repeated indices does not apply to index R, while

$$\overline{m}_{RR} \equiv g_{RR} = c_R^i g_{ij} c_R^j, \quad \overline{m}_{R0} \equiv \overline{g}_{R0} = c_R^i(g_{ij}c_{R0}^j + \overline{g}_{i0}), \quad \overline{c}_{RR} = -c_R^i\frac{\partial f_i}{\partial v^j}c_R^j - c^i_{R,0}g_{ij}c_R^j, \quad \overline{k}_{RR} = -c_R^i f_{i,j}c_R^j$$

$$\text{and} \qquad \bar{f}_R = c_R^i f_i + c_{R,0}^i (g_{ij} c_{R0}^j + \bar{g}_{i0}) . \tag{4}$$

A complete mathematical formulation is obtained by incorporating the k constraint equations. In particular, a second order ordinary differential equation (ODE) is obtained for each holonomic constraint, with form

$$(\bar{m}_{RR}\dot{\phi}^R)^{\cdot} + \bar{c}_{RR}\dot{\phi}^R + \bar{k}_{RR}\phi^R = 0 , \tag{5}$$

using geometrical arguments. Likewise, each nonholonomic constraint gives rise to a scalar ODE with form

$$(\bar{m}_{RR}\dot{\psi}^R)^{\cdot} + \bar{c}_{RR}\dot{\psi}^R = 0 . \tag{6}$$

Next, by introducing the matrix notation

$$\underline{\bar{q}} = (\bar{q}^1 \quad \cdots \quad \bar{q}^n)^T , \quad \underline{\bar{\lambda}} = (\bar{\lambda}^1 \quad \cdots \quad \bar{\lambda}^k)^T , \quad \underline{\bar{v}} = (\bar{v}^1 \quad \cdots \quad \bar{v}^n)^T \quad \text{and} \quad M = [g_{ij}] ,$$

Eq. (2) can be put in the following general form

$$(M(\underline{\bar{q}},t)\underline{\bar{v}})^{\cdot} + \underline{\bar{h}}(\underline{\bar{q}},\underline{\bar{v}},t) = A^T(\underline{\bar{q}},t)[(\bar{M}\underline{\dot{\bar{\lambda}}})^{\cdot} + \underline{\bar{h}}(\underline{\bar{\lambda}},\underline{\dot{\bar{\lambda}}},t)] . \tag{7}$$

The array $\underline{\bar{h}}(\underline{\bar{q}},\underline{\bar{v}},t)$ includes all the terms in Eq. (2) multiplied by the affinities or originating from the components $\bar{g}_{i0}$ of the metric on the event manifold $\bar{M}$, together with the applied forces f_i. Likewise, the elements of the diagonal matrix $\bar{M} = diag(\bar{m}_{11} \quad \cdots \quad \bar{m}_{kk})$ and the array

$$\underline{\bar{h}} \equiv \bar{C}\underline{\dot{\bar{\lambda}}} + \bar{K}\underline{\bar{\lambda}} + \underline{\dot{\bar{m}}}_0 - \underline{\bar{f}} ,$$

including the diagonal matrices $\bar{C} = diag(\bar{c}_{11} \quad \cdots \quad \bar{c}_{kk})$ and $\bar{K} = diag(\bar{k}_{11} \quad \cdots \quad \bar{k}_{kk})$ and the arrays $\underline{\dot{\bar{m}}}_0 = (\dot{\bar{m}}_{10} \quad \cdots \quad \dot{\bar{m}}_{k0})^T$ and $\underline{\bar{f}} = (\bar{f}_1 \quad \cdots \quad \bar{f}_k)^T$, are determined through application of Eq. (4). Finally, when a standard basis is employed on both manifolds $\bar{M}$ and $\bar{M}_R$, Eq. (7) is simplified to

$$(M(\underline{q},t)\underline{\dot{q}})^{\cdot} + \underline{h}(\underline{q},\underline{\dot{q}},t) = A^T(\underline{q},t)[(\bar{M}\underline{\dot{\lambda}})^{\cdot} + \underline{\bar{h}}(\underline{\lambda},\underline{\dot{\lambda}},t)] . \tag{8}$$

In summary, Eq. (2) furnishes a set of n second order ODEs. These equations together with Eqs. (5) and (6) form a set of $n+k$ second order ODEs in the $n+k$ unknown coordinates q^i and λ^R, describing the behavior of mechanical systems with an arbitrary (but finite) number of coordinates, possessing a time dependent original configuration manifold and being subject to time dependent and acatastatic motion constraints. In general, solution of these equations can only be achieved by numerical means, after applying appropriate methodologies leading to a suitable numerical discretization. For the scleronomic case, these equations are simplified considerably and become identical to those presented in [6].

The ODE form of the set of equations derived is associated with several advantages over formulations leading to sets of algebraic-differential equations (DAEs) [2]. It also presents advantages over previous formulations leading to an ODE form after elimination of the redundant coordinates or the Lagrange multipliers from the equations of motion, since this is done at the expense of violating the motion constraints at the lower kinematical levels [2]. Finally, another advantage of the present approach is that the affinities are independent and not derived from the metric components (i.e., the connection is not necessarily metric compatible). This allows for the most general and consistent derivation of the equations of motion. As a consequence, both the metric components and the affinities appear in Eq. (2). For instance, this is similar to the case where a body frame is used in expressing Euler equations for rigid body rotation [4]. For a metric compatible connection, the affinities can be derived in terms of the metric components and are thus be eliminated from the final set of equations of motion.

References

[1] Arnold, V.I., *Mathematical Methods of Classical Mechanics, second ed*. Springer-Verlag, Berlin, 1989.

[2] Bauchau, O.A., *Flexible Multibody Dynamics*, Springer Science+Business Media B.V., London, 2011.

[3] Bejancu, A. and Farran, H.R., *Foliations and Geometric Structures*, Springer, Netherlands, 2006.

[4] Bloch, A.M., *Nonholonomic Mechanics and Control*, Springer-Verlag, New York, 2003.

[5] Frankel, T., *The Geometry of Physics: An Introduction*, Cambridge University Press, New York, 1997.

[6] Natsiavas, S. and Paraskevopoulos, E., "A set of ordinary differential equations of motion for constrained mechanical systems", *Nonlinear Dyn.,* Vol. 79, 2015, pp. 1911-1938.

ON KINEMATIC AND SELF-EXCITED RAIL VEHICLE-TRACK INTERACTION

Prof. R. Bogacz[1], **Prof. W. Kurnik**[2]
[1,2]Warsaw University of Technology and [1]IPPT PAN, Poland

Abstract: *The paper contains description of certain dynamical problems connected with the self-excitation and kinematic excitation of rail vehicle and railway track. Some phenomena are given which may create high loads, track degradation and fatigue of wheelset axles. An alternative approach to rail vehicle hunting are proposed. some examples of experimental investigations are given which show that the dynamical load acting on the track can be much higher as the static load.*

1. Introduction

The dynamic interaction of rail vehicles with the track is very complex, some effects are still not well understood even by specialists in this field. A wide palette of models is required to cover majority of aspects of the topic. Majority of experimental observations on real vehicle-track systems can be explained using theoretical foundations and numerical investigations. It may help to improve the security and comfort of travel and reduce maintenance costs of track. A study of some selected problems concerning the influence of system parameters on the stability of track-train system in relative motion will be presented.

2. Hunting as classic train-track instability of subsystems in relative motion

Let us consider a classic train-track system or a MAGLEV train composed of two continuous systems interacting by elastic or visco-elastic layers of stiffness c_0**.** It is assumed that the train of stiffness E_0I_0 and mass density μ_0 is moving with constant speed U_0 along track of stiffness E_1I_1 and mass density μ_1 laterally interacting with elastic Winkler foundation of stiffness c_1 (Fig. 1).

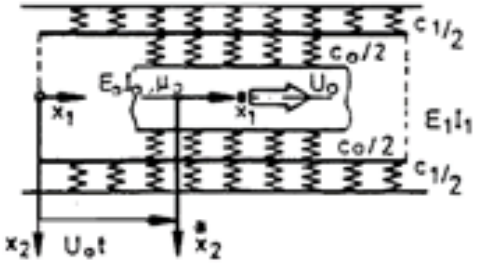

FIGURE 1. Model of train-track interaction

Coupled linear equations of transverse vibrations of system shown in Fig. 1 are as follows:

$$E_1I_1w_{,xxxx}+\mu_1w_{,tt}+c_1w+c_0(w-y)=0 \qquad (1)$$

$$E_0I_0y_{,xxxx}+\mu_0(y_{,tt}-2U_0y_{,xt}+U_0^2y_{,xx})+c_0(y-w)=0 \qquad (2)$$

where: $x=x_1$, w denotes displacement of track and y is lateral displacement of train as a beam in direction of x_2. Assuming solutions of equations of motion in the following forms of traveling waves:

$$w(x,t)=A\exp[ik(x-vt)], \qquad y(x,t)=B\exp[ik(x-vt) \qquad (3)$$

we obtain the characteristic equation:

$$\Phi(v,v_0)=[\mu(S^2-v^2)-\alpha^2](\alpha^2-v_0^2)-\alpha^2=0 \qquad (4)$$

where: $v_0=v-U_0$, $S^2=(E_1I_1k^2+c_1/k^2)/\mu_1$, $\mu=\mu_1/\mu_0, \alpha^2=c_0/k^2$ *and* k denotes wave number. In the case of four real roots v for a real value of U_0 the motion is stable, in case of two complex roots the motion is unstable $(v_i=v^*\pm i\varepsilon,\ \ i=1,2)$. Equation (4) allows one to determine the critical speed which is the boundary at which periodic transverse motion appears around unstable equilibrium (like hunting with a limit cycle in the nonlinear case).

3. Wheel-rail self-excited vibration

The next case under consideration is concerned with friction-induced vibration which is found to be a reason of many serious damages of trains and tracks, such as corrugation, sleep waves, damages of axles as result of wheelset torsional self-excitation etc. (Fig. 2). The breaking of wheelset axle (2008 accident at line Köln-Düsseldorf) was a results of fatigue due to friction-induced vibration of wheelset-track system with frequency of ca 100Hz [3]. The central part of the Fig. 2 shows a relatively simple (reversible) dependences of

the friction force f_c vs. creepage S. An another effect of friction induced vibration are slip waves occurring on low rail of curved track. As was pointed out experimentally by DB AG/ÖBB/SBB in Brixental and during simulation using the model shown on the right-hand side of Fig. 2, [4,5], that is why the intensity of vibration and amplitudes of wavy shape of rails corrugation decrease in the case of the vibrational external excitation. That is why the corrugation on steel bridges are relatively small.

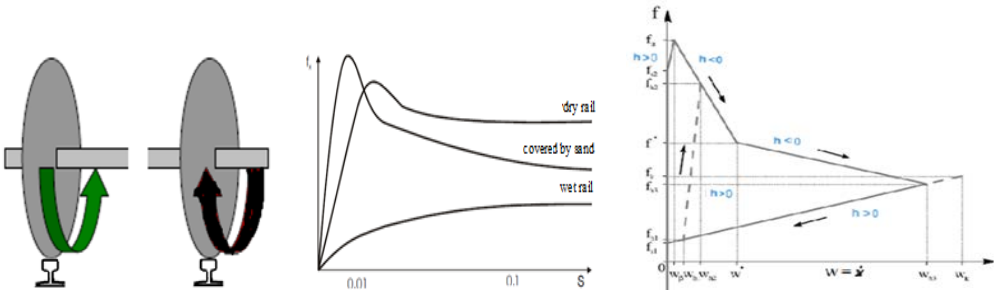

FIGURE 2: Scheme of wheelset-track self-excited vibration and two models of friction force vs. slip rate

The model of friction used in simulation [4] was assumed as dependent on relative speed (creepage), force rate, time of sticking and sign of acceleration (visible on the right hand side of Fig. 2). As a supplement to the above study also a few kinds of kinematic excitation of rail vehicles will be presented. The source of such an excitation we can mention: periodically spaced corrugation, sleepers, supports (trestle bridge) and the out-of-round railway wheels creating also structure of periodic kinematic excitation. The kinematically excited vibration will be solved using Floquet's theory and a travelling wave form of solution. Contrary to a wavy form of interaction between two continuous systems (Fig. 1), in the case of train modeled as lumped system the problem of travelling and oscillating concentrated load (force) acting on a beam must be solved. Such a problem was formulated by Mathews in 1958 [6] who proposed the solution in the form of standing waves with not properly formulated boundary condition as the condition of radiation. The correct formulation of boundary solution by means of the group velocity of generated waves was given in 1986 by Bogacz and Krzyżyński and formulated also in [2]. Such a solution allow us to solve various problems of discrete dynamical interaction of the train as a lumped system with a track as continuous systems. As the practical example we can call the train - track dynamical interaction and its stability.

4. References

[1] Bogacz, R., Popp, K., "Dynamics and stability of train-track-systems", *Proc. 2nd Intern. Conf. on Recent Advances in Structural Dynamics*, Southampton 1984, pp. 711-726.

[2] Bogacz, R., Kurnik, W. "On Some Rotor-Dynamical Phenomena of High-Speed Trains", *Archive of Applied Mechanics*, (2015) 85: pp.1343-1342.

[3] Konop, J. "Dynamics of Rail Vehicle -Track System. Simulation and Experimental Study", *Ph.D. Thesis*, Warsaw University of Technology, 2015.

[4] Bogacz, R., Ryczek, B., "Frictional phenomena in dynamical systems with external excitation", *Meccanica*, Kluwer Ac. Press, 2003, pp. 711-717.

[5] Bogacz R., Meinke P., "On evaluation of wheelsets and railway track quality", *Scientific Papers of Institute of Vehicles*, Warsaw University of Technology, 1(60)/2006, pp. 15-20.

[6] Mathews, P.M., "Vibration of beam on elastic foundation", *ZAMM*, 38, 1958, pp. 105-115.

9th German-Greek-Polish Symposium
Recent Advances in Mechanics
September 04-09, 2016
Kolympari, Chania, GREECE

SIMULATION OF CONFINED BENDING OF CONTINUOUSLY DISLOCATED CRYSTALS

Christian B. Silbermann[1], **Jörn Ihlemann**[1]
[1]Department of Solid Mechanics,
Technische Universität Chemnitz,
Reichenhainer Straße 70,
09126 Chemnitz, Germany

Abstract: *In this study, geometrically linear Continuum Dislocation Theory (CDT) is applied in order to investigate the collective behavior of dislocations during a confined bending test. The governing field equations of the CDT for dislocation glide in one active slip system are used. Numerical solutions of the corresponding initial boundary value problem are presented for the case of plane deformations using a finite difference simulation code. The resulting plastic slip field indicates dislocation movement from the border to the middle of the specimen.*

1. Introduction Governing field equations

The plastic behavior of metallic crystals strongly depends on the underlying defect structure. Dislocations – line defects that carry plastic deformation - are of special relevance. The Continuum Dislocation Theory (CDT) takes them into account by considering the incompatibility of elastic (or plastic) deformation and is thus an appropriate means to model the behavior of continuously dislocated crystals.

2. Governing field equations

The kinematics of continuously distributed dislocations in the *geometrically linear* theory is based on the split of the displacement gradient into elastic and plastic parts: $\operatorname{grad}(\underline{u}) =: \underline{\underline{\beta}} = \underline{\underline{\beta}}_e + \underline{\underline{\beta}}_p$. The additional primary field $\underline{\underline{\beta}}_p$ (second rank tensor) is considered a result of the collective motion of continuously distributed dislocations. The free energy density of the dislocated crystal depends on the thermodynamical state variables $\underline{\underline{\alpha}} = -\operatorname{curl}(\underline{\underline{\beta}}_e)$ (Kröner-Nye-Bilby-tensor) and $\underline{\underline{\varepsilon}}_e = \operatorname{sym}(\underline{\underline{\beta}}_e)$ (elastic strain tensor). An additive decomposition $\phi = \phi_e(\underline{\underline{\varepsilon}}_e) + \phi_p(\underline{\underline{\alpha}})$ is assumed. The elastic strain energy is given by Hooke's law: $\phi_e(\underline{\underline{\varepsilon}}_e) = \mu \|\underline{\underline{\varepsilon}}_e\|^2 + \frac{1}{2}\lambda \operatorname{tr}(\underline{\underline{\varepsilon}}_e)^2$ with the Lamé constants. The dislocation energy in case of one active slip system is given by $\phi_p(\underline{\underline{\alpha}}) = k\mu \ln[(1 - \|\underline{\underline{\alpha}}\|/b\rho_s)^{-1}]$ (cf. Berdichevsky [1]) where k is a dimensionless constant, b is the magnitude of the Burgers vector and ρ_s denotes a saturation value of the dislocation density.

The field equations of the CDT can be obtained exploiting the laws of thermodynamics in the form of the Clausius-Duhem inequality. Using a dissipation potential, dissipative phenomena of dislocation motion are incorporated as well, e.g. dislocation motion requires exceeding a critical resolved shear stress τ_{cr}. For single slip the plastic distortion is $\underline{\underline{\beta}}_p = \beta_p \, \underline{s} \otimes \underline{m}$ and the resulting field equations read as:

$$(\lambda + \mu)\underline{\nabla} \otimes \underline{\nabla} \cdot \underline{u} + \mu \underline{\nabla} \cdot \underline{\nabla} \otimes \underline{u} - \mu(\underline{s} \otimes \underline{m} + \underline{m} \otimes \underline{s}) \cdot \underline{\nabla}\beta_p = \underline{0} \,,$$

$$\mu(\underline{s} \otimes \underline{m} + \underline{m} \otimes \underline{s}) \cdot\cdot \underline{\nabla} \otimes \underline{u} - \mu\beta_p + \frac{k\mu}{(b\rho_s)^2} \, \underline{s} \cdot \underline{\nabla} \otimes \underline{\nabla}\beta_p \cdot \underline{s} \left(1 - \frac{|\underline{\nabla}\beta_p \cdot \underline{s}|}{b\rho_s}\right)^{-2} = \tau_{cr} \operatorname{sign}(\dot{\beta}_p) \,,$$

where $\underline{\nabla}$ denotes the Nabla operator. Defining proper initial and boundary conditions, this set of partial differential equations can be solved. Numerical solutions of the corresponding initial boundary value problems are obtained for the case of plane deformations using an in-house finite difference simulation code.

3. Simulation results and interpretation

As an example of the effects of inhomogeneous deformation, a confined bending test is considered, i.e. Dirichlet boundary conditions are applied for the displacement field and free boundary conditions are assumed for the plastic slip field. Further, zero initial conditions are used. The material constants are given in the following table:

μ/MPa	λ/MPa	b/µm	ρ_s/µm^{-2}	k	τ_{cr}/TPa
26900	40400	$2,86 \cdot 10^{-4}$	$4 \cdot 10^2$	$4 \cdot 10^{-4}$	$5 \cdot 10^{-6}$

TABLE 1: Material constants used for the numerical simulation

The single crystal's shape, the slip system and the boundary conditions for the displacement field are shown in Fig. 1 (left). The slip system is oriented at the angle $\varphi = 30°$. Plastic slip initiates when the resolved shear stress exceeds the value τ_{cr}.

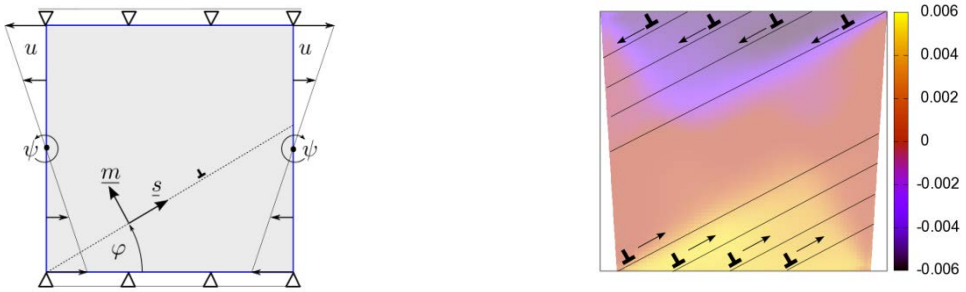

FIGURE 1: Bending test setup (left) and simulation results for the plastic slip field β_p (right). Dislocation movement is illustrated by the edge dislocation symbols (T) on the slip planes.

From the resulting field β_p is inferred that dislocations nucleate at the upper and lower surface and then glide on the parallel slip planes (single slip) towards the middle line of the beam, as illustrated in Fig. 1 (right). This corresponds to well-known simulation results from Discrete Dislocation Dynamics.

In the CDT, zones of high dislocation density result from plastic slip gradients $\underline{\nabla}\beta_p$ in the slip direction $\underline{s}$. Consequently, the simulation result suggests that dislocations moving inwards accumulate inside the beam. Analytical simulations from Le [2] show also a dislocation pile-up against the middle line. Further numerical simulation results will be presented in a forthcoming article.

4. Acknowledgements

This research was supported by the German National Science Foundation (DFG) within the Collaborative Research Centre 692 HALS.

5. References

[1] Berdichevsky, V., “Continuum theory of dislocations revisited”, *Cont. Mech. and Thermodyn.*, Vol. 18, 2006, pp. 195–222.

[2] Le, K.C., and Nguyen, B.D., “On bending of single crystal beam with continuously distributed dislocations”, *Int. J. of. Plasticity.*, Vol. 48, 2013, pp. 152–167.

CYCLIC PLASTICITY AND DAMAGE OF STRUCTURES

Prof. D. Šumarac[1]
[1]Faculty of Civil Engineering, University of Belgrade, Serbia

Abstract: *In the present paper, the Cyclic plasticity and Damage of Structures is investigated using Preisach model of hysteresis. Model is updated introducing the so called damage element in order to analyze the softening of structural components. Some advantages of this approach are underlined, compared with already existing procedures in the literature, such are the Bouc-Wen and GP (Generalized Plasticity) model.*

1. Introduction

Civil and mechanical engineering structures are usually exposed to alternate loadings such are earthquake, heavy traffic etc. During this loading the stresses in structural components usually exceed elastic limit and the response becomes nonlinear causing plastic strains and damages. This paper intends to make comprehensive model to cover these phenomena including both plasticity and damage.

2. The Preisach model for cyclic plasticity and damage

Damage can be included in three element unit, Šumarac and Perović [3], using brittle element with rupture limit Y_D, as shown in Fig.1b. Corresponding elastoplasic behavior is shown in Fig.1a. When tension stress in material reaches limit Y_D, complete failure of element is achieved.

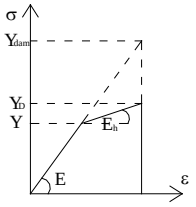

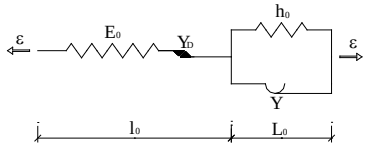

FIGURE 1a. Stress-strain curve for elem. in Fig.1b **FIGURE 1b. 3 element unit with brittle element**

For a system consisting of infinitely many three-element units (Fig.2.b), connected in parallel, with uniform yield strength distribution $Y_{min} \leq Y \leq Y_{max}$, and with uniform damage threshold distribution $Y_{D1} \leq Y_D \leq Y_{DN}$, stress-strain curve is ploted in Fig. 2a.

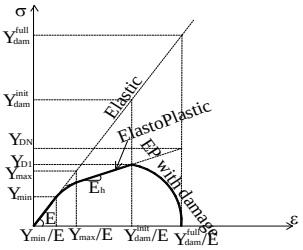

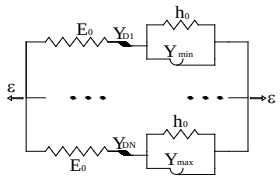

FIGURE 2a. Stress-strain curve for material in Fig.2b **FIGURE 2b. Model for real material**

3. Numerical examples

In order to emphasize the advantages of the present model, in the first example, one bar (area 0.02m^2) is subjected to cyclic loading in plastic domain, where input function, for loading, is displacement shown in Fig.3.a.

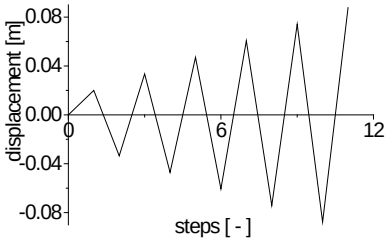

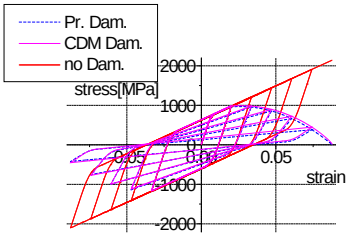

FIGURE 3a. Time history of displacement **FIGURE 3b. Resulting hysteretic loops**

When displacement history function is used for loading to the maximum damage limit, complete degradation of both elastic and hardening modulus is occurred (Fig.3b).

In the second numerical example, truss structure shown in Fig.4. is subjected to cyclic loading, where time history functions are displacement as shown in Fig.5a. Each bar of truss structure has cross sectional area equal to 0.02m^2.

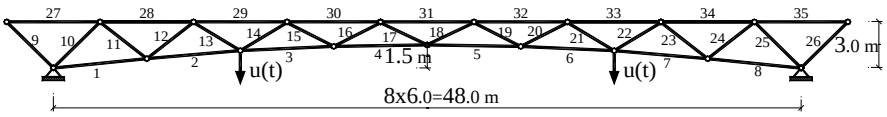

FIGURE 4 Truss structure

The typical results, stress-strain loops, are shown in Fig.5b for several bars.

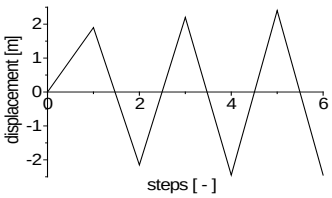

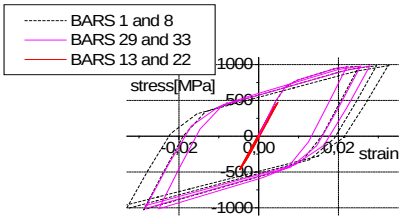

FIGURE 5a. Time history of displacement **FIGURE 5b. Resulting hysteretic loops**

4. References

[1] F. Preisach, Über die magnetische Nachwirkung, *Z . Phys*, 94,1935, pp. 277- 302.

[2] D. Šumarac and Z. Perović, Cyclic plasticity of trusses, *Archive of Applied Mechanics*: Vol. 85, 9, 2015, pp. 1513-152.

CULTURAL HERITAGE RC STRUCTURES UPGRADED BY TIES UNDER MULTIPLE EARTHQUAKES

PhD Student Angelos LIOLIOS [1], Assoc. Prof. George HATZIGEORGIOU [2], Prof. Antonia MOROPOULOU [3], and Prof. Asterios LIOLIOS [1]

[1]Democritus-University of Thrace, Department of Civil Engineering, Xanthi, Greece
[2] Hellenic Open University, Patras, Greece
[3]National Technical University of Athens, School of Chemical Engineering, 9 Iroon Polytechniou Street, Zografou Campus, Athens, Greece

Abstract: *Old industrial reinforced concrete (RC) structures, which are elements of the recent Cultural Heritage, are considered. A numerical approach is presented for the earthquake analysis of such existing RC structures concerning the case of their seismic upgrading by ties elements under seismic sequences. A double discretization is applied by using the Finite Element Method and damage indices are computed in order to select the optimum ties version*

1. Extended abstract

As well-known, the recent Cultural Heritage includes, besides the usual historic monumental structures (churches, stone bridges, old masonry buildings etc.) [1], also existing industrial buildings of reinforced concrete (RC), e.g. old factory premises. Non-usual extremal actions (seismic, environmental etc.) can cause significant strength degradation and damages on such existing RC structures, which are elements of the Cultural Heritage. To overcome these strength degradation effects, various repairing and strengthening procedures can be used for the seismic upgrading of existing RC buildings [2-3]. Among them, cable-like members (ties) can be used as a first strengthening and repairing procedure [4].

These cable-members can undertake tension, but buckle and become slack and structurally ineffective when subjected to a sufficient compressive force. So, in the mathematical problem formulation, the constitutive relations for cable-members include also inequality conditions. Such inequality conditions govern also the piece-wise linearized constitutive relations describing the non-linear behavior of the usual RC structural elements. Thus the problem becomes a high nonlinear one. For the strict mathematical treatment of the problem, the concept of variational and/or hemivariational inequalities can be used and has been successfully applied [5]. As concerns the numerical treatment, non-convex optimization algorithms are generally required [6].

On the other hand, current seismic codes (e.g. EC8) suggest the exclusive adoption of the isolated and rare “design earthquake”, while the influence of repeated earthquake phenomena is ignored. This is a significant drawback for the realistic design of building structures. Despite the fact that the problem has been qualitatively acknowledged, few studies have been reported in the literature, especially the last years, regarding the multiple earthquake phenomena.

The present study deals with a numerical approach for the earthquake analysis of Cultural Heritage existing RC building frames, which after their seismic assessment have to be strengthened by cable elements and are subjected to seismic sequences excitations. For details see [7]. The proposed method uses the finite element method, an incremental formulation and the Ruaumoko software. The decision about a possible strengthening for an existing structural system, damaged by a seismic or environmental event, can be taken after an assessment realization [2-3]. This is here obtained by using a relevant evaluation of suitable damage indices, which are also used for the selection of the optimal ties system [7]. The applicability of the proposed method is verified in numerical examples, e.g. as shown in Fig. 1. The numerical results prove that the optimal system is that one of Fig. 1.D.

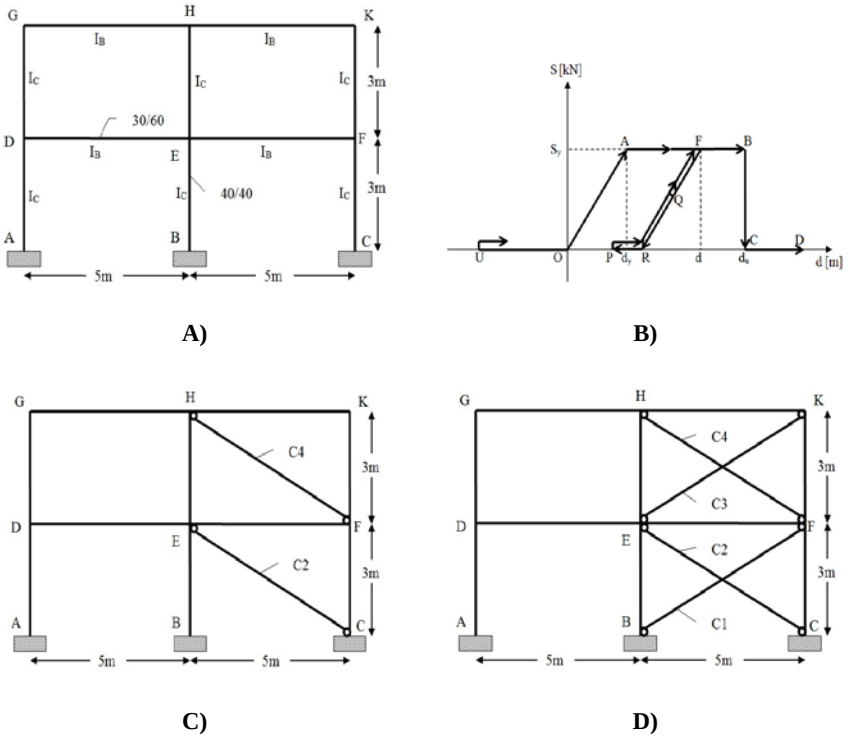

A) **B)**

C) **D)**

FIGURE 1: Numerical example: a) The two-bays two-storey RC frame, b) The constitutive law of the cable-elements, c) The F2 ties-system, d) The F4 ties-system.

2. References

[1] B. Leftheris, A. Sapounaki, Maria E. Stavroulaki, George E. Stavroulakis, (2006), *Computational Mechanics for Heritage Structures*, WIT Press, Southampton, Boston.

[2] Penelis Ge. and Penelis Gr. (2014), *Concrete Buildings in Seismic Regions*. CRC Press.

[3] Fardis, M. N. (2009). *Seismic design, assessment and retrofitting of concrete buildings: based on EN-Eurocode 8* ,Springer.

[4] Markogiannaki O., & Tegos I. (2011). *Strengthening of a Multistory R/C Building under Lateral Loading by Utilizing Ties.* Applied Mechanics and Materials, 82, 559-564.

[5] Panagiotopoulos, P.D. (1993). *"Hemivariational Inequalities. Applications in Mechanics and Engineering"*. Springer-Verlag, Berlin, New York, (1993).

[6] Mistakidis, E.S. & Stavroulakis, G.E., (1998). *Nonconvex optimization in mechanics. Smooth and nonsmooth algorithmes, heuristic and engineering applications*. Kluwer, London.

[7] Liolios Ast., Liolios Ang. & Hatzigeorgiou G. (2013). *"A Numerical Approach for Estimating the Effects of Multiple Earthquakes to Seismic Response of Structures Strengthened by Cable-Elements"*. Journal of Theoretical and Applied Mechanics, 43(3), 21-32.

9th German-Greek-Polish Symposium
Recent Advances in Mechanics
September 04-09, 2016
Kolympari, Chania, GREECE

DERIVATION OF NEWTON'S LAW OF MOTION FROM KEPLER'S LAWS OF PLANETARY MOTION

Prof. John T. Katsikadelis
School of Civil Engineering, National Technical University of Athens, Greece

Abstract: *Newton's law of motion is derived from Kepler's laws of planetary motion. This is achieved by applying a simple system identification method using numerical data from the planet's orbits and the concepts of the derivative, differential equation and Leibnitz product rule for differentiation. Moreover, the employed procedure permits the evaluation of the standard gravitational parameter, which paves the way for establishing Newton's law of universal gravitation. As the employed mathematical tools and the theory were available before 1686, we are allowed to state that the equation of motion could have been established from Kepler's law of planetary motion, before Newton had published his law of motion.*

1. Introduction

Newton's law of motion (second law) was presented in his book "Philosophiae Naturalis Principia Mathematica" published on July 5 1686 [1]. This law in the original Latin text reads [1, p. 12]:

Lex II: Mutationem motus propotionalem esse vi motrici impressae, ac fieri secundum lineam rectam qua vis illa imprimitur.

which is translated in English as [2, p. 83]

Law II: The alteration of motion is ever proportional to the motive force impressed; and is made in the direction of the right line in which that force is impressed.

By **motus** (motion) or **quantitas motus** (quantity of motion) Newton defined the product of the mass (**quantitas materiae**) times the velocity (**velocitas**) [1, Def. I and II. p. 2], i.e. what we refer to as *momentum*. Thus in mathematical language Newton's second law of motion is expressed as

$$\frac{d}{dt}(mv) = f \qquad (1)$$

where m is the mass, v the velocity and $f = f(t)$ the impressed external force in the direction of v.

Newton presented this law as an *axiom* (**Axiomata sive Leges Motus, Lex II** [1, p.12]). He did not mention anything about how he arrived at this statement. But he was aware of the work of other scientists before the publication of the *Principia*. In his Scholium [1, p.20] he mentioned.

"**Hactenus principia traditi a Mathematicis recepta & experimentia multiplici confirmata**".

which is translated [2, Scholium p.89].

"Hitherto I have laid down such principles as have been received by mathematicians, and are confirmed by abundance of experiments."

This is also attested by a letter of Newton to Robert Hook on 15 February 1676, where he had written: "*If I have seen further it is by standing on the shoulders of Giants*". Undoubtedly, Galileo Galilei (1564 – 1642) and Johannes Kepler (1571 – 1630) are two of these giants.

In a recent paper by this author [3], it was shown that Newton's law of motion could have been derived using Galileo's experiments with the inclined plane before this law was published by Newton. In the present paper, it is shown that Newton's law of motion can be also derived from Kepler's laws of planetary motion in conjunction with the inverse square law of attraction between planets and the concept of the derivative and the differential equation.

Kepler used the measurements from Tycho Brahe's astronomical observations to deduce the laws of planetary motion about the Sun stating the following [4]

1. *The orbit of a planet is an ellipse with the Sun at one of the two foci.*
2. *The line segment joining the Sun and a planet sweeps out equal areas during equal intervals of time.*
3. *The square of the orbital period of a planet is proportional to the cube of the semi-major axis of its orbit*.

Johannes Kepler published his first two laws about the planetary motion in 1609, while the third law was published in 1619. These three laws together with the inverse square law for the attracting force between the Sun and the planets are used to derive Newton's law of motion by applying the system identification procedure developed in [3]. Besides, this procedure gives the value of the *standard gravitational parameter*, if the employed data refer to the planets of the solar system or to the planets and their moons (Table 1).

Table 1 Standard gravitational parameter

	Body	Satellite or planet	r_{min} (km)	r_{max} (km)	Period (days)	m (ms^{-2}) Present	m (ms^{-2}) [5]
1	Sun	Mercury	46001009	69817445	87.969	1.3271e+20	1.3271e+20
2	Earth	Moon	363104	405696	27.321	4.0241e+14	4.0350e+14
3	Mars	Phobos	9234.42	9517.58	0.31891	4.2862e+13	4.2828e+13
5	Jupiter	Ganymede	1069200	1071800	7.155	1.2669e+17	1.2671e+17
6	Saturn	Titan	1186675	12570547	15.95	3.7921e+16	3.7941e+16
7	Uranus	Umbriel	255626	276374	4.144	5.7961e+15	5.7945e+15
8	Neptune	Triton	354753	354765	5.877	6.8363e+15	6.8365e+15

2. References

[1] Newton, Isaac, *Philosophiae Naturalis Principia Mathematica*, Royal Society Press, London (1686).

[2] Newton, Sir Isaac, *The Mathematical Principles of Natural Philosophy*; Translated into English by Andrew Motte, published by Daniel Adee, New York (1846).

[3] Katsikadelis J.T. "Derivation of Newton's law of motion using Galileo's experimental data", *Acta Mechanica*, Vol. 226, (2015), pp. 3195–3204.

[4] Murray, C.D. and Dermott, S.F., *Solar System Dynamics*, Cambridge University Press, 1999

[5] Solar System Dynamics, Astrodynamic Constants, Jet propulsion Labora-tory, Caltec, http://ssd.jpl.nasa.gov/?constants. (Retrieved 6 June 2015).

SECOND HARMONIC LAMB WAVES IN UNIDIRECTIONAL COMPOSITE

N Rauter[1], **R Lammering**[1]
[1]Helmut-Schmidt-University / University of the Federal Armed Forces Hamburg
Holstenhofweg 85, 22043 Hamburg, Germany

Abstract: *A new nonlinear hyperelastic material model is introduced to model unidirectional composite, where the nonlinear material behavior is represented by just 1 material parameter in contrast to the five constant nonlinear elastic theory, where 9 material parameter are required. It is shown that the presented material model can be used to simulate the cumulative second harmonic mode generation in unidirectional composite.*

1. Introduction

The nonlinear wave propagation is a recently developed technique to monitor and detected even micro-structural damage in isotropic and more important in composite structures [1,2]. This method is based on the second harmonic Lamb wave generation at material and geometrical nonlinearities. Due to the very small amplitude of these higher harmonic modes a cumulative effect is used, which ensures an adequate amplitude extraction [3].

So far the numerical simulations of the second harmonic Lamb wave generation in composite structures is done using the five constant nonlinear elastic theory by Murnaghan, a nonlinear hyperelastic material model [4]. For transversely isotropic material the behavior is described by 5 linear (second order) and 9 nonlinear (third order) elastic constants [5]. However, the determination of the third order elastic constants, which give the relation between the wave speed and a prestress, is very complex. Therefore, in this study a new approach for a nonlinear hyperelastic transversely isotropic material model is presented, which is based on an existing linear model by considering the compressibility of the matrix material. In a second step the presented model is used to simulate the cumulative second harmonic mode generation in composite structures.

2. Hyperelastic material model

Hyperelastic material models are characterized by the existence of a strain potential, which can be written in terms of a strain measure or its invariants. The linear behavior of transversely isotropic material is given by the potential [6]

$$\begin{aligned}\Psi_{\mathbf{C}} = \quad & c_1(I_1-3)^2 + c_2(I_2-3) - 2c_2(I_1-3) + c_3(I_4-1)^2 \\ & + c_4(I_5-1) - 2c_4(I_4-1)^2 + c_5(I_4-1)(I_1-3), \end{aligned} \tag{1}$$

where I_1, I_2, I_4 and I_5 are the invariants of the right Cauchy Green deformation tensor $\mathbf{C}$ and $c_1, ..., c_5$ are the five independent material parameters. This potential does not cover any compressibility effects. However, considering fiber reinforced plastic commonly used matrix material like Epoxy usually shows compressible behavior, which is not affected by the fibers. Therefore, a further part, representing the compressibility, is added to the potential given in (1). The new nonlinear hyperelastic potential reads

$$\Psi_{tr} = \Psi_C + \frac{K}{4}\left(J^2 - 1 - 2\ln J\right). \tag{2}$$

Here, K is the bulk modulus and J the determinant of the deformation gradient $\mathbf{F}$.

Based on strain energy potential the stress and stiffness tensor are obtained by

$$\mathbf{S} = 2\frac{\partial \Psi}{\partial \mathbf{C}} \qquad \mathbb{C} = 4\frac{\partial^2 \Psi}{\partial \mathbf{C}^2}. \tag{3}$$

To determine the material parameters for the hyperelastic material model K is set to 3.89 GPa, the bulk modulus of Epoxy. Afterwards the remaining five material parameter can be calculated by the method of equation the coefficients using the stiffness matrix for linear elastic behavior. The results are provided in Table 1.

Linear	E_1	E_2	G_{12}	G_{23}	ν_{12}	ρ
	121 GPa	8 GPa	4 GPa	3.75	0.33	1.47
Hyperelastisch	c_1	c_2	c_3	c_4	c_5	K
	0.527	-1.875	13.66	1.25	0.568	3.89

TABLE 1: Linear and hyperelastic material parameters for the unidirectional lamina

3. Numerical Simulations

The numerical simulation of the second harmonic Lamb wave generation in a unidirectional lamina is done in FEAP. A two-dimensional model consisting of 9 node elements is used assuming a plane strain state. The model is 1 mm thick and has a length of 1 m. To satisfy the conditions for a cumulative second harmonic mode generation an excitation frequency of 2.3 MHz mm is chosen. The excitation of the primary wave field is realized by a turn burst signal consisting of 40 sine cycles. After a propagation distance of 15 cm the in-plane displacement component is extracted at several points with an interval of 5 mm. At each point the second harmonic amplitude is determined by a Wavelet-Transform using the Morlet-Wavelet as the Mother-Wavelet.

FIGURE 1: Amplitude of the second harmonic S_1-mode over the propagation distance based on the numerical simulation of the wave propagation using FEAP

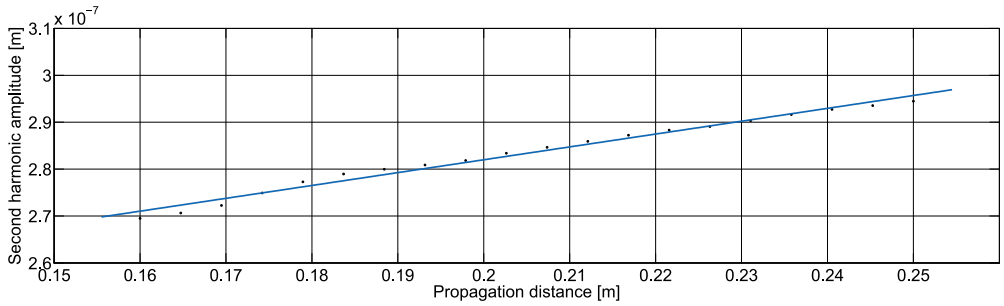

In Figure 1 the result of the second harmonic mode amplitude is plotted over the propagation distance. A linearly increasing behavior with the propagation distance is recognizable, characterizing the cumulative effect of the second harmonic generation. Therefore, the presented material model can be used to simulate the cumulative second harmonic Lamb wave generation in a lamina.

4. Conclusion

It has been shown that the presented material model is an adequate alternative to simulate the cumulative second harmonic generation in unidirectional composite. In contrast to the five constant nonlinear elastic theory, where nine nonlinear parameters are required, the number is reduce to one coefficient covering the nonlinear material behavior.

5. References

[1] Xiang, Y., Zhu, W., Liu, C.-J., Xuan, F.-Z., Wang, Y.-N. and Kuang, W.-C., “Creep degradation characterization of titanium alloy using nonlinear ultrasonic technique”, *NDT&E Int.*, Vol. 72, 2015, pp. 41-49.

[2] Rauter, N. and Lammering, R., “Impact damage detection in composite structures considering non-linear lamb wave propagation”, *Mech. Adv. Mater. Struc.*, Vol. 22, No. 1-2, 2015, pp. 44-51.

[3] de Lima, W. and Hamilton, M.F., “Finite-amplitude waves in isotropic elastic plates”, *J. Sound Vib.*, Vol. 265, No.4, 2003, pp. 819- 839.

[4] Zhao, J., Chillara, V.K, Ren, B., Cho, H., Qiu, J. and Lissenden, C.J., “Second harmonic generation in composites: Theoretical and numerical analyses”, *J App. Phys.*, Vol. 119, No. 6, 2016, pp. 064902.

[5] Prosser, W. H., *Ultrasonic characterization of nonlinear elastic properties of unidirectional graphite/epoxy composite*, USA, NASA Contractor Report 4100, 1987.

[6] Reese, S., Raible, T. and Wriggers, P., “Finite element modelling of orthotropic material behaviour in pneumatic membranes”, *Inter. J. Solid Struct.*, Vol. 38, No. 52, 2001, pp. 9525-9544.

BIGONI AND NOSELLI EXPERIMENT – IS IT EVIDENCE FOR FLUTTER IN THE ZIEGLER COLUMN?

Prof. W. Kurnik[1], **Prof. R. Bogacz**[1,2], **Prof. P. Przybyłowicz**[1]
[1]Warsaw University of Technology, Poland
[2]Institute of Fundamental Technological Research, Poland

Abstract: *The paper is inspired by recent experiment with a two-member discrete column subjected to dry friction force of interaction between the moving column and a moving plane. Experiment was presented in form of a YouTube film and recommended as an experimental evidence for flutter in the Ziegler column. We show that the tested mechanism, although subjected to a circulatory load, can not be identified with the original Ziegler column.*

1. Introduction

The history of studies on stability of columns subjected to compressive forces goes back to Euler who analyzed the static buckling of elastic compressed rods and formulated the theory of buckling even now being used in the courses of strength of materials as a first attempt to address the stability problems of light load-carrying structures [1]. The problem was refreshed and attracted much attention of scientists in structural mechanics in the 60-s of the last century when flutter was theoretically found as a result of so called follower forces that change their direction, following the current configuration of a system they act on (Bolotin [2]). Earlier, Ziegler [3] found flutter instability in a discrete two-degree-of-freedom double-rod system, now well known as the Ziegler column. The dynamical behavior of systems under assumed compressive follower forces showing flutter (like classical Beck and Leipholz columns) is not questionable and there are numerous studies of such systems demonstrating their specific properties, optimization and control. However, still rather little is known about the physics behind pure follower forces and there is skepticism among some scientists about the technical sense of the follower forces. Koiter [4] denied the importance of such forces even knowing the results by Sugiyama [5] concerning the effect of rocket propulsion as a source of a follower load acting on a beam. An impressive overview of rich literature on systems under follower forces was given by Elishakoff [6] who, being inspired by discussion between Koiter and Sugiyama, first wrote “Essay on the So-Called Follower Forces”, addressing it to a group of scientists for their opinions (Besseling, Bogacz, Bolotin, Dimitriyk, Doak, Herrmann, Karihaloo, Kounadis, Maier, Nemet-Nasser, Païdoussis, Panovko, Seyranian and Sugiyama).

The most important reference for the present paper is the experiment by Bigoni and Noselli [7] - a YouTube film recommended as evidence for flutter in the Ziegler column. In the following we show the differences between the tested real mechanism and the Ziegler column in its original concept and formulation.

2. Models of Ziegler’s column and the mechanism being tested

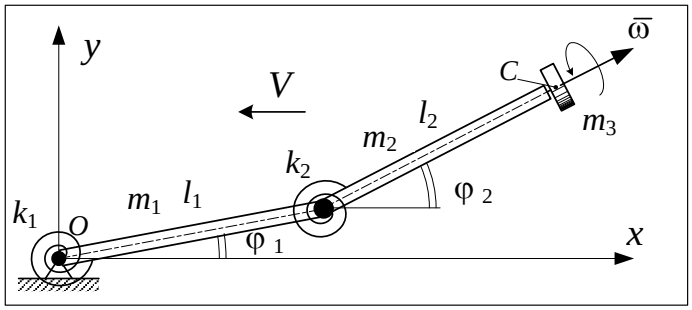

FIGURE 1: Mechanism being tested [7]

The mechanism tested by Bigoni and Noselli consists of two rigid rods linked and supported like the two members of the Ziegler column. At the end of the second member a thin roller is mounted to transfer slip dry friction force T to the column, generated at the point of its contact with a moving plane. Normal force N between the roller and the plane is controlled so that the magnitude of the friction force is constant while its direction coincides with the relative velocity of the roller and the plane at the instantaneous point of their contact. Velocity V of the plane is constant and directed along the column at its straight equilibrium position. The tested mechanism has 3 degrees of freedom and its Lagrangian equations of motion are as follows:

$$\begin{cases} \left(\frac{1}{3}m_1+m_2+m_3\right)l_1^2\ddot{\varphi}_1+\left(\frac{1}{2}m_2+m_3\right)l_1l_2\cos(\varphi_2-\varphi_1)\ddot{\varphi}_2+k\varphi_1-k_2(\varphi_2-\varphi_1)- \\ -\left(\frac{1}{2}m_2+m_3\right)l_1l_2\sin(\varphi_2-\varphi_1)\dot{\varphi}_2^2+F_nl_1\sin(\varphi_2-\varphi_1)-F_\tau l_1\cos(\varphi_2-\varphi_1)=0, \\ \left(\frac{1}{3}m_2l_1^2+m_3l_2^2+m_3r^2\right)\ddot{\varphi}_2+\left(\frac{1}{2}m_2+m_3\right)l_1l_2\cos(\varphi_2-\varphi_1)\ddot{\varphi}_1+k_2(\varphi_2-\varphi_1)+ \\ +\left(\frac{1}{2}m_2+m_3\right)l_1l_2\sin(\varphi_2-\varphi_1)\dot{\varphi}_1^2-F_\tau l_2=0, \\ m_3\ddot{\psi}-F_\tau r=0. \end{cases} \qquad (1)$$

where φ_1,φ_2,ψ denote general coordinates and F_n,F_τ are forces expressed as:

$$F_{n,\tau}=\mu N\frac{w_{n,\tau}}{w},\quad w_n=V\cos\varphi_2+l_1\sin(\varphi_2-\varphi_1)\dot{\varphi}_1,$$
$$w_\tau=V\sin\varphi_2-l_1\cos(\varphi_2-\varphi_1)\dot{\varphi}_1-l_2\dot{\varphi}_2-r\dot{\psi},\quad w=\sqrt{w_n^2+w_\tau^2} \qquad (2)$$

The corresponding equations of the original Ziegler column can be obtained from (1) by neglecting the third equation and assuming $F_n=const,\ F_\tau\equiv 0,\ m_3=0,\ r=0$.

In the paper a detailed analysis of stability of the experimentally tested mechanism is presented and the results are compared with those known for the original Ziegler column. Special attention is paid to the existence of flutter and divergence in the tested system in order to answer the basic question of whether and to what extent the experiment reflects dynamical properties of the ideal Ziegler column.

3. References

[1] Euler, L., "Determinatio onerum, quae columnae gestare valent" (in Latin), *Acta Academiae Scientiarum Petropolitanae*, 1, 1778, pp. 121-145.

[2] Bolotin, V.V., *Nonconservative Problems in the Theory of Elastic Stability*, Pergamon, N.Y., 1964.

[3] Ziegler, H., „Die Stabilitätskriterien der Elastomechanik", *Ingenieria*, 20 (1), 1952, pp. 49-56.

[4] Koiter, W.T., "Unrealistic Follower Forces", *Journal of Sound and Vibration*, 194, 1996, pp. 636-638.

[5] Sugiyama, Y., Katayama, K., Kinoi, S., „Flutter of Cantilever Column under Rocket Thrust", *Journal of Aerospace Engineering*, 8(1), 1995, pp. 9-15.

[6] Elishakoff, I., Controversy Associated With the So-Called «Follower Forces»: Critical Overview", *Applied Mechanics Reviews*, Vol. 58, 2005, pp. 117-142.

[7] Bigoni, D., Noselli, G., „Experimental Evidence of Flutter and Divergence Instabilities Induced by Dry Friction", 2011, http://www.youtube.com./watch?v=RtyHSjMVcB4.

9th German-Greek-Polish Symposium
Recent Advances in Mechanics
September 04-09, 2016
Kolympari, Chania, GREECE

PROBLEMS IN PARAMETER IDENTIFICATION WITH APPLICATION TO ARTERY MODELING

S. Hartmann[1], **R. R. Gilbert**[1]
[1]Institute of Applied Mechanics, Clausthal University of Technology, Germany

Abstract: *Arteries are composed of two mechanically contributing layers. Each layer shows at least an anisotropic viscoelastic response. Even in the case of assuming hyperelasticity with two fiber directions, a number of material parameters have to be identified for each layer. It can be shown that inflating the artery with an internal pressure and combining it with an axial stretch, the parameter identification yields correlated parameters (even between the models of different layers). Thus, fundamental investigations are performed to show the reasons of this effect.*

1. Introduction

Parameter identification using finite elements for solving an entire initial boundary-value problem is well-established today, see, for example, [1,2]. In this case use is made of experimental data in form of resulting forces, torques, displacements, or full-field measurement information to calibrate the mathematical model to the experimental observation. Both data is drawn on for determining the residual between simulation and experimental data, which should be a minimum for a particular material parameter set. This automatic procedure can be – theoretically – applied to any kind of experiments. The question is, however, whether the data is sufficient, or what the quality of the parameters, which are obtained by the optimizer, is. In [3] such quality measures are transferred from the mathematical literature to problems in solid mechanics.

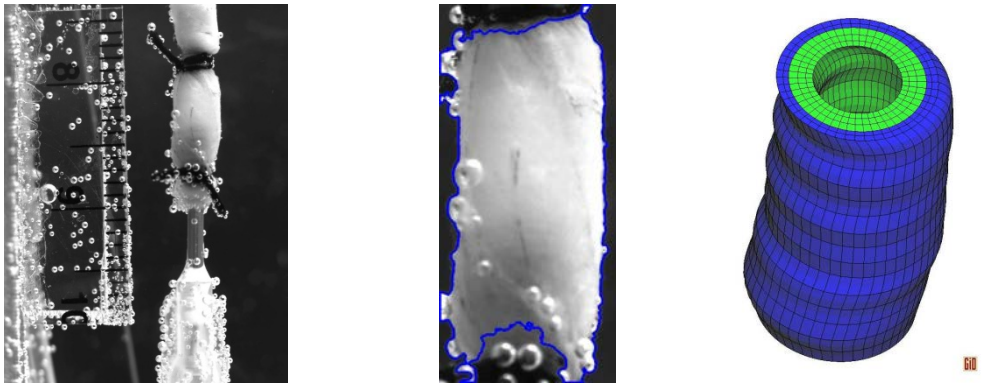

FIGURE 1: Contour detection of an artery from digital image analyses and mesh generation for material parameter identification purposes

In the experimental investigations of arteries one possibility is to stretch such materials in an experimental setup by prescribed axial displacements while it is inflated by a pressuring device. A force gauge can be used to measure the axial force and optical contour measuring systems can be applied to determine the radial displacements in one plane. It turns out that quality indicators show a correlation between the material parameters of the different layers (and in each layer itself as well). In Fig. 1 such a picture sequence is shown.

The reason of this behavior is studied at the following examples: first, we start with uniaxial tensile test for small deformations since this problem provides the reason of the problem. Additionally, the thick-walled tube under internal pressure with one or two layers is studied as well. For the latter case, a solution is derived. The quality measures of the identification process are investigated at such problems. Finally, we can look which further experiment can be provided – if possible – so that the material parameters are addressed in a more sufficient manner.

2. References

[1] Hartmann, S.: Numerical studies on the identification of the material parameters of Rivlin's hyperelasticity using tension-torsion tests, *Acta Mechanica* **148**, 2001, 129-155.

[2] Hartmann, S., Tschöpe, T., Schreiber, L., Haupt, P.: Large deformations of a carbon black-filled rubber. Experiment, optical measurement and parameter identification using finite elements, *European Journal of Mechanics, Series A/Solids* **22**, 2003, 309-324.

[3] Krämer, S., Rothe, S., Hartmann, S.: Homogeneous stress-strain states computed by 3D-stress algorithms of FE-codes. Application to material parameter identification, *Engineering with Computers* **31**(1), 2015, 141-159.

9th German-Greek-Polish Symposium
Recent Advances in Mechanics
September 04-09, 2016
Kolympari, Chania, GREECE

MODEL-BASED DETECTION OF LOCAL DEFECTS IN GEARS

Jędrzej Mączak[1], **Marcin Jasiński**[1]
[1]Institute of Vehicles, Warsaw University of Technology, Poland

Abstract: *In the paper several new methods of local faults detection in helical gears were discussed. They were tested on the helical gearbox model and verified on the back-to-back test stand. All the described methods are based on analysis of the time signals and contrary to the methods based on spectral analysis they allow for precise localization of gear defects like pitting and tooth fracture linking them to the particular pinion or gear teeth.*

1. Introduction

Local damages to the gear teeth causes short-term, local impulses in gear vibration signal repeated every rotation of the shaft and resulting in the phenomenon of amplitude and phase modulation [1,2]. The latter effect dominates in the initial stage of failures development, when the energy changes of signal are particularly small [3]. This type of disturbances are referred to as low-energy effects [4]. Low-energy means that the power increase of the vibroacoustic signal as a result of the development of failures is small compared to the changes in the power structure of the individual meshing harmonic. That small changes in signal energy causes problems in their detection forcing development of new methods of signal analysis.

The main imperfection of most methods currently used in gear diagnostics is that they use integration that is by default averaging analyzed signals. In this way, small changes in the signals appropriate for the initial phases of failure development are further minimized by the use of signal analysis algorithms.

The aim of this study was to present diagnostic methods enabling the identification of local damages of gears, allowing at the same time precise localization of the damage. The common feature of these methods is the direct use of time signal processing algorithms. Their advantage is the simplicity and speed of action that is of great significance for the implementation in the autonomous transmission diagnostic systems and diagnostic systems working online. These methods were first tested on a simulation model of the gear assembly and later tested during the experiments on a back-to-back test stand.

2. Model of the helical gear

In the used model of the helical gear [5] it is assumed that both wheels have the possibility of making an additional rotation in relation to the motion resulting from the revolution of their base circles. The resulting interference of tooth profiles can be determined by taking into account the meshing geometry and is being compensated by the flexible deformation of teeth. The meshing stiffness and the changes of its value for the entire path of contact were defined using a FEM models of toothed wheels. Its modification allows introducing local faults related to the teeth (e.g. pitting or tooth fracture). The model takes into account variable distance between axes (shaft runout or flexible shaft deformation), instantaneous errors of standard contact angle, pitch errors, variable meshing stiffness along the path of contact, etc.

3. Methods for local faults detection

Several methods based on the energetic operators were proposed and tested on the above gearbox model and also verified in practice on the back-to-back test stand allowing finding local nonstationarities in the time-domain signals caused by tooth defects like pitting and tooth fracture. These methods directly uses the signal segmentation in time domain. Beginnings and the lengths of consecutive segments are defined according to the geometry of gears (they are related to the transverse radial pitch) with use of the trigger signal. Most of the methods are based on instantaneous power of the signal (signal's envelope) and Teager-Kaiser energy operator and use differential parameters of the acceleration signal calculated for the consecutive meshes (segments). Segmentation of the signal allows presenting results on the so-called meshing plane, a plane in coordinates *pinion teeth* vs. *gear teeth* [6]. Signal representation on this plane allows to link local nonstationarities in the signal to the relative positions of both shafts (gear teeth) so that the visible changes in the signal are directly linked to the tooth fatigue damages such as pitting and tooth base fracture as well as manufacturing errors (e.g. imbalance or misalignment of shafts) in gearbox.

4. Conclusions

All the described methods are based on analysis of the time-domain signals. Contrary to the integral methods based on spectral analysis these methods allow not only for precise localization of local gear defects like pitting and fatigue fracture at the tooth base but also to link them to the particular pinion or gear teeth with the possibility of quantification of the size of the fault. The common feature of developed methods is a segmentation according to the kinematic of the machine of resampled and averaged acceleration signal so the results can be related to the accuracy of the cooperation (meshing) of the individual teeth of the pinion (or

wheel).

5. References

[1] Randall, R. B., *A new method of modelling gear faults*, J. Mech. Des., 104 (1982) 259–267

[2] McFadden, P. D., *Determining the location of a fatigue crack in a gear from the phase of the change in the meshing vibration*, Mech. Syst. Signal Process., 2(4) (1988) 403–409.

[3] Mączak, J., Radkowski, S., *Low-energy spectrum components as a symptom of failure*, Mach. Dyn. Probl., 8 (1994) 45–64.

[4] Radkowski, S., *Vibroacoustic diagnostics of low energy failures*, Institute for Sustainable *T*echnologies, Radom 2002.

[5] Maczak, J., Diagnostics of local faults in gears (in Polish), Institute for Sustainable Technologies, Radom 2013.

[6] Maczak, J., 2013, Local meshing plane analysis as a source of information about the gear quality, Mechanical Systems and Signal Processing, 38(1), 154–164.

MATERIAL POINT METHODS FOR BRITTLE FRACTURE

S. P. Triantafyllou[1], E. Kakouris[2]
Centre for Structural Engineering and Informatics
Faculty of Engineering
The University Of Nottingham
University Park, NG7 2RD, Nottingham, UK
e-mail: [1]savvas.triantafyllou@nottingham.ac.uk, [2]evxek3@nottingham.ac.uk

Abstract: *In this work, the material point method is reformulated and originally upgraded to simulate brittle fracture phenomena. A phase field description of brittle fracture is employed. Experimental results validate the proposed method.*

1 Introduction

Robust and accurate simulation of fracture processes is a challenging and intriguing task relevant to a series of real-life applications, e.g., in ice-mechanics, composite material behaviour and concrete fracture. Traditional approaches to simulating brittle fracture include the implementation of element deletion and re-meshing strategies within the standard finite element method, cohesion based finite element strategies and the extended finite element method. Recently Phase-field methods (see, e.g., Borden et al. [1]) have been introduced to address brittle fracture. Phase-field fracture represent cracks by means of an additional continuous field (Phase-field) that smoothly varies from zero (inside the crack) to one (away from crack). This field is then discretised using appropriate strategies; to this point the standard finite element method as well as its isogeometric variant have been emplyed. The Material Point Method is effectively an Arbitrary Lagrangian Eulerian method which inherits all the advantages from the Lagrangian and Eulerian descriptions of continuum mechanics. In this, the continuum is represented by a set of material points that are moving within a fixed computational grid where solution of the governing equations is performed. A notable merit is that the accuracy of the method does not depend on the quality of the underlying mesh as the latter can be conveniently chosen to be orthonormal.

2 Phase field material point method

In the following derivations, the case of an elastic domain Ω is considered subject to body forces only for brevity. The corresponding equilibrium equations are readily defined as

$$\mathrm{Div}(\boldsymbol{\sigma}) + \mathbf{b} = \mathbf{0} \quad (1)$$

where $\boldsymbol{\sigma}$ is the stress tensor and $\mathbf{b}$ the vector of body forces. The domain is considered sufficiently supported to prevent rigid body motion. The phase field method approximates the line integral of the fracture energy, i.e. the energy released due to crack opening along a path Γ with a volume integral over the volume of the elastic domain Ω according to the following expression

$$\int_{\Gamma} G_c dx \approx \int_{\Omega} G_c \left[\frac{(c-1)^2}{4l_0} + l_0 \frac{\partial c}{\partial x_i} \frac{\partial c}{\partial x_j} \right] dx \qquad (2)$$

where c is the phase field, G_c is the critical fracture energy density and l_0 is a length scale. The evolution of the phase field parameter is further governed by the differential equation (3) below

$$\left(\frac{4l_0 H}{G_c} + 1 \right) c - 4l_0^2 \frac{\partial^2 c}{\partial x_i^2} = 1 \quad (3)$$

where $i = 1,2,3$ and H is a history field satisfying the following Kuhn-Tucker conditions

$$\psi_{el}^{+} - H \le 0 \quad \dot{H} \ge 0 \quad \dot{H}\left(\psi_{el}^{+} - H\right) = 0 \qquad (4)$$

Equations (4) essentially enforce the irreversibility condition of the crack problem when no healing mechanisms exist. In equations (4), ψ_{el}^{+} denotes the elastic energy density corresponding to the positive components of the strain tensor. This is conveniently evaluated through a polar decomposition of the stress and strain tensor. Further information can be found in Miehe et al. [2]. Within this setting, the elastic energy density is additively decomposed as

$$\psi_{el} = c^2 \psi_{el}^{+} + \psi_{el}^{-} \quad (5)$$

where ψ_{el}^{-} is the elastic energy corresponding to the negative part of the stress and strain tensor (see, e.g., Miehe et al. [2]). Equation (5) essentially establishes that (i) decreasing values of c result in a degrading

material response; $c=1$ being a limit value where no degradation takes place and (ii) this degrading behaviour is imposed only on the positive part of the energy density, thus allowing crack propagation due to tensile stresses only. Equations (1) and (3) form a coupled system of differential equations. Coupling is introduced at the constitutive material level, through consideration of the effect of the phase field on the positive elastic density (equation (5)) and the Kuhn-Tucker conditions introduced in equation (4). Herein, the coupled system is solved by reverting to a Material Point Method. To achieve this, the weak form of the coupled system is derived and appropriately redefined over a set of material points. Consider the case of a set of material points n_p within an Eulerian element of n_n nodes, the resulting discrete equations assume the following form

$$\sum_{p=1}^{n_p} \rho_p \ddot{\mathbf{u}}_p N_I(\mathbf{x}_p)\Omega_p + \sum_{p=1}^{n_p} (\boldsymbol{\sigma}_p \cdot \nabla N_I(\mathbf{x}_p))\Omega_p = 0,\ I=1,..n_n \qquad (6)$$

and

$$\sum_{p=1}^{n_p}\left(\frac{4l_0 H}{G_c}+1\right)\left(\sum_{J=1}^{n_n} N_J(\mathbf{x}_p)c_J\right)N_I(\mathbf{x}_p)\Omega_p + \sum_{p=1}^{n_p} 4l_{0_p}^2 \nabla N_J(\mathbf{x}_p)c_J \nabla N_I(\mathbf{x}_p)\Omega_p = \sum_{p=1}^{n_p} N_I(\mathbf{x}_p)\Omega_p,\ I,J=1,...n_n \qquad (7)$$

for the equilibrium and phase field equations respectively, where $I=1,2,...n_n$. In equations (6) and (7), N_I correspond to the shape functions of the Eulerian mesh while Ω_p corresponds to the volume of the material point p. Assembled at the structural level, equations (6) and (7) give rise to a set of nonlinear equations that can be solved with either explicit or implicit solvers.

3 L-shaped panel test

A set of cyclic experiments conducted in L-shaped reinforced concrete panels has been considered to validate the proposed scheme. The geometry, material properties, boundary conditions and loading scenario considered are shown in Figure 1(a) and (b). The width of the panel is 100mm. In Figure 1(c), the experimentally derived crack path is presented whereas in Figure 1(d) the derived force displacement path is shown. This is identical to the load path reported in Ambati et al. [3] derived using a FEM phase field approach. In Figure 1(e)-(f) snapshots of the phase-field evolution are shown; Figure 1(f) corresponds to the final state of the specimen.

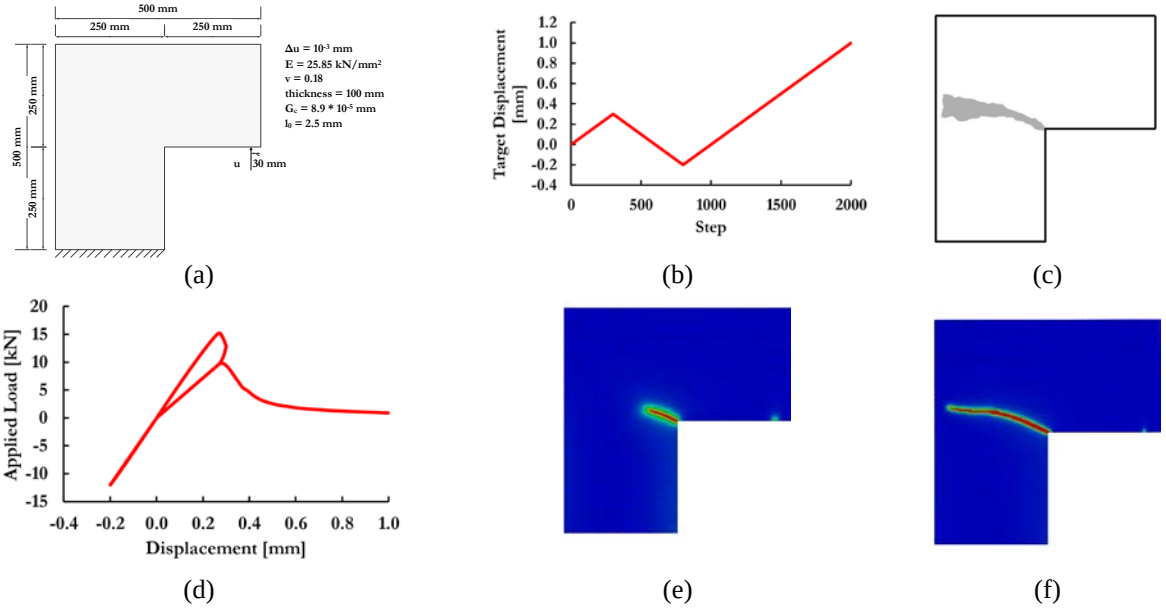

Figure 1 L-shaped concrete panel tests and numerical simulation

4 References

[1]. Borden MJ, Verhoosel CV, Scott MA, Hughes TJ, Landis CM. "A phase-field description of dynamic brittle fracture", *Computer Methods in Applied Mechanics and Engineering*, 217, 2012, pp. 77–95.

[2]. Miehe C, Welschinger F, Hofacker M. "Thermodynamically consistent phase-field models of fracture: Variational principles and multi-field FE implementations", *International Journal for Numerical Methods in Engineering*, 83(10), 2010, pp. 1273–1311.

[3]. Ambati M, Gerasimov T, De Lorenzis L., "A review on phase-field models of brittle fracture and a new fast hybrid formulation. Computational Mechanics", 55(2), 2015, pp. 383–405.

REQUIREMENTS ON CONSTITUTIVE MODELING OF HIGH-TEMPERATURES MATERIALS BEHAVIOR

Prof. Dr.-Ing. habil. K. Naumenko, Prof. Dr.-Ing. habil. H. Altenbach
Otto-von-Guericke-University Magdeburg, Institute of Mechanics, PF 4120, D-39016 Magdeburg, Germany

Abstract: *Many materials and structures are subjected to complex mechanical loading and high-temperature environment. Examples include heat resistant steels, nickel-bases alloys, age-hardened aluminum alloys, cast iron and metal matrix composites for materials as well as turbine blades, turbine housings, rotors, turbochargers, steam pipework and microelectronics components for structures. In the last decades, numerous approaches to the description of the material behavior at high temperature have been developed and efficiently used for the analysis and life assessment of components. The aim of this presentation is to discuss requirements on the constitutive models and underline several open questions based on examples from the engineering practice as well as micromechanics simulations.*

1. Introduction

To illustrate the structural behavior under thermo-mechanical loading let us consider a turbine rotor. The steam temperature on the surface of the rotor is changing according to hot start-up, steady running and hot shut-down sequence. The results of the heat transfer analysis are discussed in detail in [1]. Figure 1a shows the temperature vs time plots for the points *A* and *B* of the rotor.

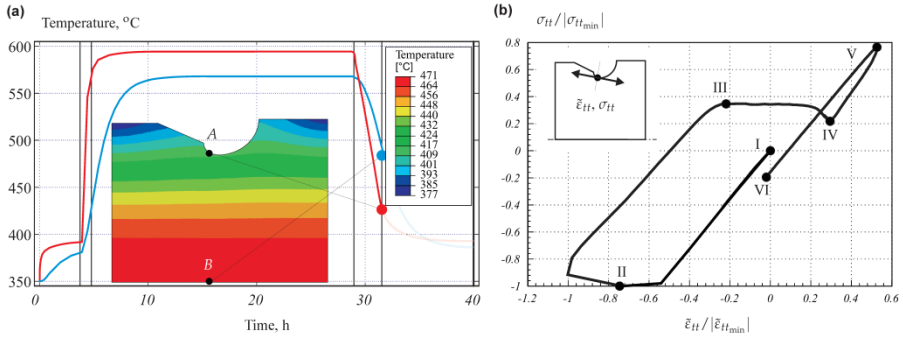

FIGURE 1: Results of thermo-mechanical analysis for a turbine rotor. (a) temperature distribution during cool-down and temperatures in two points vs time, (b) normalized tangential stress vs mechanical strain for one cycle, after [1]

The greatest difference between temperatures of these points is observed during the heat up regime. Within the steady running stage the temperature attains steady state. During the cool-down the temperature difference increases such that the temperature of the surface is lower than the temperature of the symmetry axis. The temperature field for a time step of cooling is shown in Fig. 1a. Figure 1b illustrates the normalized tangential stress vs mechanical strain loop in the notch area. The part I-II is the response during the warm-up stage with the increasing temperature difference between the surface and the core point of the rotor. Here the tangential stress and strain decrease down the minimum (negative) values in the inelastic range. The part II-III corresponds to the warm up stage with the decreasing temperature difference. The part III-IV results from the steady running stage with a slow increase in the strain and decrease in the stress (creep regime). The part IV-V is the tensile regime during the cool-down stage with an increase in the temperature difference. The part V-VI is the final cool-down stage with a decrease of temperature gradient. This example illustrates that both slow and transient inelastic processes of material behavior have to be described by a constitutive model in a unified manner. Several phenomena can be observed experimentally over many load cycles only. Examples include cyclic softening, ratcheting and fatigue damage. The local loading profile determined within one cycle, such us hot start, is crucial for the material behavior over the longer operation time. This should be reflected by evolution equations for internal state variables.

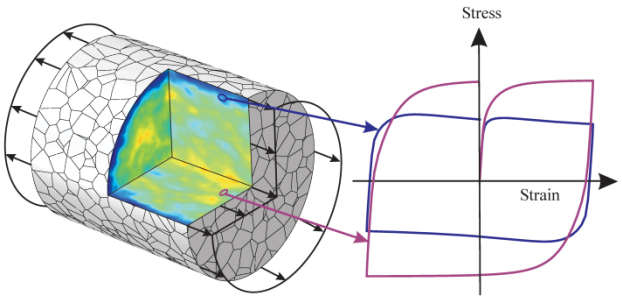

FIGURE 2: Surface layer effect in a polycrystal cylindrical specimen, after [2]

Many features of inelastic material behavior can be qualitatively illustrated and explained based on micromechanical analysis. Figure 2 shows a geometric model of a polycrystal specimen created using a Voronoi diagram [2]. Applying the homogeneous displacements on the edges the low cycle fatigue behavior was investigated numerically. To get smooth deformation and stress fields, N model specimens were randomly generated and the results of analysis were averaged. Figure 2 illustrates the stress field and the hysteresis loop. The results show the surface effect of the stress distribution: the stress values at the surface are substantially lower than the stress values in the bulk of the sample. To capture microscale inelastic phenomena the constitutive model should meet several requirements. First the slip geometry inside individual grains (slip planes and directions) is not always well-defined at high temperature. In the creep range, complex dislocation substructures like cells and subgrains may form and/or evolve leading to additional hardening/softening effects. Furthermore stress and strain states exhibit surface layer and gradient effects.

2. References

[1] Naumenko, K and Altenbach, H. Modeling High Temperature Materials Behavior for Structural Analysis. Part I: Continuum Mechanics Foundations and Constitutive Models. Springer, 2016.

[2] Prygorniev, O. Statistical analysis of stress and deformation state in polycrystalline aggregates with a large number of grains. Dissertation, Otto-von-Guericke-Universität Magdeburg, 2015.

ANALYSIS OF RC FRAMES UNDER SEVERE CYCLIC LOADING USING SMOOTH PLASTICITY AND DAMAGE MODELS

V.K. Koumousis[1], **I.A. Gkimousis**[1]

[1] Institute of Structural Analysis and Aseismic Research, NTUA, Greece

Abstract: *In this work a new method for analyzing RC members until collapse due to severe cyclic loading is presented. It accounts for failure due to core crushing, cover spalling and/or inelastic buckling of longitudinal rebars. Steel and concrete are independently modeled on the basis of new developed smooth plasticity and damage models, while their combined effects are incorporated into a fiber beam-column finite element based on mixed energy principles. This formulation allows for effective solutions adequate for earthquake engineering applications.*

1. Introduction

Modeling Reinforced Concrete (RC) behavior under monotonic and cyclic loading is of particular interest in earthquake engineering due to its decisive role in computer simulations of frame structures. Various models have been proposed either resulting from phenomenological description of experimental behavior, or originating from theoretical considerations.

2. Concrete cyclic behavior

Plain concrete can be modeled using plasticity and damage theories. Soon after initial elastic loading, friction along initial cracks is manifested as elastoplastic behavior with a nonlinear isotropic hardening branch. At later stages, due to extensive cracking the effective reference volume at the critical region of the RC member is reduced resulting to a softening branch. During unloading concrete exhibits nonlinear behavior, while in reloading it remains linear. Particularly, when unloading from tensile stresses, permanent tensile strains settle due to incomplete crack closure caused by misfits at crack edges. If loading at compression field follows, stiffness gradually obtains its compressive value as cracks close. All these physical phenomena are implemented in the following smooth rate stress-strain law [1]:

$$\dot{\sigma}_C = E_{C,t}\cdot\dot{\varepsilon}_C,\ E_{C,t} = \left\{(1-D_i)\cdot\left[1-(1-a_i)\cdot H_{C1}\cdot H_{C2}\right] - \left(H_{C4}\cdot H_{C2}\cdot\frac{dD_i}{dk_i}\cdot\frac{\bar{\sigma}_C}{E_i}\right)\right\}\cdot r_{un}\cdot r_{rec}\cdot E_i \qquad (1)$$

where the first and the second term in the bracket refer to the plastic and damage behavior respectively, while functions r_{un} and r_{rec} describe nonlinear unloading and crack closure phenomena. Verification of the proposed concrete model with experimental data is shown in Figure 1.

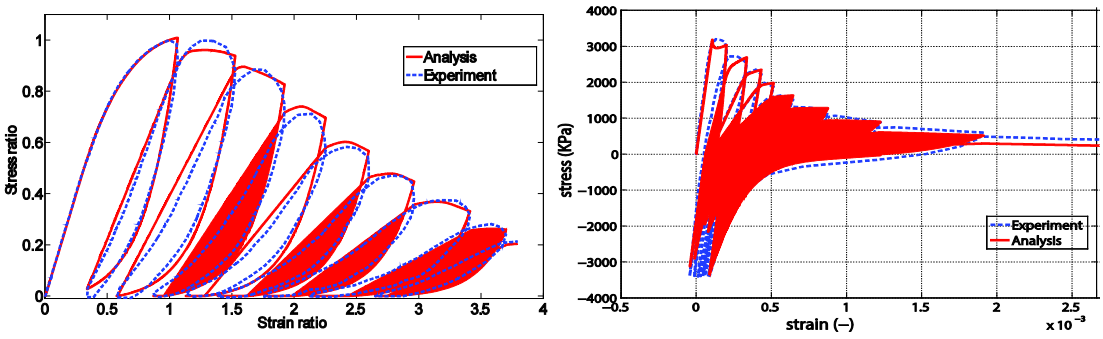

Figure 1: Verification of the compressive and tensile behavior of the proposed concrete model

3. Rebar cyclic behavior

Steel rebar is modeled via a smooth rate model incorporating a combined nonlinear kinematic and isotropic hardening law. It is also valid with plasticity postulates and as a result it can simulate short reversals accurately without overshooting problems [2]. The general steel constitutive relation is presented below in relation (2) where function $\alpha(\varepsilon_p)$ incorporates nonlinear hardening and Heaviside functions H_1 and H_2 describe yielding and unloading conditions.

$$\dot{\sigma}_S = E_{S,t} \cdot \dot{\varepsilon}_S, \quad \dot{\sigma}_S = \left[1-(1-\alpha)\cdot H_1 \cdot H_2\right] \cdot E_S \cdot \dot{\varepsilon}_S \tag{2}$$

At large tensile strains an iterative procedure is developed that can describe inelastic buckling which is reflected in the average stress-strain curve as negative stiffness in the compressive range. Correlation of the proposed model and experimental results of steel rebars are presented in Figure 2.

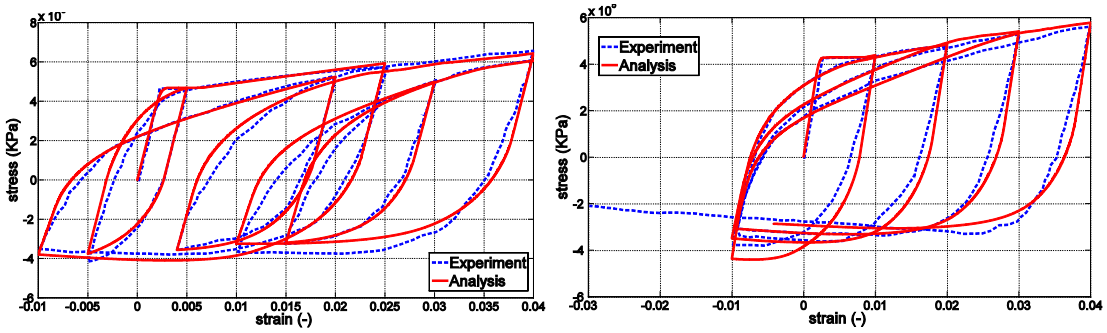

Figure 2: Verification of rebar cyclic behavior exhibiting inelastic buckling

4. Variational beam formulation

RC members describe a softening branch which results in equilibrium errors when classical displacement based finite elements are used. For this reason the proposed material models were incorporated to a mixed beam finite element based on the two-filed Hellinger – Reissner potential. The rate structure of the constitutive equations leads to numerical solution schemes with either linearization of the equations [2] or with solution as an ODE system in state space form.

5. Numerical results

The developed beam-column element is compared against experimental data of RC columns under severe cyclic loading. Such a comparison is presented in **Figure 3** where the column-pier specimen fails due to inelastic buckling of longitudinal rebars.

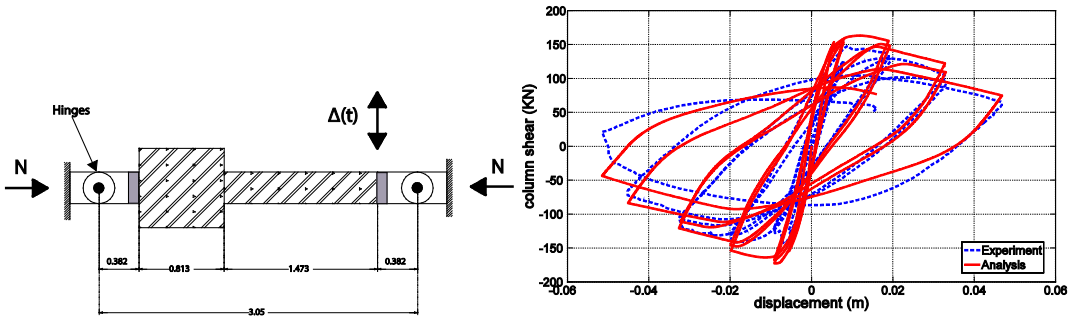

Figure 3: Analysis of an RC column and comparison with experimental results

6. References

[1] Andriotis, C., Gkimousis, I., Koumousis, V. (2015). "Modeling Reinforced Concrete Structures Using Smooth Plasticity and Damage Models." J. Struct. Eng., Volume 142, Issue 2.

[2] Gkimousis, I.A., Koumousis, V.K. (2016). "Inelastic mixed fiber beam finite element for steel cyclic behavior." Engineering Structures 106, pp. 399-409.

9th German-Greek-Polish Symposium
Recent Advances in Mechanics
September 04-09, 2016
Kolympari, Chania, GREECE

ANALYTICAL MINIMUM WEIGHT DESIGN OF TRUSSES USING CYLINDRICAL ALGEBRAIC DECOMPOSITION

Dr. A. E. Charalampakis[1]
[1]Gediz University, Izmir, Turkey

Abstract: *A methodology for the discovery of globally optimal analytical solutions for the minimum weight design of trusses, including stress, displacement and frequency constraints, is presented. The methodology is based on the Cylindrical Algebraic Decomposition (CAD) algorithm, in tandem with powerful symbolic computation. To the best of our knowledge, no similar attempt can be found in the literature.*

1. Introduction

In this work, a methodology for the derivation of exact, globally optimal solutions to truss weight minimization problems is presented. The basis of the methodology is the Cylindrical Algebraic Decomposition (CAD) algorithm, in tandem with powerful symbolic computation for the discovery of stationary points.

2. Cylindrical Algebraic Decomposition

Given a finite set $P \subset R[x_1, x_2, ..., x_n]$ of polynomials in n variables, a P-invariant cylindrical algebraic decomposition is a special partition of $\mathbb{R}^n$ into components, called *cells*, over which each of the polynomials from P has constant sign on each cell of the decomposition. The cylindrical algebraic decomposition (CAD) *algorithm* is an algorithmic procedure proposed by Collins [1] which constructs these decompositions; it also provides a point in each cell, called *sample point*, which can be used to determine the sign of the polynomials.

Further, given a logical combination of polynomial equations and inequalities in n real unknowns, one can use the CAD algorithm to find a cylindrical algebraic decomposition of its solution set [2]. This decomposition provides the feasible domain in a suitable form for exact global optimization, as shown next.

3. Example: 3-bar truss

The well-known 3-bar truss (Figure 1a) is used to demonstrate the method:

$$\begin{aligned}
&\text{Minimize } f(x_1, x_2) = \left(2\sqrt{2}x_1 + x_2\right)L \text{ subject to} \\
&c_1(x_1, x_2) = \frac{\sqrt{2}x_1 + x_2}{\sqrt{2}x_1^2 + 2x_1x_2}P - \sigma \le 0 \\
&c_2(x_1, x_2) = \frac{x_2}{\sqrt{2}x_1^2 + 2x_1x_2}P - \sigma \le 0 \qquad (1) \\
&c_3(x_1, x_2) = \frac{1}{x_1 + \sqrt{2}x_2}P - \sigma \le 0 \\
&\text{where } 0 < x_1 < 1;\ 0 < x_2 < 1;\ L = 100cm;\ P = 2kN;\ \sigma = 2\,kN/cm^2.
\end{aligned}$$

Applying the CAD algorithm in the sequence $\{x_1, x_2\}$, the following is derived:

$$\frac{1-\sqrt{2}+\sqrt{3}}{2} < x_1 < 1 \cap \frac{\sqrt{2}(x_1-1)x_1}{2x_1-1} \le x_2 < 1. \qquad (2)$$

The above describes *precisely* the coordinates of all the points $(x_1, x_2) \in \mathbb{R}^2$ for which the constraints $c_1 \le 0$, $c_2 \le 0$ and $c_3 \le 0$ hold simultaneously. The algorithm could have been applied to even more constraints (representing stress, displacement, frequency, or any other kind of constraint). After the discovery of stationary points, the analytical solution is derived (Figure 1b), which is compared to the results of other researchers in Table 1.

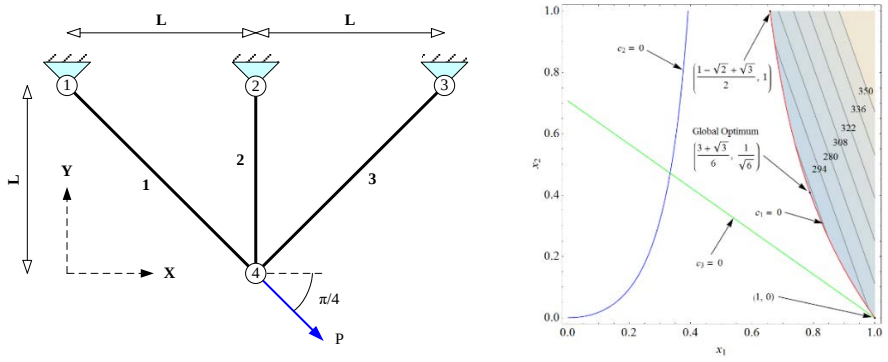

(a) (b)

FIGURE 1: (a) 3-bar truss (b) feasible domain, constraints, and global optimum.

	Ray and Liew [3]	Liu et al. [4]	This study (analytically)	This study (numerically)
x_1	0.7886210370	0.788675134746	$\left(3+\sqrt{3}\right)/6$	0.788675…
x_2	0.4084013340	0.408248290037	$1/\sqrt{6}$	0.408248…
min f	263.8958466	263.895843376468	$L\left(\sqrt{2}+\sqrt{3/2}\right)$	263.895843…

TABLE 1: Results for the 3-bar truss

4. References

[1] Collins, G.E., "Quantifier elimination for the elementary theory of real closed fields by cylindrical algebraic decomposition", *LNCS*, Vol.33, 1975, pp. 134-183.

[2] Strzeboński, A., "Solving systems of strict polynomial inequalities", *J Symb Comput*, Vol. 29, 2000, pp. 471–480.

[3] Ray, T., and Liew, K.M., "Society and Civilization: An Optimization Algorithm Based on the Simulation of Social Behavior," *IEEE Trans on Evol Comput*, Vol. 7(4), 2003, pp. 386–396.

[4] Liu, H., Zixing, C., and Wang, Y., "Hybridizing particle swarm optimization with differential evolution for constrained numerical and engineering optimization," *Appl Soft Comput*, Vol. 10, 2010, pp. 629–640.

COMPUTATIONAL HOMOGENIZATION OF DIFFUSION PROBLEMS

S. Kaessmair[1], **Prof. Dr.-Ing. habil. P. Steinmann**[1]
[1]Chair of Applied Mechanics,
Friedrich-Alexander University Erlangen-Nuremberg, Germany

Abstract: *In the present contribution, we address computational first-order homogenization of transient diffusion problems. There, two different cases are considered. Firstly, when the size of the representative volume element (RVE) is negligibly small and secondly, when a finite RVE size is assumed. These cases result in stationary and transient microscale solutions, respectively.*

1. Introduction

Diffusion is essential for many processes observed in nature like drug transport in biological tissue or mineral unmixing. In order to determine the response of a macroscopic body with heterogeneous microstructure, we use computational first-order homogenization. The well-known assumption of scale separation, i.e. the existence of different length scales l (micro) and ${}^{M}l$ (macro) with $l << {}^{M}l$, results in a stationary microscale problem, see Özdemir et al. [1]. For a relaxed version of this condition, that is for a finite size of the RVE, this is not necessarily the case. See Larsson et al. [2] and Pham et al. [3], where the formulation on the micro-level is fully transient.

2. Computational Homogenization

In the following, the superscript M labels macroscopic quantities. Consider a macroscopic body B with boundary ∂B and a microstructural representative volume element V with boundary ∂V attached to macroscopic particles with placement ${}^{\mathrm{M}}\boldsymbol{X}$. Particles on the microscale are located at positions $\boldsymbol{X}$. We assume that the RVE is centered at ${}^{\mathrm{M}}\boldsymbol{X}$. On the micro- and macroscale, respectively, the species transport is governed by the following balance equations

$$\mathrm{D}_t c - \mathrm{Div}\,\boldsymbol{H} = 0 \quad \text{in} \quad V \quad \text{and} \quad \mathrm{D}_t {}^{M}c = -{}^{M}\mathrm{Div}\,{}^{M}\boldsymbol{H} = 0 \quad \text{in} \quad B. \tag{1}$$

The chemical potential $\mu = \mu(\boldsymbol{X},t)$ is used in order to describe the microscale concentration $c = c(\mu)$ and the microscale species flux $\boldsymbol{H} = \boldsymbol{H}(c, \mathrm{Grad}\,\mu)$. Their macroscopic counterparts are denoted ${}^{M}c$ and ${}^{M}\boldsymbol{H}$. Multiplication with the scalar-valued test functions $\delta\mu$ and $\delta^{M}\mu$ and application of the divergence theorem yields the corresponding weak formulations on the microscale

$$\int_V \mathrm{D}_t c\,\delta\mu - \boldsymbol{H}\cdot\mathrm{Grad}\,\delta\mu\,\mathrm{dV} - \int_{\partial V^H} \delta\mu\, H^{\mathrm{p}}\,\mathrm{dA} = 0 \quad \forall\,\delta\mu \in H_0^1\,, \tag{2}$$

and on the macroscale

$$\int_B \mathrm{D}_t {}^{M}c\,\delta^{M}\mu - {}^{M}\boldsymbol{H}\cdot{}^{M}\mathrm{Grad}\,\delta^{M}\mu\,\mathrm{dV} - \int_{\partial B^H} \delta^{M}\mu\,{}^{M}H^{\mathrm{p}}\,\mathrm{dA} = 0, \forall \delta^{M}\mu \in H_0^1 \tag{3}$$

The quantities ${}^{M}H^{\mathrm{p}}$ and H^{p} denote the species flux across the boundary.

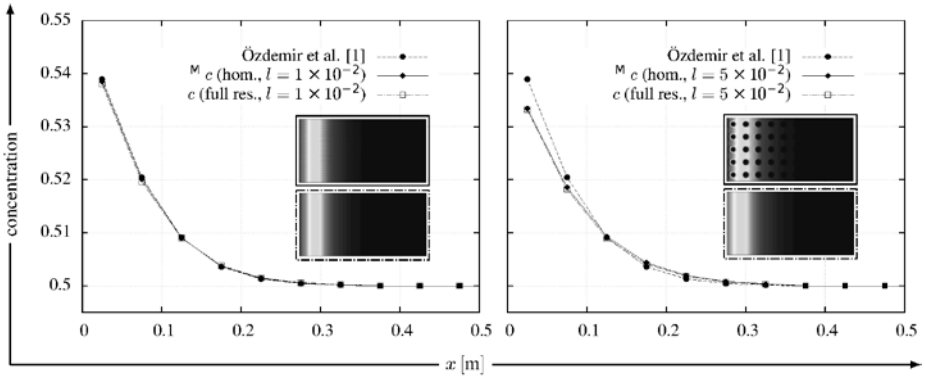

FIGURE 1: Comparison of the homogenized solutions with the solution of the corresponding full resolution models. The length of the underlying microstructure is denoted *l*. As benchmark the solution using the model of Özdemiret al. [1] with stationary microscale is given.

When using first-order homogenization, the microscopic chemical potential decomposes into a linear

macroscopic contribution and fluctuations $\tilde{\mu}$, that is

$$\mu = {}^{M}\mu + {}^{M}\mathrm{Grad}\,{}^{M}\mu \cdot \left[\boldsymbol{X} - {}^{M}\boldsymbol{X}\right] + \tilde{\mu}\,. \tag{4}$$

The fluctuations vanish on the boundary of the RVE in order to enforce ${}^{M}\mathrm{Grad}\,{}^{M}\mu = \langle \mathrm{Grad}\,\mu \rangle$. Here, $\langle \circ \rangle$ is the spatial averaging operator. A Hill-Mandel like statement is used to equate the dissipation power at both scales, i.e.

$$\mathrm{D}_t{}^{M}c\;\delta^{M}\mu \; - {}^{M}\boldsymbol{H} \cdot {}^{M}\mathrm{Grad}\;\delta^{M}\mu = \; \langle \mathrm{D}_t c\;\delta\mu \rangle \; - \langle \boldsymbol{H} \cdot \mathrm{Grad}\;\delta\mu \rangle. \tag{5}$$

With the aid of equations (1), (4), and (5) we eventually find

$$\mathrm{D}_t{}^{M}c = \; \langle \mathrm{D}_t c \rangle \quad \text{and} \quad {}^{M}\boldsymbol{H} = \langle \boldsymbol{H} - \mathrm{D}_t c \left[\boldsymbol{X} - {}^{M}\boldsymbol{X}\right] \rangle. \tag{6}$$

The last term on the right hand side can be interpreted as microscale inertia to a change in the macroscopic species concentration. For a vanishingly small RVE, this term vanishes and the macroscopic flux is equal to the averaged flux on the microscale. This behavior can be observed in figure 1, the bigger the RVE size the slower the species transport through the body. When the size of the RVE decreases the model of Özdemir et al. [1] is approached.

Acknowledgements The support by the German Research Foundation (DFG) grant STE 544/48-1 is gratefully acknowledged.

3. References

[1] Özdemir, I., Berkelmans, W.A.M., and Geers, M.G.D., "Computational homogenization for heat conduction in heterogeneous solids", *Int. J. Numer. Meth. Engng.*, Vol. 73, 2008, pp. 185-204.

[2] Larsson, J., Runneson, K., and Su, F., "Variationally consistent computational homogenization of transient heatflow", *Int. J. Numer. Meth. Engng.*, Vol. 81, 2010, pp. 1659-1686.

[3] Pham, K., Kouznetsova, V.G., and Geers, M.G.D., "Transient computational homogenization for heterogeneous materials under dynamic excitation", *J. Mech. Phys. Solids*, Vol. 61, 2013, pp. 2125-2146.

9th German-Greek-Polish Symposium
Recent Advances in Mechanics
September 04-09, 2016
Kolympari, Chania, GREECE

EFFICIENT ASYMPTOTIC STATE SOLUTIONS OF CYCLICALLY LOADED ELASTOPLASTIC STRUCTURES

K.V. Spiliopoulos[1], **K.D. Panagiotou**[1]
[1]National Technical University of Athens, Greece

Abstract: *RSDM and RSDM-S are two recent numerical procedures that constitute a most physical way to estimate the long-term response and to provide safety margins for cyclically loaded elastoplastic structures. In this work, their combined application to benchmark structures is discussed. Moreover, advances concerning their quicker convergence as well as extensions to provide shakedown boundaries in multiple loading domains are proposed.*

1. Introduction

The exposition of a civil or mechanical engineering structure or structural component to high levels of variable repeated loading may lead them to asymptotic limit states related to global excessive deformations (ratcheting) or local ones (e.g. low cycle fatigue). Typical cyclic loadings may be heavy traffic, earthquakes or waves on civil engineering structures, like bridges, pavements, buildings, and offshore structures. On the other hand, in mechanical engineering structures, like nuclear reactors, aircraft propulsion engines, the co-existence of cyclic mechanical together with high temperature loads may be possible cases of collapse. Below a certain level of the applied loading, a favorable limit state exists that, after some initial plastic straining, the structure eventually adapts itself to a steady condition with elastic straining only (shakedown). This is a safe state which extends the life cycle of a structure.

The determination of the long-term asymptotic states of elastoplastic structures, loaded cyclically is normally done using cumbersome time stepping calculations. A much better alternative, that requires much less computing time, is offered by the direct methods. On the other hand, if the exact loading time history inside the cycle is not known, but only its variation intervals, then direct methods are the only way to establish safety margins.

2. The Residual Stress Decomposition methods (RSDM & RSDM-S)

Most direct methods are based on the two theorems of plasticity and they are formulated within the framework of mathematical programming. A different procedure called Residual Stress Decomposition method (RSDM) [1] has appeared, which assumes the exact cycle time history of the loading. The procedure exploits the fact of the expected cyclic nature of the residual stresses at the asymptotic state. Thus it decomposes them into Fourier series whose terms are evaluated iteratively by satisfying equilibrium and compatibility at several time points inside the cycle. With roots on this method, an approach (RSDM-S) [2, 3] has been formulated that may evaluate the shakedown load factor of a loading consisting of two different loads varying between an upper and a lower limit that must be estimated. The loads may be applied either proportionally or independently. Loading domains consisting of two mechanical or one mechanical and a thermal load have been considered [2-4]. The domain is converted to an equivalent time history loading by drawing smooth curves that pass through these two limits. The loading domain may be isotropically varied through the multiplication by a load factor. The shakedown load factor is estimated through iterations by continuously shrinking the loading domain so that a constant distribution of residual stresses may evolve, which is the criterion for elastic shakedown to occur. Inside an iteration, the RSDM is used to provide the residual stress distribution, as well as its Fourier coefficients, for the loading corresponding to the current load factor.

Both the procedures are implemented through the discretization of the structure with finite elements assuming an elastic-perfectly plastic material with a von Mises yield criterion. They are formulated within the framework of the stiffness method and may thus be implemented in any standard finite element program with no need to use any optimization algorithm. To add to the procedures' numerical efficiency, the stiffness matrix needs to be formed and decomposed only once.

In the present work the two methods are successfully combined [5] offering a valuable help to understand complex phenomena, such as shakedown, alternating plasticity, and ratcheting. Advances of the methods, like different tolerance criterion, that improves their computational time, are also discussed. The RSDM-S is also herein extended to thermomechanical loadings that consist of three loads. Further possible extension of the method to multiple loading domains is also presented.

Examples of application for various structures and loadings will be presented during the workshop.

3. References

[1] Spiliopoulos, K.V. and Panagiotou, K.D., "A direct method to predict cyclic steady states of elastoplastic structures", *Comput. Methods Appl. Mech. Eng*. Vol. 223–224, 2012, pp. 186–198.

[2] Spiliopoulos, K.V. and Panagiotou, K.D., "A Residual Stress Decomposition based Method for the Shakedown analysis of structures', *Comput. Methods Appl. Mech. Eng*., Vol. 276, 2014, pp. 410-430.

[3] Spiliopoulos, K.V. and Panagiotou, K.D., "RSDM-S: A Method for the Evaluation of the Shakedown Load of Elastoplastic Structures", *Direct Methods for Limit and Shakedown Analysis of Structures,* Springer Intnl. Publish., 2015, pp. 159-175.

[4] Spiliopoulos, K.V. and Panagiotou, K. D., "A numerical procedure for the shakedown analysis of structures under cyclic thermomechanical loading" *Arch. Appl. Mech*., Vol. 85, 2015, pp. 1499-1511.

[5] Panagiotou, K.D. and Spiliopoulos K.V., "Assessment of the Cyclic Behavior of Structural Components Using Novel Approaches", *ASME J. Press. Vess. Techn*., Vol. 138, 2016, 041201.

9th German-Greek-Polish Symposium
Recent Advances in Mechanics
September 04-09, 2016
Kolympari, Chania, GREECE

ON THE EXPERIMENTAL TECHNIQUES FOR THIN SHEETS TESTING AT LARGE DEFORMATIONS

Prof. Z.L. Kowalewski[1], **Prof. L. Dietrich**[1], **Prof. G. Socha**[2]
[1]Institute of Fundamental Technological Research, Poland
[2]Institute of Aviation, Poland

Abstract: *Problems associated with material testing on flat specimens under large deformation due to compression or cyclic tension-compression are discussed. A short review of the anti-buckling fixtures developed up to now is given with special emphasis on the new fixture elaborated at the Institute of Fundamental Technological Research in Poland.*

1. Introduction

Material characterization using flat specimens under compression within large deformation range procure many difficulties. The buckling effect is regarded as the most significant. Among many important phenomena observed during cyclic tests carried out on the flat specimens one can distinguish: (a) changes of the hardening modulus of a material due to variation of the loading direction; (b) strain-hardening stagnation observed after change of the loading direction; (c) relationship between strain amplitude and stress saturation; (d) changes of the elastic modules due to cyclic loading. Tension-compression tests are especially important for materials exhibiting mechanical properties to be dependent on the first stress invariant. One can indicate the magnesium alloys for example.

The fixture elaborated by the team from IPPT changes its length with specimen elongation or shrinkage during a test which allows application of cyclic load, Fig. 1. The friction force, which is generated due to a movement of both parts of the fixture, is measured by the special strain gauge system during each test. It allows eliminating friction force influence on the stress-strain characteristics.

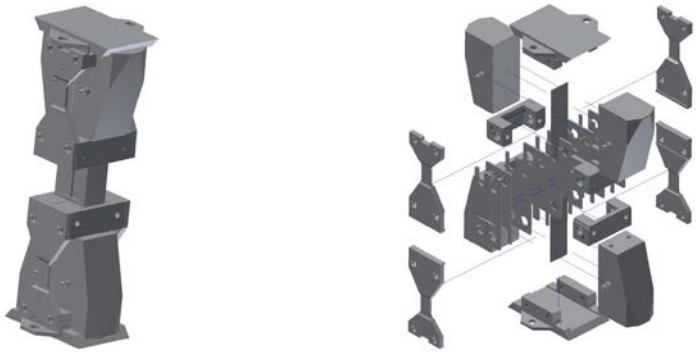

FIGURE 1: Scheme of general and exploded views of the fixture

The results of investigations carried out on steel, brass and aluminium alloy using the new fixture were captured. Selected examples are presented in Fig. 2 for the brass. It shows the results from strain controlled tension-compression cycles performed for the constant strain amplitude equal to ±2%, Fig. 2a, and variable strain amplitude within the range ±4%, Fig. 2b. Variations of the strain control signal are presented for both tests in graphs (c) and (d) of Fig. 2, respectively. Force responses into those programmes together with friction force measurements are documented in graphs (e) and (f) of Fig. 2. As it is clearly shown, the brass exhibits softening effect. Also, the so called strain-hardening stagnation observed after change of the loading direction may be noticed.

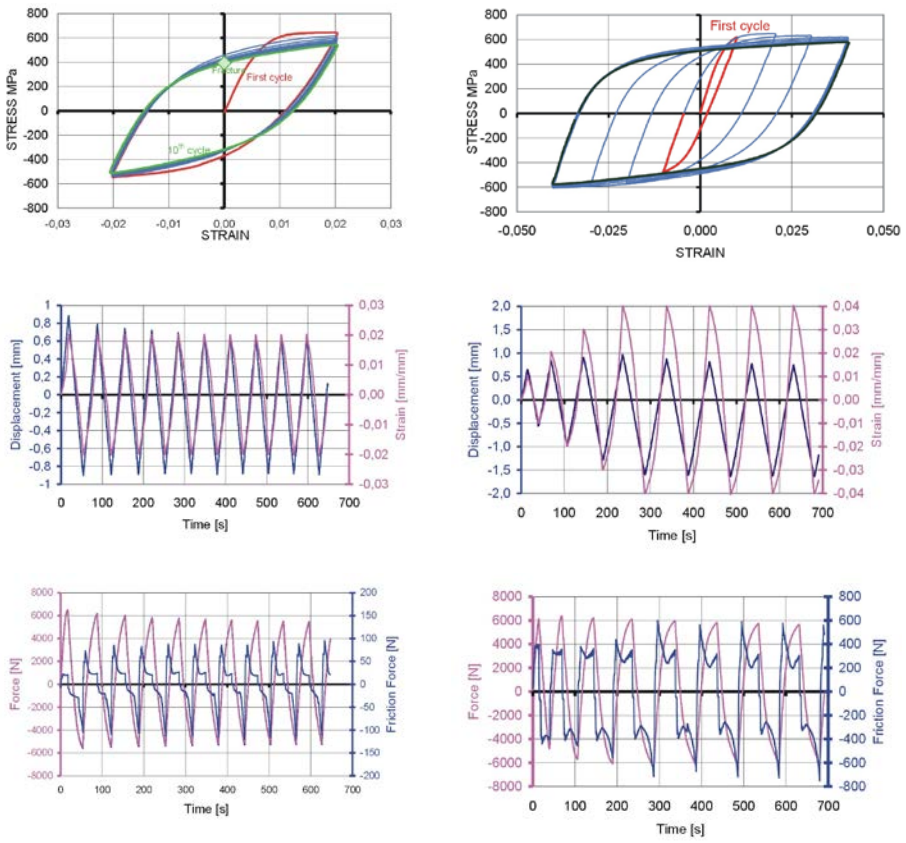

FIGURE 2: Hysteresis loops under cyclic tension-compression for: (a) constant; and (b) variable strain amplitude; graphs (c) and (d) represent strain control signal and displacement; graphs (e) and (f) show force responses into the strain control signals in graphs (c) and (d), respectively

2. References

[1] Dietrich L., et al., Anti-buckling fixture for large deformation tension-compression cyclic loading of thin metal sheets, *Strain Int. J. Exp. Mech.*, **50**, 2014, pp. 174-183.

9th German-Greek-Polish Symposium
Recent Advances in Mechanics
September 04-09, 2016
Kolympari, Chania, GREECE

ASPECTS OF THE PROPER ORTHOGONAL DECOMPOSITION TECHNIQUE APPLIED TO THE DYNAMIC FIBRE PULL-OUT

Wolfgang E. Weber, Daniel Balzani, Yannick F. Fangye, Bernd W. Zastrau
Technische Universität Dresden, Institute of Mechanics and Shell Structures,
Dresden, Germany

Abstract: *To adequately describe the pull-out of reinforcing fibres is both a challenging and time consuming task. Thus an efficient solution procedure is required. A powerful projection-based reduction method is the proper orthogonal decomposition (POD). Herein, the problem is projected into a lower dimensional subspace built up from so-called snapshots. However, the choice of these snapshots does influence both the accuracy of the numerical results and the numerical effort. Within this contribution the applicability of the POD is discussed.*

1. Introduction

In civil engineering and mechanical engineering many structures are made from fibre reinforced materials. If such structures are exposed to impulsive loads, cracks may occur which are bridged by the reinforcing fibres. The amount of load bearing capacity of the structure clearly depends on, amongst others, this crack bridging. The crack bridging itself is strongly influenced by the dynamic pull-out of the reinforcing fibres. That is, a deeper understanding of the mechanical effects taking place during the dynamic fibre pull-out helps in increasing the resistance of structures to impulsive loads. However, in general the simulation of the fibre pull-out is numerically expensive, see Fig. 1. Thus, strategies are sought which allow for reducing the numerical effort. One of these strategies – the POD [1] – is discussed in this contribution.

2. Fibre pull-out

The dynamic pull-out of a fibre from the surrounding host material is characterized by e. g. the stiffness and density of the fibre, the host material, and – if existent – the interphase between both constituents. Additionally, the bond behaviour fibre-host (or fibre-interphase-host) is of interest, as a fibre pull-out is only possible if the bond fails along the fibre. That is, something like a moving load front will appear. Concerning the load, its time-dependence and magnitude are of major concern. As can readily be seen, an advanced numerical model is necessary for adequately modelling the fibre pull-out. In order to provide a reference solution for the numerical model, in Weber *et al.* [2] a simplified analytical model is introduced which however is taking into account major effects occurring in the advanced model, too. By means of this analytical model the time-dependent behaviour of the displacement along the fibre as plotted in Fig. 2 can be described qualitatively. The validation of the numerical model allows for deeper investigations, which as expected is time-consuming. Consequently, a method is sought which reduces the computational effort while maintaining a good quality of the results obtained subsequently. Within this contribution the POD is chosen. The main idea is to project the original system to a lower dimensional one. This reduction is achieved by multiplying the system's stiffness matrix $\boldsymbol{K}$, the vector of the incremental nodal displacements $\Delta\boldsymbol{D}$, and the residual vector $\boldsymbol{R}$ by the so-called subspace matrix $\boldsymbol{\phi}$

$$\boldsymbol{\phi}^T \boldsymbol{K} \Delta\boldsymbol{D} = \boldsymbol{\phi}^T \boldsymbol{R} \quad .(1)$$

Herein, $\boldsymbol{\phi}$ is the (subspace) matrix of the left-singular vectors of the so-called snapshot matrix $[\boldsymbol{D}^1, \boldsymbol{D}^2, \ldots, \boldsymbol{D}^l]$ containing the nodal displacements of the system at l time steps for a given load [3]. The quality of the approximation of the reduced system strongly depends on the amount n of left-singular vectors taken into account (Fig. 2). These left-singular vectors are assigned to the n largest singular values.

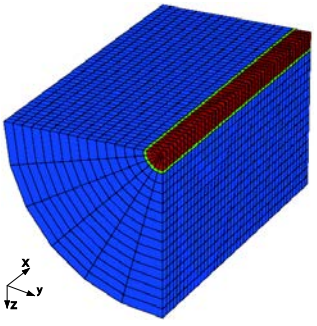

FIGURE 1: FE-Model

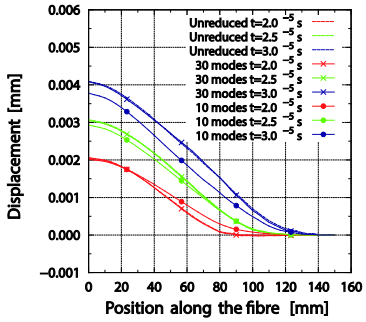

FIGURE 2: Displacement distribution

3. Results

The POD is an efficient model order reduction method. Depending on the amount of left-singular vectors used for the computations accurate results compared to the unreduced system can be achieved. As these eigenvectors only contain the system's information up to the last time step taken into account, only an interpolation of the systems behaviour with respect to the time is possible, while an extrapolation is difficult. If the snapshots are generated for different load magnitudes (that is, a lower and an upper bound), an interpolation of the system's behaviour for loads between these bounds is possible, too.

4. References

[1] Chatterjee, A., "An introduction to the proper orthogonal decomposition", *Current science*, Vol. 78, No. 7, 2000, pp. 808-817.

[2] Weber, W. E., Balzani, D., Fangye, Y. F., Zastrau, B. W.: "Analytical and Numerical Modelling of a Sub- and Supersonic Moving Load Front Along a Rod's Skin", in: *Advanced Methods of Continuum Mechanics for Materials and Structures*, eds.: Naumenko, K., Aßmus, M., 2016, pp. 469-489.

[3] Fangye, Y. F., Weber, W. E., Zastrau, B. W., Balzani, D.: "Some Basic Ideas for the Simulation of Wave Propagation in Microstructures using Proper Orthogonal Decomposition", *PAMM*, Vol. 16, No. 1, 2016, to appear.

9th German-Greek-Polish Symposium
Recent Advances in Mechanics
September 04-09, 2016
Kolympari, Chania, GREECE

DYNAMIC STABILITY OF ROTATING NANOSHAFTS

Professor A. Tylikowski
Warsaw University of Technology, Poland

Abstract: *Using the direct Liapunov method, stability of carbon nanotube rotating with constant angular velocity is analysed. A modified nonlocal beam model is used to describe two- dimensional transversal beam displacements. The nanobeam is axially loaded by a constant and time-dependent wide-band Gaussian force. The critical angular velocity is written as a function of beam mechanical parameters, axial force characteristics and the nanoscale coefficient.*

1. Analysis

Among other applications carbon nanotubes are also expected to be used as elements of nanomachines, e.g. nanoshafts used as driving elements. They can be modeled as the Bernoulli-Euler beam rotating with constant angular velocity ω, with respect to own axis and subjected to an axial force. The Erringen-Lim [1] formulation of nonlocal elasticity is used to describe bending of nanobeam with the constant bending stiffness EJ, length l, transversal displacements u,v, axial coordinate x, transversal loading q_u , q_v , and nanoscale $\tau = e_o\, a/l$, where e_o material parameter, a inner scale

$$EJ\, u_{,xxxx} - \tau^2\, EJ\, u_{,xxxxxx} = q_u \tag{1}$$

$$EJ\, v_{,xxxx} - \tau^2\, EJ\, v_{,xxxxxx} = q_v \tag{2}$$

Eq. (1) and (2) have the similar form as the equations derived in the frame of gradient elasticity by Papargyri-Beskou and Beskos [2]. Natural boundary conditions in the first approximation have form

$$\begin{aligned} &u(0,t)=u(1,t)=v(0,t)=v(1,t)=0 \\ &u_{,xx}(0,t)=u_{,xx}(1,t)=v_{,xx}(0,t)=v_{,xx}(1,t)=0 \\ &u_{,xxxx}(0,t)-\tau^2\, u_{,xx}(0,t)=u_{,xxxx}(1,t)-\tau^2\, u_{,xx}(1,t)=0 \\ &v_{,xxxx}(0,t)-\tau^2\, v_{,xx}(0,t)=v_{,xxxx}(1,t)-\tau^2\, v_{,xx}(1,t)=0 \end{aligned} \tag{3}$$

Finally, taking into account the internal and external damping forces with constant proportionality coefficients β_1 , h_1, respectively, dynamics equations in nonrotating coordinate system in dimensionless coordinates have the form

$$\begin{aligned} &u_{,tt} + h_1 u_{,t} + e u_{,xxxx} - e\tau^2\, u_{,xxxxxx} + \beta_1 e\left(u_{,xxxxt} + \omega v_{,xxxx}\right) + f_o\, u_{,xx} = 0 \\ &v_{,tt} + h_1 v_{,t} + e v_{,xxxx} - e\tau^2\, v_{,xxxxxx} + \beta_1 e\left(v_{,xxxxt} - \omega v_{,xxxx}\right) + f_o\, v_{,xx} = 0 \end{aligned} \tag{4}$$

In order to examine stability of the undeflected equilibrium of nanoshaft (the trivial solution) the energy-like functional have the form Tylikowski [3]

$$\begin{aligned} V = \int_0^1 \Big[& u_{,t}^2 + \left(u_{,t} + h_1 u + \beta_1\, u_{,xxxx}\right)^2 + v_{,t}^2 + \left(v_{,t} + h_1 v + \beta_1\, v_{,xxxx}\right)^2 + \\ & + 2e\left(u_{,xx}^2 + v_{,xx}^2\right) + 2e\tau^2\left(u_{,xxx}^2 + v_{,xxx}^2\right) - 2 f_o\left(u_{,x}^2 + v_{,x}^2\right)\Big] dx \end{aligned} \tag{5}$$

If the axial force has a stochastic wide-band Gaussian component Eqs(4) are written as a system of stochastic Itô equations and using the same functional (5) sufficient conditions of uniform stochastic stability can be obtained.

2. Results

Applying the direct Liapunov method to functional (5) along dynamic equations assuming the bending stiffness e = 10^{-6}, the internal damping coefficient equal to thermoelastic damping coefficient $\beta_1 = 10^{-4}$ and $\beta_1 = h_1$ Liapunov stability domain is calculate for deterministic force and shown in Figure1

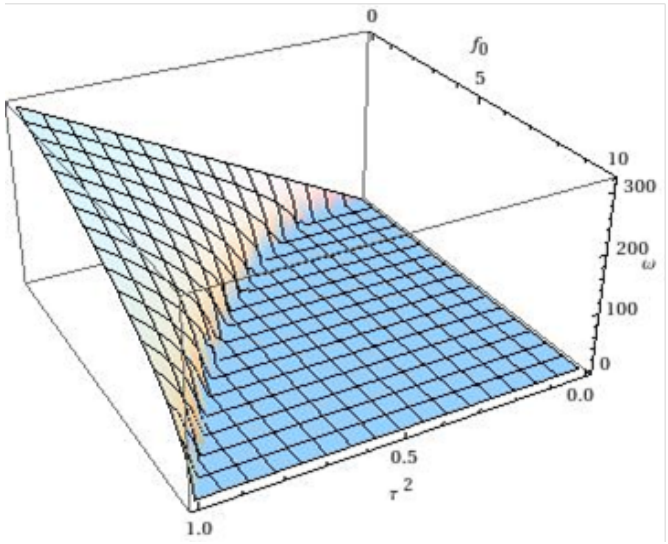

FIGURE1 : Influence of constant axial force and scale coefficient on critical angular velocity

3. References

[1] Lim, C.W., "On the truth of nanoscale for nanobeams based on nonlocal elastic stress field theory: equilibrium, governing equations and static deflection", *Appl. Math. Mech. Engl. Ed.,* Vol. 31, 2010, pp. 37- 54. 218- 232.

[2] Papargyri-Beskou, S. and Beskos, D.E., "Static, stability and dynamic analysis of gradient flexural Kirchhoff plates", *Arch. Appl. Mech.*, Vol. 78, 2008, pp. 625-635.

[3] Tylikowski, A., "Dynamic stability of rotating shafts", *Ing. Arch*., Vol.50, 1981, pp. 41-48.

AUXETIC STRUCTURES SUBJECTED TO DYNAMIC LOADS

Prof. G.E. Stavroulakis[1], Dipl.Eng.MSC A. Syntzanakis[1], Dipl.Eng. A. Georgellis[1], Asst.Prof. G.A. Drosopoulos[2],
[1]Technical University of Crete, School of Production Engineering and Management, Greece
[2]University of KwaZulu-Natal, Department of Civil Engineering, South Africa

Abstract: *Auxetic microstructures have a beneficial effect in dynamic behavior, as it is shown with the example of a plate. Further optimal design work is required for specific applications.*

1. Introduction

Auxetic structures and materials are metamaterials with negative Poisson's ratio. Static behavior or even complicated auxetic materials resulting from topology optimization in the nonlinear range, including contact and plasticity has been studied and verified using numerical homogenization [1].

Vibration suppression within specific frequencies can be achieved with auxetics. A plate with classical and auxetic core is studied numerically using finite elements in order to demonstrate this effect, see Figure 1.

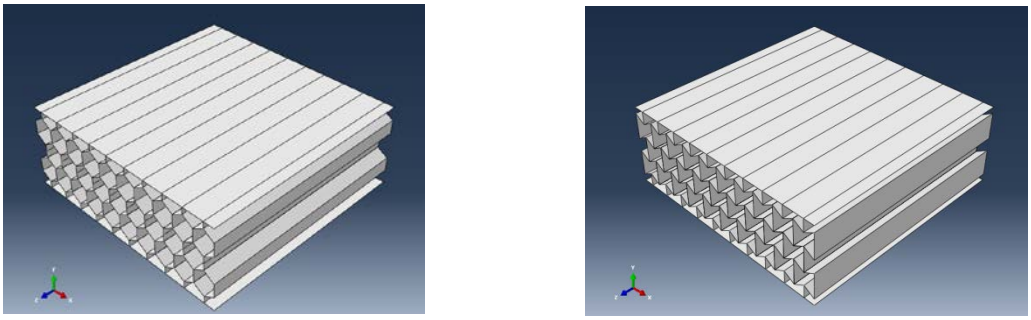

FIGURE 1: Plate with classical and auxetic microstructure

The results demonstrate that frequency response is influenced from the microstructure, depending on the frequency of excitation, see Figures 2 and 3, respectively. Extenssion to other dynamical loads, like impacts, has not been straightforward [2]. Further study using structural optimization in frequency domain is required, cf. [3].

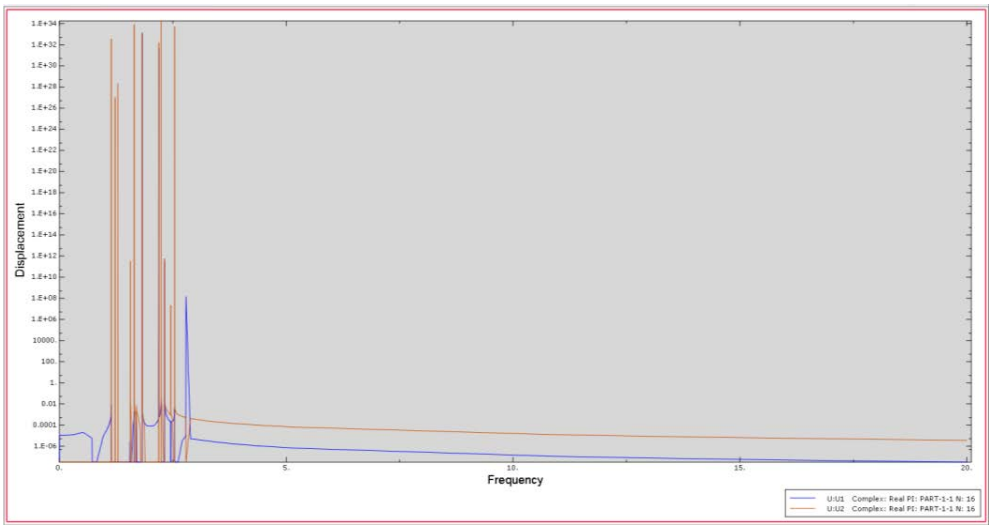

FIGURE 2: Classical plate, frequency response 0-20 Hz

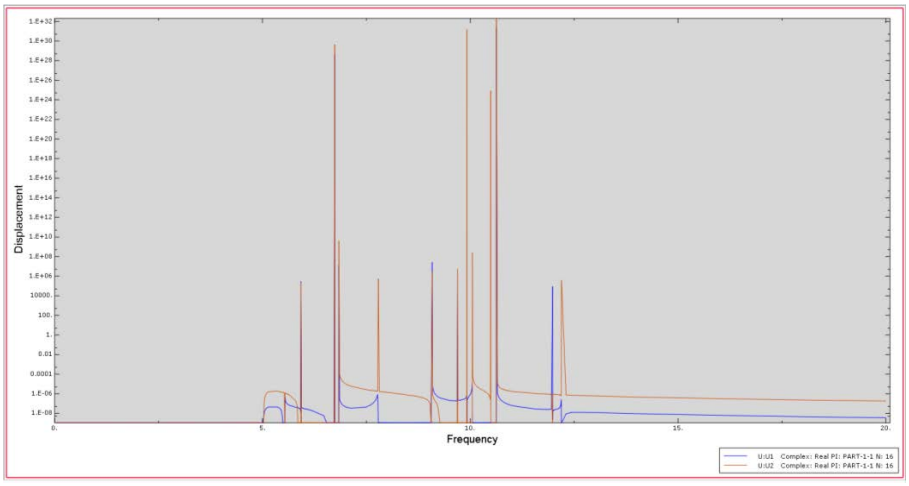

FIGURE 3: Auxetic plate, frequency response 0-20 Hz

2. References

[1] Drosopoulos, G.A., Kaminakis, N., Papadogianni, N., and Stavroulakis, G.E., "Mechanical Behaviour of Auxetic Microstructures Using Contact Mechanics and Elastoplasticity", *Key Engineering Materials*, Vol. 681, 2015, pp. 100-116.

[2] Georgellis, A., *Diploma Thesis*, Technical University of Crete, 2016 (in Greek, available through *http://dias.library.tuc.gr/view/manf/66034*)

[3] Schanz, M., Stavroulakis, G.E., and Alvermann, S., "Effective dynamic material properties for materials with non-convex microstructures", Ch. 4 In: Kompis, V. (ed.), *Composites with Micro- and Nano-Structure*, Springer, Ch. 4, 2008, pp. 47-65.

GEOMETRICALLY NONLINEAR MIXED LEAST-SQUARES FINITE ELEMENT FORMULATIONS

Dr.-Ing. A. Schwarz[1], **K. Steeger, MSc.** [1], **M. Igelbüscher, MSc.** [1],

Prof. Dr.-Ing. J. Schröder[1]

[1]Institute for Mechanics, Faculty of Engineering, University of Duisburg-Essen, Universitätsstr. 15, 45141 Essen, Germany

Abstract: *The main goal of this contribution is the solution of geometrically nonlinear problems using the mixed least-squares finite element method. An investigation of a hyperelastic material law based on logarithmic deformation measures, compare e.g. Simo [1] and Miehe and Lamprecht [2], as an elastic basis for further studies within finite elasto-plasticity is performed. The basis for the proposed formulation is a classical div-grad first-order system consisting of the equilibrium condition and a constitutive equation, see e.g. Cai and Starke [3].*

1. Introduction

In the recent years the complexity of numerical simulations is still increasing. Various modifications and extensions of finite element technologies aim for an improvement of the performance and stability of element formulations. In this work we present a geometrically nonlinear mixed least-squares finite element method (LSFEM) with stresses and displacements as the basic variables. The regarded hyperelastic material is formulated in terms of logarithmic deformation measures, compare e.g. Simo [1] and Miehe and Lamprecht [2]. Furthermore, the performance of the presented formulation is investigated in a numerical example by a comparison of the approximation quality of the formulation.

2. Theoretical framework

The advantages of using LSFEMs lie e.g. in a posteriori error estimator, no restriction to the LBB-condition due to the fact that least-squares functionals lead to a minimization problem and an uniform structure for almost all kinds of DE, see Cai and Starke [3]. For the construction of least-squares functionals $L^2(B)$-norms are applied on the single residuals in general, which leads in the presented work to functionals depending on displacements and stresses. The system with *i* differential equations and *U* unknowns written in residual form ($R_i=0$) and with the corresponding weightings ω_i is given by

$$\mathcal{F}(U) = \sum_i \frac{1}{2} \parallel \omega_i R_i \parallel^2_{L^2(B)} = \sum_i \int_B \frac{1}{2} \omega_i^2 R_i \cdot R_i dV.$$

For the interpolation of stresses and displacements approximation spaces are declared with *m* defining the interpolation order regarding the approximation of the stresses using vector-valued Raviart-Thomas (*RT*) functions and *k* denotes the polynomial order for the Lagrange interpolation (*P*) of the displacements. The resulting element structure is therefore given by RT_mP_k. The considered material model is based on a free energy function formulated in terms of logarithmic deformation measures as

$$\psi(b) = \frac{\Lambda}{2}(\varepsilon_1 + \varepsilon_2 + \varepsilon_3)^2 + \mu((\varepsilon_1)^2 + (\varepsilon_2)^2 + (\varepsilon_3)^2)$$

with $b = \lambda_1^2 n_1 \otimes n_1 + \lambda_2^2 n_2 \otimes n_2 + \lambda_3^2 n_3 \otimes n_3$ and $\varepsilon_i = \ln(\lambda_i)$.

Therein, the Lame constants are given by Λ and μ. Additionally, the left Cauchy-Green deformation tensor $\boldsymbol{b}=\boldsymbol{F}\boldsymbol{F}^T$ is introduced in terms of the eigenvector basis $n_{1,2,3} \otimes n_{1,2,3}$ and the eigenvalues $\lambda_{1,2,3}$ of the stretch tensor $\boldsymbol{V}$ following from $\boldsymbol{F}=\boldsymbol{V}\boldsymbol{R}$ where $\boldsymbol{R}$ is a proper orthogonal rotation tensor. The resulting least-squares functional reads after reformulation and consideration of an isotropic case for the Kirchhoff stresses $\tau=PF^T = 2\frac{\partial \psi}{\partial b} b$ as

$$\mathcal{F}(P,u) = \frac{1}{2}\int_B \omega_1^2 (DivP + f) \cdot (DivP + f)\ dV + \frac{1}{2}\int_B \omega_2^2 \left(PF^T - 2\frac{\partial \psi}{\partial b} b\right) \cdot \left(PF^T - 2\frac{\partial \psi}{\partial b} b\right) dV.$$

3. Numerical Example

The numerical example is given by the Cook's membrane problem where we consider RT_mP_k element formulations with a polynomial order of $m=0,1,2$ and $k = m+1$. The geometrical setup, material parameters, boundary conditions and the results are given in Figure 1. The results show clearly the raise of performance for the higher order elements of the presented classical LSFEM.

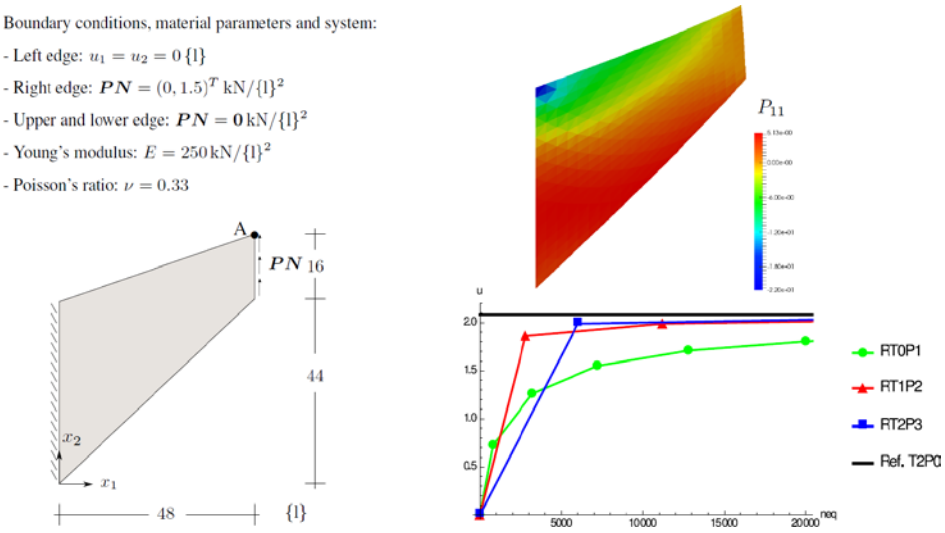

FIGURE 1: Geometry setup, material parameter and displacement convergence for u_2 of the upper right node (48,60) over number of equations (neq) of the final system of equations.

Acknowledgements The authors gratefully acknowledge the support by the Deutsche Forschungsgemeinschaft in the Priority Program 1748 "Reliable simulation techniques in solid mechanics. Development of non-standard discretization methods, mechanical and mathematical analysis" under the project "First-order system least squares finite elements for finite elasto-plasticity" (SCHR 570/24-1, SCHW 1355/2-1).

5. References

[1] Simo, J.C., "Algorithms for static and dynamic multiplicative plasticity that preserve the classical return mapping schemes of the infinitesimal theory", *Comput. Methods in Appl. Mech. Eng.*, Vol. 99, No. 1 ,1992, pp. 61-112.

[2] Miehe, C., and Lamprecht, M., "Algorithms for computation of stresses and elasticity moduli in term of Seth-Hill's family of generalized strain tensors", *Commun. Numer. Meth. En.*, Vol. 17, 2001, pp. 337-353.

[3] Cai, Z., and Starke, G., "Least-squares methods for linear elasticity", *SIAM Jour. on Num. Anal.*, Vol. 42, No. 2, 2004, pp. 826-842.

9th German-Greek-Polish Symposium
Recent Advances in Mechanics
September 04-09, 2016
Kolympari, Chania, GREECE

ENGINEERING ANALYSIS USING CAD-BASED MACROELEMENTS

Prof. Dr.-Ing. C. G. Provatidis[1]
[1]National Technical University of Athens, Greece

Abstract: *Older and contemporary CAD-based interpolations, either for surfaces or for volume blocks, create corresponding sets of basis functions on which finite-element (Galerkin) and global collocation procedures are supported. The paper investigates the quality of the relevant numerical solution in several 2D and 3D engineering problems. The study deals with Poisson equation and acoustics, as well as with elastostatics and elastodynamics.*

1. Introduction

CAD formulas have appeared for the first time by S. Coons (at MIT in the period 1964-1967), whereas the coupling between CAD and CAE (mainly FEM) ideas has been later proposed by Gordon and Hall [1]. One of the first paper in treating a large domain as a single Coons macroelement is due to Kanarachos and Deriziotis [2] for potential problems as well as Kanarachos et al. [3] for static and dynamic elasticity problems. A state-of-the-art review paper was presented by Provatidis [4].

In a chronological sense, CAD formulas have passed through five main stations, i.e. (i) boundary-only Coons interpolation, (ii) internal-point Gordon-Coons interpolation, (iii) Bézier formulation, (iv) B-splines, and (v) NURBS. Each of these formulations describes a geometric object, i.e. a curved surface of a volume block. The connection between CAD and CAE is immediately understood as follows. For example, in the case of a 2D elliptic problem, the 3D plot of solution $z = u(x,y)$ versus the axes x and y will be a surface in the space, and being such a surface can be mathematically described by a CAD-based interpolation formula. Moreover, since each of the abovementioned CAD formulas include a corresponding 'hidden' complete set of basis functions, these can be used to treat the computational problem, implementing any known computational method such as FEM, BEM or collocation techniques.

2. Details and Performance of Macroelement Analysis

Despite the excellent performance of "C-elements" in several potential problems [2], it was later found that under certain conditions they may coincide with the well-known Serendipity elements [5], which obviously share an incomplete functional basis. Therefore, the boundary-only Coons interpolation [case (i) of CAD stations] is not of general applicability and should be applied with reservation.

Instead, Gordon-Coons transfinite interpolation may be successfully used and generally it leads to excellent numerical results [6]. Under certain conditions, this formulation coincides with the well-known elements of Lagrangian type. To give an idea about the numerical performance of these elements, let us consider the case of an elliptical section ($2a \times 2b = 4 \times 2$) of a prismatic beam in torsion. Using 48 triangular finite elements (with 33 nodal points) the error in the calculation of the torsional rigidity ($J_{exact} = 5.025$) is about 30%, whereas using 24 quadratic triangular elements (with 6-node each, 65 nodes totally) the error reduces to 5%.

Interestingly, using the same number of boundary descritization (16 equal segments) but now in conjunction with a single Lagrangian type macroelement (25 nodes), the error entirely vanishes. Similar behavior has been noticed to many other 2D problems [4].

In this paper we continue the investigation in 3D problems, for which only boundary-only formulations have been previously presented [7]. As the equations of elastodynamics split in four sets of acoustic equations (due to Helmholtz decomposition: $\vec{u} = grad\Phi + curl\vec{\Psi}$), and due to the fact that simple closed form formulas exist in acoustics, a main part of our work is spent on the eigenvalue analysis of a rectangular acoustic cavity of dimensions $2.5 \times 1.1 \times 1.0$, as well as a spherical one. For both cases it is shown that boundary-only Coons formulation works but a single Lagrangian macroelement is still better. Moreover, it was found that transfinite elements of which the number of internal nodes is slightly less than those existing on their boundary, lead again to reliable numerical eigenvalues .

Then it was found that the functional set of Bézier (Bernstein) polynomials lead to identical results as those obtained using the aforementioned single Lagrangian macroelement, and a theoretical explanation is provided as a result of basis change. The collection of numerical results is completed using B-splines and NURBS for the same mesh density of breakpoints.

A similar high quality of calculated eigenfrequencies was also found for elastic structures, where the numerical solution that was obtained using fine meshes in the commercial code ANSYS was taken as a reference.

3. References

[1] Gordon, W.J., and Hall, C.A., "Transfinite element methods: blending-function interpolation over arbitrary curved element domains", *Numerische Mathematik*, Vol. 21 (2), 1973, pp 109-129.

[2] Kanarachos, A., and Deriziotis, D., "On the solution of Laplace and wave propagation problems using `C-elements`", *Finite Elements in Analysis and Design*, Vol. 5 (2), 1989, pp. 97-109.

[3] Kanarachos, A., Provatidis, Ch., Deriziotis, D., and Photeas, N., "A new approach of the FEM analysis of two-dimensional elastic structures using global (Coons') interpolation functions", In: W. Wunderlich (ed.), CD Proceedings *European Conference on Computational Mechanics (ECCM'99)*: (Paper 763.pdf: pages 1-19), 28 Aug-3 Sept. 1999, Munich, Germany.

[4] Provatidis, C.G., "A Review on Attempts towards CAD/CAE Integration Using Macroelements", *Computational Research*, Vol. 1 (3), 2013, pp. 61-84.

[5] Provatidis, C.G., "Coons-patch macroelements in two-dimensional parabolic problems", *Applied Mathematical Modelling*, Vol. 30 (4), 2006, pp. 319-351.

[6] Provatidis, C.G., "Two-dimensional elastostatic analysis using Coons-Gordon interpolation", *Meccanica*, Vol. 47 (4), 2012, pp. 951-967.

[7] C. G. Provatidis, C. G., "Analysis of box-like structures using 3-D Coons' interpolation", *Communications in Numerical Methods in Engineering*, Vol. 21 (8), 2005, pp. 443-456.

9th German-Greek-Polish Symposium
Recent Advances in Mechanics
September 04-09, 2016
Kolympari, Chania, GREECE

NONLINEAR BEHAVIORS OF UNDERACTUATED SYSTEMS IN THE TRAJECTORY TRACKING TASKS

M.Sc. S. Korczak
Warsaw University of Technology, Poland

Abstract*: This contribution presents some nonlinear behaviors of an underactuated mechanical system under the trajectory tracking task. The system is fully controlled with a computed torque algorithm with the pseudoinverse operation and a proportional-derivative feedback. Control errors present irregular and chaotic behaviors because of the input force limitations.*

1. Introduction

The dynamic system described by a set of second order ODE in form

$$\ddot{\boldsymbol{q}}(t) = \boldsymbol{f}_1 + \boldsymbol{f}_2\boldsymbol{u}(t) \tag{1}$$

with generalized coordinates $\boldsymbol{q}(t) = [q_1, q_2, \dots, q_n]$ and inputs $\boldsymbol{u}(t) = [u_1, u_2, \dots, u_w]$ is called underactuated if the unbounded control inputs $\boldsymbol{u}(t)$ cannot produce accelerations $\ddot{\boldsymbol{q}}$ in arbitrary direction. This could be verified by the condition $\mathrm{rank}\boldsymbol{f}_2 < \dim\boldsymbol{q}$. The situation of less number of inputs than the number of degrees of freedom is called trivial underactuation. There are many systems with the underactuated property, e.g. acrobot, pendubot, cart-pole, the beam-and-ball, inertia-wheel pendulum, airplane and multicopter, hovercraft, surface vessel. A recent review of underactuated systems and their control is presented by Liu and Yu [1].

2. Input coupling problem in trajectory tracking task

One of not enough studied problems related to underactuated systems is the input coupling. The system described by equation (1) has input coupling if at least one input acts on at least two accelerations. This situation causes big problems in the trajectory tracking task.

The most popular method of tracking control of underactuated systems with the input coupling effect is based on the change of variables that converts this problem into noncoupled. Then some accelerations are separately controlled by inputs and some stay without control (selective control method). This contribution presents a new method of full state control based on the Moore-Penrose pseudoinverse operation combined with a computed torque technique and PD feedback presented by Korczak [2,3]. The inputs are then proposed as

$$\boldsymbol{\tau}(t) = \boldsymbol{f}_2^{+}\left(\ddot{\boldsymbol{d}}(t) - \boldsymbol{f}_1 + \boldsymbol{K_D}\dot{\boldsymbol{e}}(t) + \boldsymbol{K_P}\boldsymbol{e}(t)\right) \tag{2}$$

where $\boldsymbol{f}_2^{+}$ is a pseudoinverse of $\boldsymbol{f_2}$, $\boldsymbol{d}(t)$ is a vector of desired trajectory functions, $\boldsymbol{K_D}$ and $\boldsymbol{K_P}$ are diagonal matrices of coefficients and $\boldsymbol{e}(t) = \boldsymbol{d}(t) - \boldsymbol{q}(t)$ is a vector of tracking errors. Substitution of the control method proposed by equation (2) into system of equations of motion (1) yields the errors dynamic equation

$$\ddot{\boldsymbol{e}}(t) + \boldsymbol{f_2}\boldsymbol{f}_2^{+}\boldsymbol{K_D}\dot{\boldsymbol{e}}(t) + \boldsymbol{f_2}\boldsymbol{f}_2^{+}\boldsymbol{K_P}\boldsymbol{e}(t) = (\boldsymbol{f_2}\boldsymbol{f}_2^{+} - \boldsymbol{I})\left(\boldsymbol{f_1} - \ddot{\boldsymbol{d}}(t)\right) \tag{3}$$

3. Exemplary underactuated system

In this paper, one of the simplest underactuated models is described [3]. It can be used for basic representation of a hovercraft, rocket or sliding vehicle. Consider a planar rigid body moving on a plane (Fig. 1). The object has mass m and inertia I_C in the center of mass (point C). Coordinates $x(t)$ and $y(t)$ describe its position, $\varphi(t)$ denotes angle between the object symmetry line and X axis of the global coordinate system O_{XY}. The vector of force $\vec{\boldsymbol{F}}$ acts on the object in a point away from the point C by distance a. Constant drag coefficients c and c_φ are used. The equations of motion for the system are as follows

$$m\ddot{x}(t) + c\dot{x}(t) = |F|\cos(\varphi(t) + \beta(t)) \tag{4}$$

$$m\ddot{y}(t) + c\dot{y}(t) = |F|\sin(\varphi(t) + \beta(t)) \tag{5}$$

$$I_C\ddot{\varphi}(t) + c_\varphi\dot{\varphi}(t) = F(t)a\,\sin\beta(t) \tag{6}$$

The most interesting behavior of tracking errors occurs in the situation of bounded inputs $\boldsymbol{u}(t)$. An exemplary phase portrait and Poincare map of the angle error are presented on the figure 2.

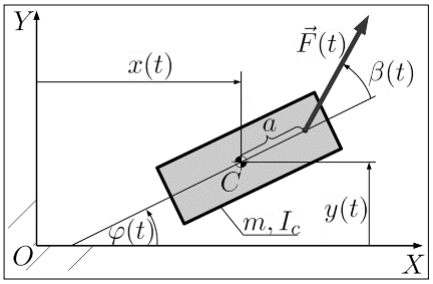

Figure 1: Object in the global coordinate system

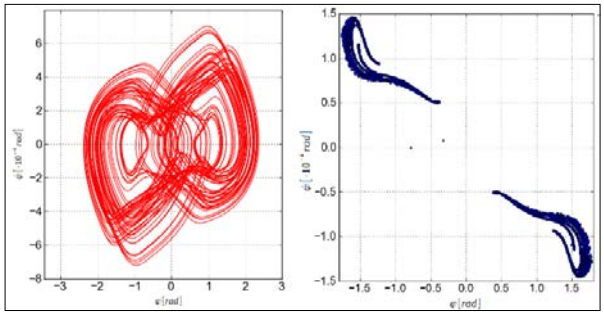

Figure 2: Phase portrait and Poincare map for the rotation error

4. Reference

[1] Liu Y., Yu H., "A survey of underactuated mechanical systems", *IET Control Theory and Applications*, Vol. 7, No. 7, 2013, pp. 921-935.

[2] Korczak S., "Dynamics and stability of underactuated systems with input coupling", PhD thesis, 2016.

[3] Korczak S., "Tracking control of an underactuated rigid body with a coupling input force", *Archives of Control Sciences*, Vo. 24, No. 3, 2014, pp. 321-332.

[4] R. Olfati-Saber, "Nonlinear control and reduction of underactuated systems with symmetry. III. Input coupling case", Proceedings of the 40th IEEE Conference on Decision and Control, Vol. 4, 2001, pp. 3778-3783.

9th German-Greek-Polish Symposium
Recent Advances in Mechanics
September 04-09, 2016
Kolympari, Chania, GREECE

ISOGEOMETRIC METHODS IN HIGHER-ORDER CURVED BEAM THEORIES

I.N. Tsiptsis[1], E.J. Sapountzakis[2]

[1] Institute of Structural Analysis and Antiseismic Research
School of Civil Engineering
National Technical University of Athens,
Zografou Campus,GR-157 80 Athens, Greece
e-mail: mrtsip@hotmail.com

[2] Institute of Structural Analysis and Antiseismic Research
School of Civil Engineering
National Technical University of Athens,
Zografou Campus,GR-157 80 Athens, Greece
e-mail: cvsapoun@central.ntua.gr,
web page: http://users.ntua.gr/cvsapoun/contact-gr.html

Abstract: In this paper, Isogeometric tools are employed for the analysis of curved homogenous beams of arbitrary cross section, taking into account nonuniform warping, shear deformation effects (shear lag due to both flexure and torsion) and cross-sectional distortion considering either a b-spline or a NURB approximation for both the numerical solution of the problem and the geometry of the beam. Different numerical methods have been employed and compared such as the Analog Equation Method (AEM), a boundary element based method, and the Finite Element Method (FEM).

1. Introduction-Statement of the problem

Most of the developed beam theories are usually based on assumptions that require special attention. Considering the most fundamental ones, cross sections are assumed 1) to remain plane with 2) their shape unchanged during deformation. Regarding the first assumption, this is relaxed by introducing independent warping parameters multiplying corresponding warping functions in the displacement field which are presented in [1-2]. In order to take into account distortional effects, another set of distortional parameters have been considered and multiplied by the corresponding distortional functions. In this paper, Isogeometric tools are employed in the AEM [3] in a general form for sixteen one-dimensional boundary value problems described by second-order differential equations, such as the nonuniform warping and distortional problem of a homogeneous beam, which are reduced to solving the second-order differential equations with respect to the components and parameters mentioned above. Comparisons to FEM solutions have been done. The introduction of b-splines or NURBS [4] either in the approximation of the AEM fictitious loads or the FEM displacement field as well as the geometry of the beam improves accuracy and reduces computational cost.

2. Conclusions

A closed one-cell thin-walled box-section beam has been studied. Figure 1 displays the distortional mode of the beam formulation shown in Figure 2 for a vertical eccentrically applied load. Figure 2 shows the difference in displacement between a beam formulation with sufficiently spaced diaphragms along the length (Figure 2a) and with one diaphragm at the free edge (Figure 2b) for a vertical load applied at the centroid of the cross section. Total translation at the free edge is almost doubled for the 3-d model with one diaphragm due to distortion along the length displayed as the shaded area at the top cross section curved plate (Figure 2b). The beam formulation suggested in this work allows an easier handling and post-processing of the curved beam model comparing to 3-d FEM solid elements with the same level of accuracy and much less computational effort.

3. References

[1] Dikaros, I.C., and Sapountzakis, E.J., “Generalized Warping Analysis of Composite Beams of Arbitrary Cross Section by BEM Part I: Theoretical Considerations and Numerical

Implementation", *Journal of Engineering Mechanics ASCE*, Vol. 140, 2014, pp. 1-14.

[2] Sapountzakis, E.J., and Tsiptsis, I.N., "Generalized warping analysis of curved beams by BEM", *Engineering Structures*, Vol. 100, 2015, pp. 535-549.

[3] Katsikadelis, J.T., "The Analog Equation Method. A Boundary – only Integral Equation Method for Nonlinear Static and Dynamic Problems in General Bodies", *Theoretical and Applied Mechanics*, Vol. 27, 2002, pp. 13-38.

[4] Hughes, T., Cottrell, J., and Bazilevs, Y., "*Isogeometric analysis: Toward Integration of CADand FEA*", Wiley, 2009.

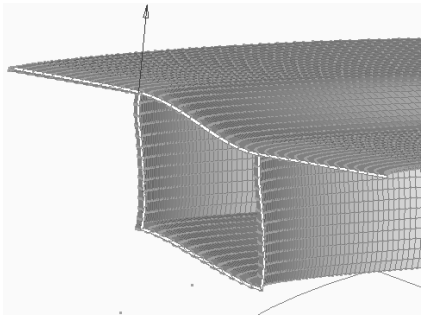

FIGURE 1: Cross-sectional in-plane deformation of a monosymmetric box-shaped curved beam.

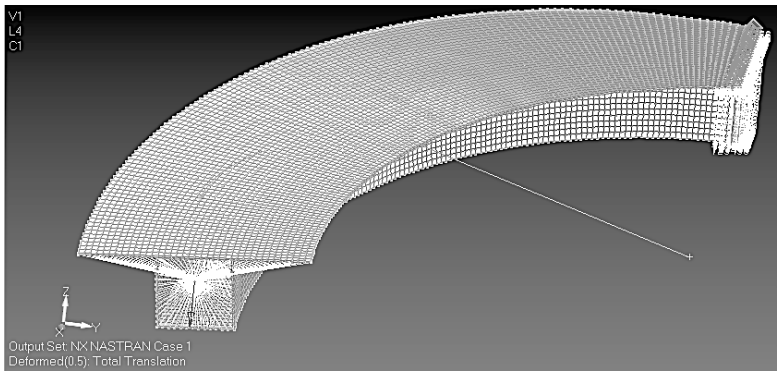

(a)

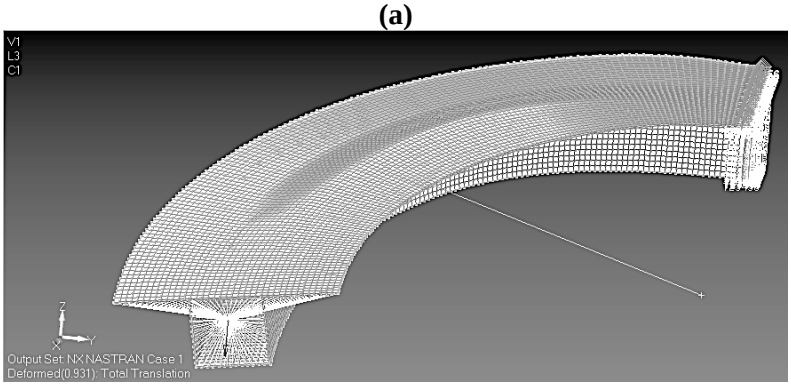

(b)

FIGURE 2. Deformed shapes of models in FEMAP employing 10976 quadrilateral solid finite elements and (a) 13 diaphragms or (b) one diaphragm.

COMPOSITE STEEL-CONCRETE BEAMS WITH PARTIAL INTERACTION: EXPERIMENT, THEORY, SIMULATION

Prof. M. Kuczma[1], **Dr B. Kuczma**[2]
[1,2]Poznan University of Technology, Institute of Structural Engineering, Poznań, Poland

Abstract: *We will present results of our experimental testing, mathematical modelling, and numerical simulations of steel-concrete composites beams bonded by traditional steel headed stud shear connectors and flexible or stiff structural adhesive layers. The mutual slip across the steel/concrete interface was observed in experiments and taken into account in the model. Good agreement of theory and experiment was obtained.*

1. Experimental testing

We deal with composite beams of steel and concrete bonded with different types of connectors: traditional steel headed stud shear connectors as well as flexible or stiff structural adhesive layers. We have carried out laboratory investigations on composite beams of length 3700 mm and the cross-section shown in Fig. 1. The composite beams were subjected to a quasi-static three-point bending test, whereas fragments related to them — to a push-out test with compression force, Fig. 2.

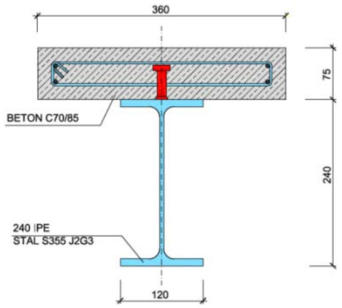

Figure 1: Cross-section of composite beam

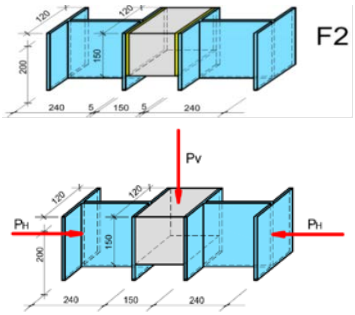

Figure 2: Fragments related to composite beam

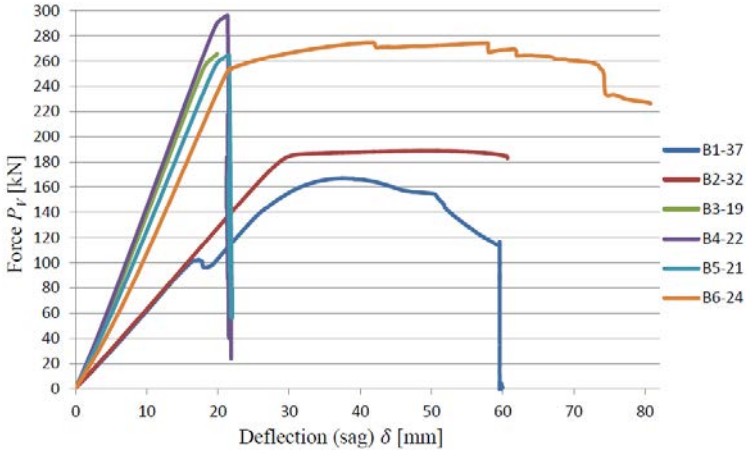

Figure 3: P-δ diagrams for ultimate load tests on composite beam with various steel-concrete bonds

Figure 3 shows the experimental results we obtained for ultimate load 3-point bending tests on the composite beams with various kinds of steel-concrete bond: beam B1 with concrete slab freely resting on steel girder through 5 mm diameter steel round bars, beam B2 with flexible structural adhesive, beams B3 and B4 with stiff structural adhesive, B5 with steel headed stud shear connectors with circle steel foot bonded to steel girder by stiff structural adhesive, and B6 with steel headed stud shear connectors welded to steel girder. As can be seen the highest limit load (296,5 kN) was reached for the composite beam with stiff structural adhesive bond.

2. Mathematical modelling and simulation

To account for a mutual slip between the concrete slab and the steel girder we have applied three kinematic fields: $w = w(x,t)$ – vertical displacement, $u_1 = u_1(x,t)$, $u_2 = u_2(x,t)$ – horizontal displacements of the girder and the slab, respectively.

The deformation process of the investigated composite beams is complex because of the nonlinear response of component materials and unilateral constraints on the steel/-concrete interface.
Having applied the finite element discretization to the governing boundary value problem for the composite beam, we can formulate it incrementally in time as a sequence of (linear) complementarity problems that take the form, for a typical time-step $t_{k-1} \rightarrow t_k$,

$$\boldsymbol{D}\boldsymbol{x}_k = \boldsymbol{b}_k$$
$$\boldsymbol{x}_k^2 \geq \boldsymbol{0}, \quad \boldsymbol{y} \geq \boldsymbol{0}, \quad \boldsymbol{x} \cdot \boldsymbol{y} = 0 \tag{1}$$

where $\boldsymbol{x_k}$ is an unknown supervector at time t_k, whose first part $\boldsymbol{x}_k^1$ is not sign-restricted but second part must not be negative, $\boldsymbol{x}_k^2 \geq \boldsymbol{0}$, and which must be orthogonal to the vector of slack variables $\boldsymbol{y}$. Vector $\boldsymbol{x_k}$ contains finite increments of nodal displacements and Lagrange multipliers corresponding to the unilateral, inequality constraints. Matrix $\boldsymbol{D}$ may, in a general case, depend on time, and the right-hand side vector $\boldsymbol{b}_k$ is known at time t_k.
The results of numerical solution of (1) will be presented at the conference. The present contribution is an extension of Kuczma B. [2] and Kuczma M. [3]. Research problems and solutions in composite structures are presented and discussed in Johnson [1] and Ranzi *et al*. [4], to cite a few, where further references can be found.

3. References

[1] Johnson, R.P., *Composite Structures of Steel and Concrete*, Blackwell Publishing, Oxford 2004.

[2] Kuczma, B., *Static-strength analysis of steel-concrete composite beams with deformable connectors* (in Polish), UZ Press, Zielona Góra, 2011.

[3] Kuczma, M., A viscoelastic-plastic model for skeletal structural systems with clearances, *CAMES*, No. 6, 1999, pp. 83-106.

[4] Ranzi, G., Leoni, G., Zandonini, R., State of the art on the time-dependent behaviour of composite steel–concrete structures. *Journal of Constructional Steel Research*, Vol. 80, 2013, pp. 252–263.

ON OPTIMALITY OF COLUMN GEOMETRY

Prof. R. Bogacz[1], Prof. K. Frischmuth[2]

[1]Politechnika Warszawska, SIMR, ul. Narbutta 84, 02-524 Warszawa
and IPPT Polska Akademia Nauk, Pawińskiego 5B, 02-106 Warszawa, Poland
[2]University of Rostock, Institute of Mathematics, Ulmenstraße 69, D-18051 Rostock, Germany

Abstract: *Critical loads of columns under compressive follower forces have been widely discussed in the literature. By means of shape optimization, improvements by factors of more than eight could be achieved. However, the obtained solutions turn out to be not robust against perturbations. The aim of this paper is to explain this sensitivity effect, basing on a study of eigenforms. Further, a robust alternative to the classical optimization approach is proposed.*

1. Introduction

The study of critical loads of constructions has a long tradition, it goes back to L. Euler, and is still of ongoing interest [3], due to new designs and new challenges as e.g. in wind turbines. In particular, variable forcing, coupling effects, passive and active control [4] are important issues. The maximization of critical loads, but also the avoidance of certain undesirable eigenfrequencies, earn a lot of attention. In this context – as well as in numerous others – it was observed that the optimization of shape and other construction parameters frequently leads to negative effects. In particular, the robustness against perturbations of design variables and of the loading conditions may be diminished. Several authors obtained astonishing critical loads for Beck's column, see Fig. 1, middle, but the results could not be confirmed by different numerical methods. In [2] we reported a severe drop in the critical load after rounding profile data from double to single floating point numbers, compare Fig. 2.

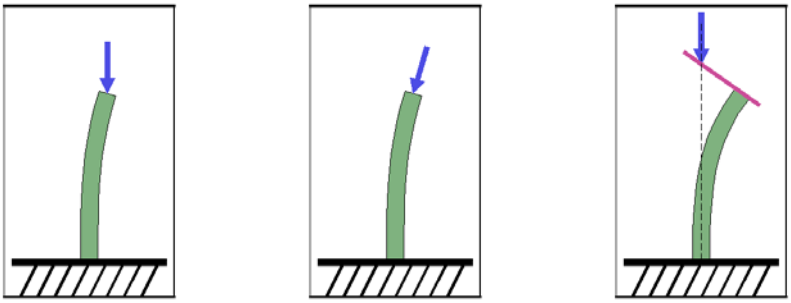

Fig. 1: Loading schemes of Euler, Beck and Reut

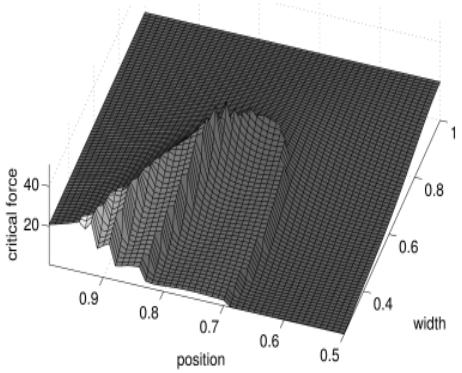

Fig. 2: Drop of critical force due to change of eigenform

The key to an understanding of the mentioned effects lies in the analysis of eigenforms of the considered constructions under loads close to the critical one. As a rule, the characteristic curves in the P-ω-plane become higher, but also more and more slender during the optimization process. Typically, in the vicinity of maximizers, one can find configurations, where neighbouring branches touch, see Fig. 3. This leads to catastrophic changes in

the topology of root curves, where a new, considerably lower local maximizer appears, with the corresponding eigenfrequency jumping and a different eigenform at the new critical point.

Notice that in the classical Euler case, Fig. 1, left, for dead load frozen at a certain low level, with frequency increasing from zero, one passes through consecutive resonances, where the number of nodes of the eigenforms is always the same as their counter indicates. However, this property is violated, if load is increased, with different thresholds for other kinds of loading, such as Beck, Reut or Lipmann cases. This effect becomes more evident, when the shape of the column, i.e. its thickness profile function, is optimized, so that the critical load of a column with uniform thickness is by far exceeded.

We propose a modification of the way nodes are defined and hence calculated. In fact, we look at changes of the sign of the curvature instead of the sign of the displacement itself. This definition is consistent with the classical approach, since in the Euler case the eigenforms are sinusoidal, and zeros of the function and its second derivatives are identical. However, in corresponding forms of oscillations in other cases we have only one point with zero displacement but also two arcs of opposite oriented curvatures, which classifies it as second eigenform.

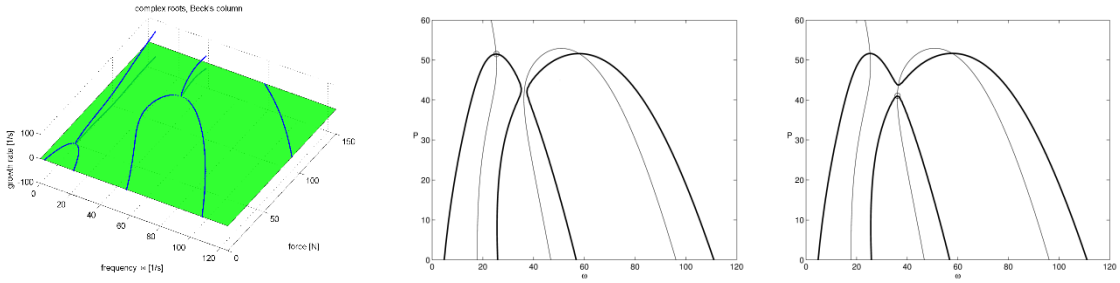

Fig. 3 Root curves, complex, optimal and suboptimal

In order to obtain practically applicable results for critical loads, we propose to evaluate the *worst case load* (WCL). Assuming a maximal tolerable measure of deviation from the given form, parameters and loading conditions, each given configuration is assigned the least critical load over all neighbouring configurations within this tolerance. This approach makes optimization more expensive, and it gives considerably smaller optimal loads. The results, however, are robust to (sufficiently small) manufacturing errors and disturbances during the exploitation of the considered construction.

2. References

[1] Beck, M. Die Knicklast des einseitig eingespannten, tangential gedrückten Stabes, *Z. angew. Math. Mech.*, Vol. 3, 225–228, 1952.

[2] Bogacz, R., Frischmuth, K. and Lisowski, K., Interface Conditions and Loss of Stability for Stepped Columns, *Applied Mechanics and Materials*, Vol. 9, 41–50, 2008.

[3] Kurnik, W. and Bogacz, R., Ziegler problem revisited – flutter and divergence interactions in a generalized system, *Machine Dynamics Research*, Vol. 37, No 4, 71–84, 2013.

[4] Preumont A. and Seto K.: *Active Control of Structures*. Wiley, 2008.

9th German-Greek-Polish Symposium
Recent Advances in Mechanics
September 04-09, 2016
Kolympari, Chania, GREECE

INDENTATION OF MICROSTRUCTURED MATERIALS

Th. Zisis[1] and P.A. Gourgiotis[2] and H.G. Georgiadis[1]

[1]Mechanics Division, National Technical University of Athens, Greece
[2]School of Engineering and Computing Sciences, Durham University, UK

ABSTRACT

In the present study, we derive general solutions for characteristic two-dimensional (2D) indentations within the framework of the generalized continuum theory of couple-stress elasticity. The results show significant departure from the predictions of classical elasticity and it thus seems inadequate to analyze indentation problems in microstructured complex materials employing only classical Contact Mechanics.

1. Introduction

In the present study, we derive general solutions for two-dimensional (2D) plane strain contact problems within the framework of the generalized continuum theory of couple-stress elasticity [1-2] – see Figure 1. This theory introduces characteristic material lengths and is able to capture the associated scale effects that emerge from material microstructure which are often observed in indentation tests used for the material characterization. The contact problems are formulated in terms of singular integral equations using a Green's function approach [3]. The pertinent Green's function obtained through the use of integral transforms corresponds to the solution of the 2D Flamant-Boussinesq half-plane problem in couple-stress elasticity. The results show a strong dependence upon the microstructural characteristics of the material when this becomes comparable to the characteristic dimension of the problem, which in the case of an indentation test is the contact length/area.

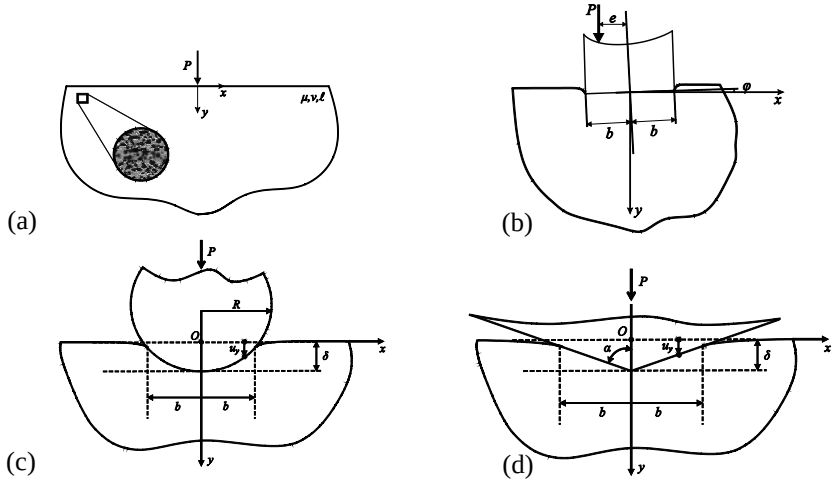

Figure 1: Definition of the problem of a (a) point load applied to an elastic half-plane (b) flat punch (c) cylindrical rigid body and (d) rigid wedge indenting an elastic half-plane.

Our objective is the determination of the contact-stress distribution below the rigid indentor and the determination of the associated contact length. Suppose that the surface of the half-plane is subjected to a distributed normal load $p(\xi)$ per unit length. The stress and displacement fields can be found by superposition using the Flamant-Boussinesq solution as the pertinent Green's function – i.e. treating distributed load as the limit of a set of point loads of magnitude $p(\xi)d\xi$.

In view of the above, the tangential gradient of the normal displacement at the surface of the half-plane assumes the following form:

$$-\frac{1-\nu}{3-2\nu}\mathrm{CPV}\int_{-1}^{1}\frac{p(\tilde{s})}{\tilde{x}-\tilde{s}}d\tilde{s}+\int_{-1}^{1}\tilde{N}(\tilde{x}-\tilde{s})\,p(\tilde{s})\,d\tilde{s}=\frac{\pi\mu}{b}\frac{d\tilde{k}(\tilde{x})}{d\tilde{x}},\quad |\tilde{x}|<1\ , \tag{1}$$

with $\tilde{x}=x/b$, $\tilde{s}=s/b$. Note that the first integral in the integral equation (1) is interpreted in the Cauchy

principal value sense (CPV). In addition, the regular kernel is defined as

$$\tilde{N}\left(\tilde{x}-\tilde{s}\right)=\frac{2\left(1-\nu\right)^{2}}{\left(3-2\nu\right)}\int_{0}^{\infty}\frac{2q^{2}\zeta^{2}\left(\sqrt{1+q^{2}\zeta^{2}}-q\zeta\right)-\sqrt{1+q^{2}\zeta^{2}}}{\sqrt{1+q^{2}\zeta^{2}}+4q^{2}\left(1-\nu\right)\zeta^{2}\left(\sqrt{1+q^{2}\zeta^{2}}-q\zeta\right)}\sin\left(\left(\tilde{x}-\tilde{s}\right)\zeta\right)d\zeta\,, \qquad (2)$$

with $\zeta=\xi b$ and $q=\ell/b$.

The numerical solution of the singular integral equation is accomplished by means of the collocation method for each indentor profile – further details can be seen in [4, 5].

Our results exhibit significant departure from the predictions of classical elasticity. Regarding the concentrated load problem, we note that although the displacement components exhibit the same asymptotic behavior as in the classical theory, their detailed structure is quantitatively different in couple-stress elasticity. Moreover, in marked contrast with the classical theory, the rotation becomes bounded when calculated in the context of couple-stress theory. The departure from the classical elasticity is more significant near the point of the application of the load, where the rotation / strain gradients are more pronounced, while as we move further from the point of the application of the load the differences decay and the couple-stress solution approaches the classical.Regarding the cylindrical and wedge indentation problems, it is shown that for decreasing ratio b/ℓ the pressure below the indentor increases significantly compared to the classical elasticity predictions - Figure 2. Moreover, it is observed that as the characteristic material length ℓ increases the contact width b decreases.

In light of the above, the elastic indentation of microstructured solids, which introduces a more complex loading situation, may also act as a good alternative to common tests like simple shear and pure bending in order to identify the characteristic material length and provide more accurate information closer to real-life conditions.

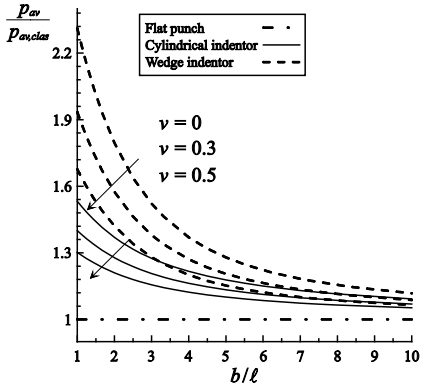

Figure 2: Dependence of the dimensionless average pressure p_{av} / $p_{av,clas}$ upon the ratio ℓ/b and the Poisson's ratio ν .

2. References

[1] Toupin, R.A. 1964. "Theories of elasticity with couple-stress". Arch. Ration. Mech. Anal. 17, pp. 85-112.

[2] Hills, D., Nowell, D., 1994. Mechanics of Fretting Fatigue. Kluwer Academic Publishers, Dordrecht.

[3] Green, A.E., Zerna, W., 1968. Theoretical Elasticity. Oxford University Press, Oxford.

[4] Gourgiotis, P.A., Georgiadis, H.G., 2008. An approach based on distributed dislocations and disclinations for crack problems in couple-stress elasticity. Int. J. Solids Struct. 45, 5521-5539.

[5] Zisis, Th., Gourgiotis, P.A., Baxevanakis, K.P., Georgiadis, H.G., 2014. Some basic contact problems in couple stress elasticity, Int. J. Solids Struct. 51, 2084–2095.

9th German-Greek-Polish Symposium
Recent Advances in Mechanics
September 04-09, 2016
Kolympari, Chania, GREECE

BUCKLING OF THICK PLATES ON BIPARAMETRIC ELASTIC FOUNDATION. A MAEM SOLUTION

Dr. A. J. Yiotis and Prof. J. T. Katsikadelis
School of Civil Engineering, National Technical University of Athens, Greece

Abstract: *The MAEM (Meshless Analog Equation Method), a purely meshless method, is developed for buckling of thick Mindlin's plates resting on biparametric elastic foundation. The solution is approximated by new RBFs, which result from the integration of the analog equations. Increased accuracy is achieved using optimal values of the involved arbitrary shape parameter. The examples demonstrate the efficiency of the method.*

1. Introduction

For the buckling analysis of moderately thick plates of uniform thickness h based on Mindlin's theory and resting on biparametric (Pasternak-type) elastic foundations the following differential equations are used [1]:

$$\frac{D}{2}[(1-\nu)\nabla^2\phi_x+(1+\nu)\frac{\partial}{\partial x}(\frac{\partial\phi_x}{\partial x}+\frac{\partial\phi_y}{\partial y})]-\kappa Gh(\frac{\partial w}{\partial x}+\phi_x)=0 \qquad (1a)$$

$$\frac{D}{2}[(1-\nu)\nabla^2\phi_y+(1+\nu)\frac{\partial}{\partial y}(\frac{\partial\phi_x}{\partial x}+\frac{\partial\phi_y}{\partial y})]-\kappa Gh(\frac{\partial w}{\partial y}+\phi_y)=0 \qquad (1b)$$

$$\kappa Gh(\nabla^2 w+\frac{\partial\phi_x}{\partial x}+\frac{\partial\phi_y}{\partial y})-(N_x w_{,xx}+2N_{xy}w_{,xy}+N_y w_{,yy})=k_f w-G_f\nabla^2 w \qquad (1c)$$

where w is the transverse deflection, ϕ_x,ϕ_y the rotations of the normal about y and x axes; E, G, ν, $D=Eh^3/12(1-\nu^2)$, Young's modulus, shear modulus, Poisson's ratio and the plate flexural rigidity; $\kappa=\pi^2/12$ the shear correction factor for Mindlin's plate theory, $\nabla^2=\frac{\partial^2}{\partial x^2}+\frac{\partial^2}{\partial y^2}$ the Laplace operator in Cartesian coordinates; N_x, N_y, N_{xy} the in-plane forces per unit length inside the domain of the plate resulting from the pre-buckled state [2] and k_f, G_f the subgrade reaction coefficient and the shear modulus of the foundation. The boundary conditions are given in Yiotis and Katsikadelis [3], which are taken homogeneous for buckling.

The boundary value problem (1) together with the boundary conditions is solved using the MAEM as in Katsikadelis [4-5]. The analog equations are :

$$\nabla^2\phi_x=b_1(\mathbf{x},t), \qquad \nabla^2\phi_y=b_2(\mathbf{x},t) \qquad \nabla^2 w=b_3(\mathbf{x},t) \qquad (2a,b,c)$$

where $b_i(\mathbf{x})$ $i=1,2,3$ are the unknown fictitious loads. Using the procedure described in Yiotis and Katsikadelis [3], we obtain the expressions for the displacements:

$$\phi_x\simeq\sum_{j=1}^{K+L}a_j^{(1)}\hat{\phi}_j(r) \quad \phi_y\simeq\sum_{j=1}^{K+L}a_j^{(2)}\hat{\phi}_j(r) \quad w\simeq\sum_{j=1}^{K+L}a_j^{(3)}\hat{w}_j(r) \qquad (3a,b,c)$$

where $r=\|\mathbf{x}-\mathbf{x}_j\|$; K and L the domain and boundary nodal points. The derivatives are obtained by direct differentiation of Eqs. (3). Finally, applying Eqs. (1) at the domain nodal points and the boundary conditions at the boundary nodal points and replacing the involved values of the displacements and their derivatives from Eqs. (3), we obtain the buckling equation:

$$\det(\mathbf{A}-\lambda\mathbf{B})=0 \qquad (4)$$

where $\mathbf{A}$ and $\mathbf{B}$ are known $(3K+3L)\times(3K+3L)$ matrices. Equation (4) yields the values of the buckling parameter λ and the coefficients $\alpha_j^{(i)}$.The buckling modes are computed from Eqs. (3). The

critical value $S_{cr} = S_x a^2 / D$ of a simply supported square plate of length a loaded with the in-plane force S_x along $x = 0$ and $x = a$ for $h/a = 0.20$ and foundation parameters $K_F = k_f a^4 / D$, $G_F = G_f a^2 / D$ is shown in Table 1 as compared with an analytical solution [1].

h/a	$K_F = 0$, $G_F = 0$		$K_F = 100$, $G_F = 10$		$K_F = 1000$, $G_F = 100$	
	[1]	Present	[1]	Present	[1]	Present
0.20	32.4414	32.5323	55.0289	55.6175	174.976	175.5923

Table 1. Critical value for $S_{cr} = S_x a^2 / D$ **(**$\nu = 0.30$**).**

2. References

[1] Akhavan, H., Hashemi Hosseini Sh., Taher Damavandi Rokni H., Alibeigloo A. and Vahabi Sh, "Exact solutions for rectangular Mindlin plates under in-plane loads resting on Pasternak elastic foundation. Part I: Buckling analysis", *Comp. Mater. Sci.*, Vol. 44, 2009, pp. 968-978.

[2] Herrmann, G., and Armenakas, A.E., "Vibrations and stability of thick plates under initial stress", *Transactions of the ASCE*, Vol. 127, 1962, pp. 458-487.

[3] Yiotis, A.J., and Katsikadelis, J. T., "Dynamic analysis of thick plates on biparametric elastic foundation. A MAEM solution", *Proceedings of the 11th HSTAM International Congress on Mechanics*, (eds. H.G Georgiadis and V. K. Koumousis), 2016, Abstract p. 175, Full Paper USB, Greece, May 25-27,2016.

[4] Katsikadelis, J. T., "The 2D elastostatic problem in inhomogeneous anisotropic bodies by the meshless analog equation method MAEM", *Eng. Anal. Bound. Elem.*, Vol. 32, 2008, pp. 997-1005.

[5] Katsikadelis, J. T., *Boundary Element Method for Plate Analysis*, Academic Press, Elsevier, Amsterdam, 2014.

SIMULATION STUDY OF WHEELS WEAR IN LOW- FLOOR TRAM WITH INDEPENDENTLY ROTATING WHEELS

Prof. A. Chudzikiewicz, Ph.D. D.Sc.[1]; **J. Korzeb, Ph.D. D.Sc.**[1]
[1]Warsaw University of Technology, Faculty of Transport, Poland

Abstract: *The paper presents an example of low-floor trams simulation tests. The tram under study was unique because of using the system of independently rotating wheels in the bogie[2]. In this paper the dynamic behavior of the vehicle was examined, and the phenomenon of wheels and rails wear during the rolling contact was subjected to the identification. For this purpose a dedicated computational model was built in Matlab environment, taking into account the phenomenon of kinematic pair wear using Archard model.*

1. Introduction

In case of two solid bodies contact, literature examines many theories taking into account phenomena in the contact area on a surface. Restraining force (frictional force) is directly proportional to the pressure force, and depends on the parameters of the rubbing surfaces: material type, surface roughness, the temperature of the surroundings, and environment properties (occurrence of factors that reduce or increase the friction), and the state of movement (sliding friction, rolling friction). In the case of metals and their technical alloys, the forces associated with the contact area generate stresses, giving in consequence the elastic deformation of surface. After crossing the plasticity limit the strengthening of material can occur by distortion of crystal structure, which translates into an increasing of hardness and strength, and reducing the plastic properties. As a result of internal friction and internal energy dissipation due to the tension and compression, the relation describing the deformation as a stress function is non- linear, and takes the form of hysteresis, called elastic hysteresis. After dividing it by the elastic deformation energy result represents the vibration reduction capability. The tribological material wear due to the friction it's caused by abrasion, cracking, material defects, adhesion of the contact surfaces and tribo-chemical reactions [2].

2. The method and results

During the study of the tribological wear phenomena, a lot of computational models were used. The classical approach describes the use of an adhesive model by Archard [1], wherein the volume and weight of material wear (in wear equation) describes the relation:

$$\begin{cases} V_w = x \cdot k \cdot \dfrac{N}{H} \\ m_w = w_r \cdot \dfrac{W_f}{s_c} \end{cases}$$

where:
V_w - the volume of wheel material wear, [m3],
m_w - mass removed due to wear, [μg/mm^2]

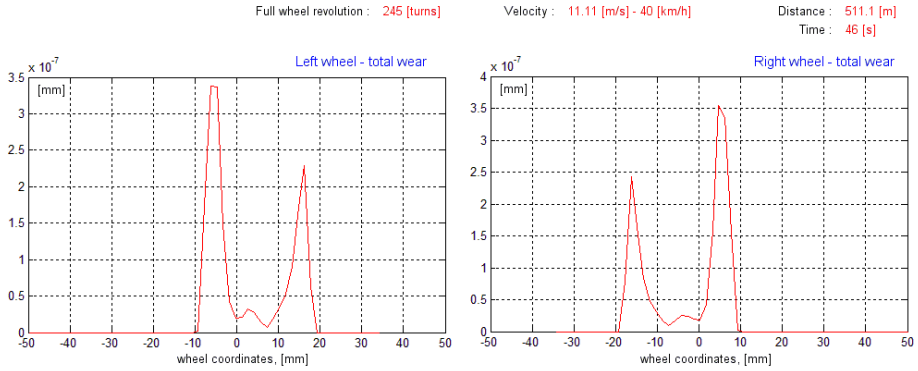

FIGURE 1: Chart of wear the wheels in bogie A, at a speed of 40 km/h; tram loaded, very good condition of the track, linear scale [2]

In the study of dynamics, modeling of rolling contact with the rail wheels, and the calculation of forces acting at the contact area is crucial. To make the calculations of contact forces according to the full theory for non-conformal contacts (adhesion area of solids is not large), commonly used algorithm for calculating the tangential forces - Fastsim developed by Kalker [4] is used. Fastsim is also successfully used for wear prediction of wheel and rail profiles - Chudzikiewicz [3].

In the simulation tests, there was no wear of the wheel rolling plane greater than 6.12e-7 mm, which is consistent with the data encountered in the literature, what indicates that wear should be smaller than 1 mm / 100 000 km.

3. Summary

Simulation studies were designed to evaluate the dynamics of the vehicle under various operating conditions, depending on: state of the track, its configuration and speed of the vehicle. Multi-variant calculations, that incorporate different operating scenarios, allowed to evaluate the wear of wheel rolling surface, preceding the introduction to exploitation of the new model of tram bogie, equipped with independently rotating wheels.

4. References

[1] Archard J.F. ”Contact and Rubbing of Flat Surfaces”, *Journal of Applied Physics*, Vol. 24, pp 981-988, 1953.

[2] Chudzikiewicz, A. et al. ”The structural design of a modern, completely low-floor tram with independently rotating wheels (Report in polish)”, *NCBiR - DEMONSTRATOR+, Warsaw University of Technology Faculty of Transport - PESA Bydgoszcz*, 2014.

[3] Chudzikiewicz A. ”Modelling of wheel and rail wear”, *The Archives of Transport*, Vol. XIII, 2001.

[4] Kalker J.J., Chudzikiewicz A. “Calculation of the evolution of the form of a railway wheel profile trough wear", *International Series of Numerical Mathematics*, Vol. 101, pp. 71-84, 1991.

CELLULAR-SOLID STRUCTURAL ELEMENTS IN SEISMIC DESIGN

P. Tsopelas, Assoc. Prof.[1], **Th. Zisis, Assist. Prof.**[1] , **S. Papathanasiou, Grad. Stud.**[1]
[1]Mechanics Division, Schol of Applied Mathematical and Physical Sciences, NTUA, Greece

Abstract: *Cellular solids show great potential for applications as response modification elements as well as load bearing elements within structural systems, due to their ultra-light properties and mechanical behavior. A light-weight cellular solid shear wall could work efficiently for vibration mitigation in large scale structural systems. Finite Element models are developed to predict the stiffness, strength, and energy dissipation effectiveness of shear wall panels with cellular solids.*

1. Introduction

Shear walls are structural members used by engineers to control displacements by providing additional stiffness to bare frame structures. A lot of effort has been spent to increase the ductility of conventional Reinforced Steel Shear Wall (RSSW) system, so as to enhance the energy dissipation capacity of shear wall under earthquake excitation. Such a system is the Steel Plate Shear Wall system (SPSW) and its modifications (e.g. [1], [2], [3]) which can limit drift effectively and can dissipate large amount of energy.

The cellular structure of the shear wall essentially eliminates the potential of out of plane buckling which is prevailing in solid steel-plate shear wall systems. In addition, macroscopically, the cellular structure is responsible for the observed pure shear behavior of the panel. A parametric study to quantify the mechanical properties of the cellular shear wall panels is conducted as a function of the thickness and length of the individual cell walls, and the orientation angle of the vertical cell walls. Finally, to evaluate the performance of a structure fitted with cellular shear wall system, a model of a three-story structural frame is developed and analyzed under seismic excitation

This work studies the static and dynamic behavior of shear walls with cellular solids. The influence of cell geometry on the behavior of cellular solids, when subjected to monotonic and cyclic shear loading, is investigated. (see Figure 1)

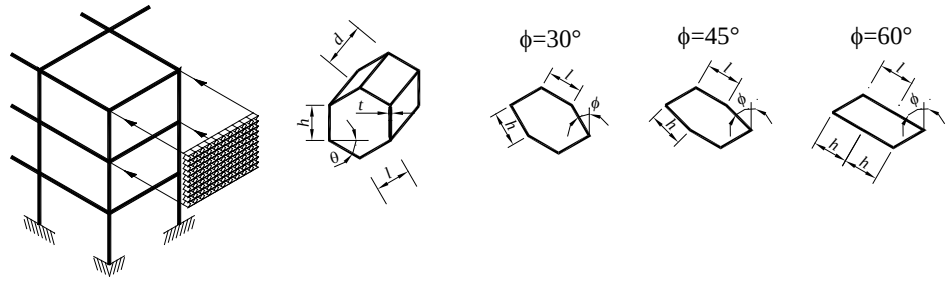

FIGURE 1. Cellular-solid shear wall panel within framed structural system. Geometrical characteristics of regular hexagonal honeycomb (for l=h and θ=30° regular honeycomb) and honeycomb with vertical walls oriented by angle ϕ.

The regular hexagonal honeycomb cell is considered as a unit cell of the proposed cellular-solid shear walls. A number of shapes based on the regular hexagonal honeycomb cell are explored in studying the behavior of shear wall elements with cellular architecture (see Figure 1). Their effect on the strength and energy dissipation properties of shear walls is quantified by analyzing detailed finite element models of a control representative volume element (RVE).

The behavior of a RVE (see Figure 2) can be used in a homogenization attempt, where an equivalent solid material element can be utilized in the place of the cellular-solid. This engineering simplification could greatly reduce computational effort and make numerical analysis more efficient when members (shear walls, response modification devices, etc.) consisting of cellular solids are to be used in full scale structural systems. Furthermore, considering the nature of cellular solids (periodicity) and the aforementioned “homogenization” approximation the behavior of a representative volume element of a cellular material, could be accurately captured by “spring” like hysteretic models.

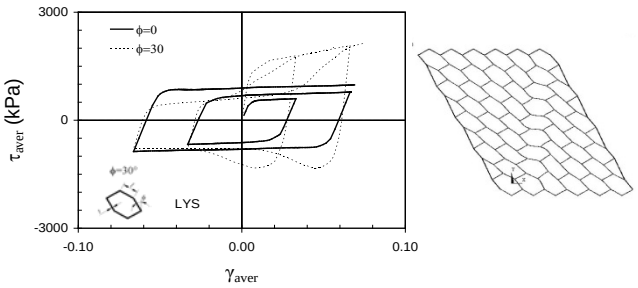

FIGURE 2. Hysteretic behavior of cellular solids under cyclic loading, and buckling-mode deformations of a column of cells with $\phi=30^{o}$ when their cell walls are in compression.

The effectiveness of the shear walls made of cellular-solids was shown from the comparison of the responses of a three-story three-bay steel frame under the seismic motion of El-Centro.

2. References

[1] Thorburn, L. J. Kulk, G.L., & Montgomery, C.J. "Analysis of Steel Plate Shear Walls." Struct. Engrg. Report No. 107. Dept. of Civil Engrg., Univ. of Alberta, Edmonton, Alberta, Canada, 1983.

[2] Berman, J.W. & Brueau, M. "Experimental Investigation of Light-Gauge Steel Plate Shear Walls for Seismic Retrofit of Buildings." Multidisciplinary Center for Earthquake Engineering Research, University at Buffalo, State University of New York. Technical Report MCEER-03-0001, 2003.

[3] Vian, D. & Bruneau M. "Steel Plate Shear Walls for Seismic Design and Retrofit of Building Structures." Multidisciplinary Center for Earthquake Engineering Research, University at Buffalo, State University of New York. Technical Report MCEER-05-0010, 2005.

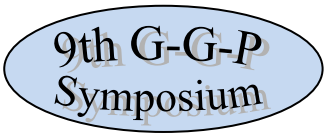

AUTHOR INDEX

The History of the 9 German-Greek-Polish Symposia

The Symposia are regularly every three years in one of the participating countries:

1st, September 1991 in Pułtusk, Poland
2nd, September 1996 in Bad Honnef, Germany
3rd, September 1998 in Xanthi, Greece
4th, September 2001 in Pułtusk, Poland
5th, September 2004 in Bad Honnef, Germany
6th, September 2007 in Alexandroupolis, Greece.
7th, September 2010 in Poznań, Poland
8th, September 2013 in Goslar, Germany
9th, September 2016 in Chania, Greece

ISBN 978-960-8475-25-0